Study of solution processable emissive materials for organic light emitting diodes

Submitted by

Benjamin Breig

A thesis submitted in fulfilment of the requirements for the degree of Doctor of Philosophy in Department of Pure and Applied Chemistry,

University of Strathclyde

2018

This thesis is the result of the author's original research. It has been composed by the author and has not been previously submitted for examination which has led to the award of a degree.

Signed:

Date:

Acknowledgement

First, I would like to thank my supervisor Prof. Peter Skabara for the opportunity he gave me to join his research group, first as an intern and later as a PhD student. I would also like to thank the Korean program KIAT for funding my research and providing us with the main chemicals for this research.

I am very grateful to Dr. Anto Regis Inigo, for teaching me everything I know on organic semi-conductors fabrication and characterisation, to Dr. Neil Findlay for giving me his precious materials and never objecting too much when I asked for more, and to Dr. Alexander Kanibolotsky, for always being available to answer all my questions. A special thanks to Dr. Joseph Cameron, for his help along all my PhD from the research to the correction of this thesis. More generally, I would like to thank every member of the group, past or present, visitor or permanent, for creating such an enjoyable work atmosphere and for helping me discover all the wonders of Scotland.

Sincere thanks to all my friends in Glasgow who made this experience in Scotland unforgettable. A special thanks to Carmelo, your constant happiness and your delicious food where always of great support. Enormous thanks also to Luis and Giuseppe for all these memorable adventures in Glasgow and abroad. Thanks also to my small French community, Alex, Charles, Fabien, Teddy, Brieuc, etc. for always being available when I needed it and for always joining me in the Ark for a good time around a beer.

I would also like to thank all my family, even if they will probably never read this thesis, for all their help and their constant support during all my life.

Finally, I would like to thank my lovely girlfriend, Tania, for all the love she gave me for this last two years. I hope to be able to give you back even just a small part of everything you are giving me.

This thesis is dedicated to all of you, to thank you for everything you bring me.

Abstract

Organic light emitting diodes have played a major role in the display industry in the last ten years. Today, they have found commercial applications in smartphones, televisions, cameras and much more. This recent commercialisation is mainly due to the large performance enhancement in luminance, efficiency and lifetime observed in the last decade. The development of new organic emitting materials is obviously a key part of this success. Consisting of polymers, oligomers or small molecules, these emitters usually follow a simple synthetic path and, thanks to a facile functionalisation, they can be easily adapted to the desired project. However, they constantly need improvement to reach their full potential as efficient, cheap and lightweight light sources. Being able to obtain good performing solution processed emissive materials would be a major step towards the achievement of these goals.

Chapter I includes a brief introduction to the history of OLEDs and their development, followed by a summarised description of the theory of OLEDs.

Chapter II studies the different factors that influence OLED performances. A well-known PPV polymer is used during this study. The emissive layer is first optimised in a conventional architecture. Then a change of architecture allows the study of optimising the transport/blocking layers on the device performance.

Chapters III introduce two novel series of materials for red and green emission. Both series are based on a benzothiadiazole core and fluorene arms. The fluorene arm length and the terminal groups are varied and the influence of these changes are studied. The knowledge acquired in the previous chapter is applied to characterise and optimise the different emissive materials.

In chapter IV the hole mobility of each material is measured in order to have a better understanding of the inner mechanisms of the devices and a solution processed electron transport is proposed as a way to improve their devices performances.

Abbreviations

3D	Three dimensions
°	Degree
%wt	Weight percent
°C	Degree Celsius
Å	Angstrom
A	Ampere
A_1	Lighting area of the device
abs	Absorbance
AFM	Atomic force microscopy
AMOLED	Active matrix organic light emitting diode
a.u.	Arbitrary unit
CCD	Charge Coupled Device
cd	Candela
CELIV	Charge extraction by linearly increasing voltage
C_i	Capacitance
CIE	Commission Internationale de l'éclairage
cm	Centimetre
CV	Cyclic voltammetry
D	Distance between the emitter and the photometer
DSC	Differential Scanning Calorimetry
EBL	Electron blocking layer
E_f	Fermi level
E_{fsm}	Semiconductor fermi level
E_g	Band gap
EIL	Electron injection layer
em	Emission
EM	Emissive material
et al.	et alii
ETL	Electron transport layer
eV	Electron volt
eV_0	Built-in potential
F	Farad
Fc	Ferrocene
FET	Field effect transistor
g	Gramme
HBL	Hole blocking layer
HIL	Hole injection layer
HOMO	Highest occupied molecular orbital
HTL	Hole transport layer
I_{ds}	Drain-source current
I_{on}/I_{off}	On/off current ratio
IR	Infrared
ISC	Intersystem crossing
ITO	Indium tin oxide
J	Current density
L	OFET channel length
LED	Light emitting diode
LCD	Liquid crystal display
lm	Lumen
LUMO	Lowest unoccupied molecular orbital
lx	Lux
m	Meter
M	mol/L
mg	Milligrams
min	Minutes
ml	Millilitre
mol	Mole

MOSFET	Metal-oxide-semiconductor
Mw	Molecular weight
nm	Nanometres
OFET	Organic field-effect transistor
OLED	Organic light emitting diode
OPV	Organic photovoltaic
Pa	Pascal
RGB	Red Green Blue
PLQY	Photoluminescence quantum yield
PPV	Polyphenylenvinylene
RISC	Reverse intersystem crossing
Rpm	Rotation per minutes
s	Second
S_0	Ground state
S_1	Excited state
SAM	Self-assembly monolayers
SCLC	Space charge limited current
SiO_2	Silicon oxide
SY	Super-Yellow (PDY-132)
t	Film thickness
T_1	Triplet state
T_g	Glass transition temperature
TADF	Thermally activated delay fluorescence
TGA	Thermal gravimetric analysis
Tm	Melting temperature
TOF	Time of flight
TOLED	Transparent OLED
TV(s)	Television(s)
V	Voltage
V_2O_5	Vanadium- oxide
Va	Applied voltage
V_{ds}	Drain-source voltage
Vg	Voltage at the gate
VTE	Vacuum thermal evaporation
V_{th}	Threshold voltage
w	OFET channel width
W	Watt
w/w	Mass fraction
$Ø_m$	Metal work function
$Ø_{sm}$	Semiconductor work function
$Ø_B$	Schottky barrier
μ	Charge carrier mobility
ε	Permittivity
χ	Electron affinity

Table of Contents

Abbreviations 5

Chapter I: Introduction and theory 1

I. A brief history of organic light emitting diode (OLED) 1

II. Band theory 4

A. Band theory in the solid 4

B. Band theory in organic materials 6

C. Metal-Semiconductor contact 8

III. OLED architecture and operation 10

IV. Deposition techniques 14

V. OLED Materials 17

A. Emissive layer 17

B. Charge transporting and blocking layers 21

VI. Bibliography 24

Chapter II: OLED optimisation and influencing factors 27

I. Introduction 27

II. Photoluminescence 28

III. Active layer optimisation 31

A. Thickness and solution concentration 31

B. Annealing 33

C. Spin-speed 35

IV. Device architecture 36

A. Inverted architecture 36

B. Molybdenum trioxide 38

C. Molybdenum bronzes 40
D. PEI concentration 44
E. PEI molecular weight 46
V. Conclusion 48
VI. Bibliography 51
Chapter III: Green and Red series materials for OLEDs application 56
I. RGB materials and OLEDs 56
II. Green OLED 58
A. Background 58
B. Materials 59
C. Devices 63
1. Concentration 63
2. Annealing 65
3. CIE coordinates emission spectrum 67
D. Conclusion and further improvement 69
III. Red OLED 71
A. Background 71
B. Materials 72
C. Devices 76
1. Concentration 76
2. Annealing 82
D. Electroluminescence 84
E. Conclusion and further work 86
IV. Bibliography 88

Chapter IV: Charge carrier mobility measurements and their influence on the performance of OLED devices 91
I. Introduction 91
II. Organic field-effect transistors 92
A. Theory 92
B. Measurement of the hole mobility for Green and Red materials 95
III. Space charge limited current 98
C. Theory 98
D. Space charge limited current for electron mobility measurement of ETLs/HBLs 100
IV. Conclusion 105
V. Bibliography 106
Chapter V: Conclusion and further work 108
I. Conclusion 108
II. Further work 113
Chapter VI: Experimental 116
I. OLED 116
A. Fabrication 116
1. Cleaning 116
2. Conventional Architecture 117
3. Inverted architecture 118
B. Characterisation 119
C. Emission spectra and CIE coordinates 120
II. Charge carrier measurement 120
A. SCLC 120

B. OFET fabrication 121

III. PLQY 123

IV. Thickness measurement AFM 125

V. Bibliography 126

Annex 128

Chapter I: Introduction and theory

I. A brief history of organic light emitting diode (OLED)

The story of the organic light emitting diode (OLED) starts with the discovery of semiconductors. In 1833, Faraday[1] reported a change in the resistance of silver sulfide with temperature, a phenomenon that had never been observed with conducting materials. This is the first documented observation of a semiconductor effect. In the following decades, research on semiconductors focused on two important properties. First, the rectification of metal-semiconductor junction, notably through the work of Braun, Marconi or Schuster[2]. Secondly, the sensitivity of semiconductors to light, primarily based on the photovoltaic effect demonstrated by Alexander Edmund Becquerel (father of Henri).[2]

It was only in 1953 (120 years after Faraday's first observations), that Bernanose *et al.*[3] reported electrically simulated light emission (known as electroluminescence) from organic fluorescent materials (acridine orange and its derivatives), deposited on a cellophane sheet, when place in an electric field. Twelve years later, Helfrich and Schneider[4] made the first organic based electroluminescent device, using anthracene crystal. However, this device, as well as the others that followed, had very low performance (with an operating voltage of around 100 to over 1000 V). Some of the major problems of the time concerned the primitive sample preparation, low purity of the organic material and an electrode-organic contact of poor quality.

Following improvements in purification methods as well as the use of vacuum processing techniques for deposition, Tang and Van Slyke,[5] in 1987, reported the first efficient light emitting diode, based on a two organic layers systems made of 4,4'-cyclohexylidenebis[N,N-bis(4-methylphenyl)benzenamine] (TAPC) and tris(8-hydroxyquinolinato)aluminium (Alq_3). The operating voltage was below 10 V for an emission over a 1 000 cd/m^2. This moment marked a turning point in the history of the organic light emitting diode (OLED). From there on, the interest in OLEDs, and

organic electronics in general, has not stopped growing. Nowadays, the field of organic electronics extends to organic photovoltaics (OPVs) and organic field-effect transistors (OFETs).

The success of OLEDs is due to their remarkable properties. Firstly, they are (mostly) made of organic materials, which means they are potentially cheaper to produce than their inorganic counterparts. Additionally, their capacity to form very thin layers (hundreds of nm) combined with their ability to be deposited on flexible substrates, makes them extremely attractive, notably for display technologies. Further advantages over their inorganic homologues include a wider viewing angle, wider operating temperature, better colour temperature tenability, higher resolution, sharper image, better contrast ratio, lower power consumption and they can also be printed, which has the potential to massively lower the cost of production.[6,7]

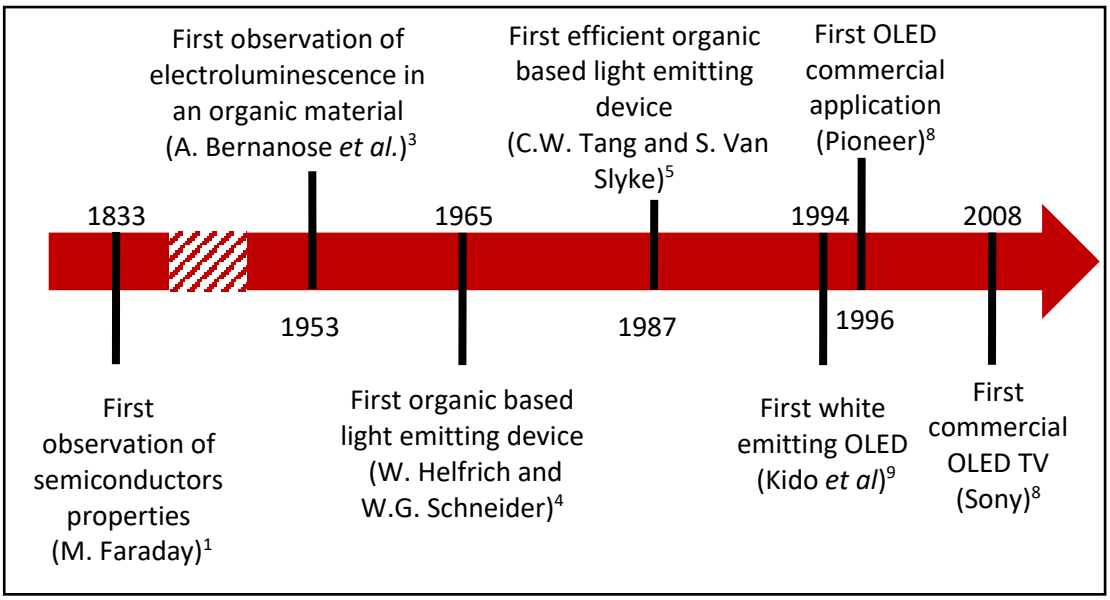

Figure I.1: Brief history of OLEDs

The first commercial OLED was released in 1996 by Pioneer - a monochrome 256x64 display for car audio systems.[8] In 2008, Sony released the first OLED TV ready for commercialisation - XEL-1 for the "modest" sum of $2500 (Figure I.2).[8] Now, organic light emitting diodes are commercialised under numerous forms. Their main application is in displays where they are available in smart-phones, smart watches,

digital cameras, tablets, and ultra-high definition (UHD) TVs. More and more companies are developing projects based on OLEDs, including Sharp, Apple, Dell, AU Optronics, BOE Display, Japan Display, Sony and Panasonic.[7] In January 2018, LG unveiled a prototype for a 65" rollable OLED TV as well as the world's first 88-inch 8K (7680x4320) OLED display.[9]

However, displays are not the only possible application for OLEDs. Indeed, in 1994, Kido *et al.*[10] reported a white emitting OLED for the first time, opening the path for OLEDs to be used in solid-state lighting. The diode was made of a double layer device with a blue emitter and an orange emitter. However, the mix of blue and orange (and later yellow) OLED emitters usually presents lower efficiency compared to their LED counterparts. One way to combat this issue is to develop hybrid inorganic/organic LEDs, where a highly efficient inorganic blue emitting LED is coated with a yellow emitting organic emitting material. The latter should absorb in the blue region, therefore it will absorb part of the blue emitted light from the inorganic material and re-emit yellow light instead. [11,12] A second option to make white light is to use a combination of red, green and blue emitters, either in the same device or in parallel (the method which is used in display with inorganic LED).[13] Using either of these systems, white OLEDs have shown competitive luminous efficiency with light bulbs and fluorescent tubes[14,15] and therefore have the potential to replace them. Nowadays, LEDs are already used in solid-state lighting since they offer a reduction in energy consummation. OLEDs could offer similar impact combined with a potential lower production cost. In 2017, IKEA launched their first OLED lamp – the Vitsand.[16]

Despite the enthusiasm over OLED technology, it still suffers from several problems. The main challenge is to improve the stability of the organic layers when exposed to common environmental aspects such as UV light, humidity or even oxygen. High band gap materials are particularly more sensitive to any degradation process, especially to oxygen, therefore blue OLEDs tend to have a shorter life span than green or red OLEDs.[6] Improvement in efficiency and lifetime are necessary for OLEDs to be more competitive in display and solid-state lighting. It is why they are

often encapsulated before being exposed to any outside agent. The most common protective layers are polyethylene terephthalate (PET) or epoxy, usually deposited on top of the devices. This step, however, complicates the fabrication process and increases the overall price.

Sony XEL-1: The world's first OLED TV[8]

LGD's newest prototype - a 65" rollable OLED TV[9]

The 7.7" Super AMOLED tablet and the 5.3" HD Super AMOLED phone by Samsung[17]

IKEA first OLED lamp, the Vitsand chandelier[16]

Figure I.2: Examples of commercial products with OLEDs

II. Band theory

A. Band theory in the solid

Although Faraday reported the properties of semiconductors in 1833, it was only in 1931 that Sir Wilson[18,19] proposed band theory, a quantum mechanical model to explain conductivity in a solid. This theory is the basis of our understanding of semiconductors.

The idea is as follows: Originally, electrons of a single isolated atom are on a discrete set of energy levels. However, when N number of atoms are brought together, the electrons follow the Pauli Exclusion Principle, which specifies that it is impossible for two electrons to occupy the exact same quantum state. To respect this principle when N atoms form a covalent bond to form a molecule the energy levels are divided into N levels of different energies. However, these energy levels are

extremely close one to another and when the number of atoms increases, , the energy levels are so close to each other that they can be considered as a bulk of levels, called bands (Figure I.3).[20,21] They are separated in two bands, the valence band and the conduction band.

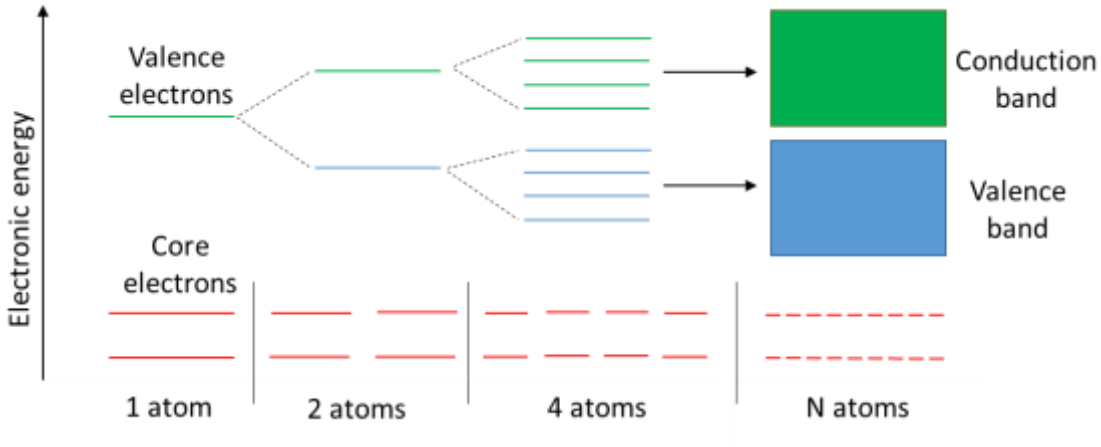

Figure I.3: Band theory from one atom to N atoms

In conducting materials the two bands overlap, therefore it is easy for an electron to be promoted from one band to the other. On the other hand, insulators possess a large (> 4 eV) forbidden band (also called band gap or E_g) between their two bands, where no electrons can exist (Figure I.4). Therefore, in order to pass to the conduction band the electron would require an enormous amount of energy.

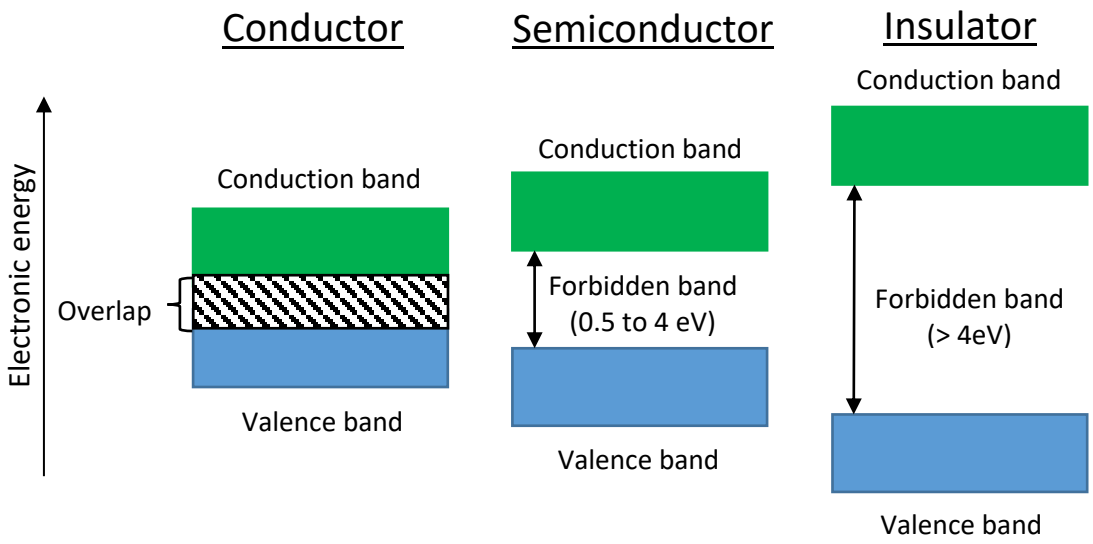

Figure I.4: Conductor, semiconductor and insulator

Semiconductors are at the interface of the other two. They do possess a band gap like the insulators, yet this band is smaller (< 4 eV)[22], which means that if a sufficient external stimulus (heat, electromagnetic, photonic energy) is applied then an electron can be excited to the conduction band. The energy to promote an electron from the valence band to the conduction band should be at least equal to the energy of the band gap.

An electron present in the valence band is considered to have not enough energy to move from atom to atom. If an electron is in the conductance band, it is considered to have a sufficient energy to move from atom to atom. Additionally, since the band is mostly empty, nothing should impair its movement. When an electron is promoted to the conduction band, it leaves an unpaired electron and an electron "hole" (or simply hole) in the valence band. To stabilise the material the hole can be filled by another electron present in the material, which will create another hole where the electron used to be. In turn, it will be filled by another electron present in the material, etc. This movement is described as a hopping mechanism. The movement of the holes combined with the free movement of electrons leads to the conduction of electricity. The movement of holes and electrons is illustrated in Figure I.5.

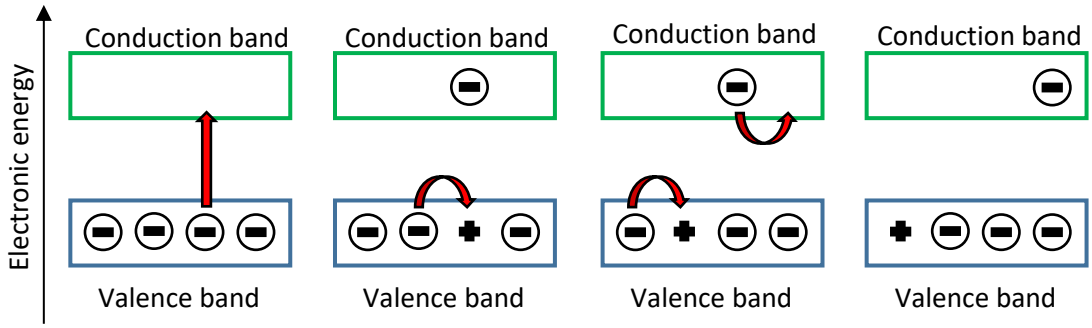

Figure I.5: Movement of electrons and holes in the energy bands in a semiconductor

B. Band theory in organic materials

Organic semiconductors are based on the notion of conjugation, which occurs when a chain of atoms alternates between single and double/triple bonds. It is this

alternation that will induce, in organic materials, a split of the energy levels as well as a delocalisation of charges in these levels and therefore conducting properties.[20]

Carbon atoms possess four valence electrons (electrons used for bonding). If we consider the formation of one double bond between two carbon atoms (like in ethylene) or between one carbon atom and another atom, three of these valence electrons are considered to be in sp^2 hybridised orbitals. These electrons will contribute to the formation of a covalent bond to another carbon or a side group (such as a hydrogen) via σ molecular orbitals. The last electron is considered to be in a p_z orbital and will be used in the formation of a second covalent bond to another carbon or a heteroatom (such as an oxygen) *via* a π molecular orbital.

When two atoms form a single covalent bond, they form at least two orbitals σ- and σ+, in the case of two carbons a non-bonding (nb) orbital is form too. When a double bond is form *via* p_z orbitals, it results in a splitting in two orbitals, π and π*. The bond formation between two atoms is illustrated in Figure I.6 with the example of a double bond between two carbon atoms in ethylene.

As the number of atoms involved in the molecules increases, the number of split orbitals increases as well. In the case of polymers, the energy of the orbitals are so close to each other that it is considered that they form two energy bands. The lowest unoccupied molecular orbital is referred to as LUMO and the highest occupied molecular orbital is referred to as HOMO. The energy gap between the two molecular orbitals previously described is simply named the HOMO-LUMO gap.

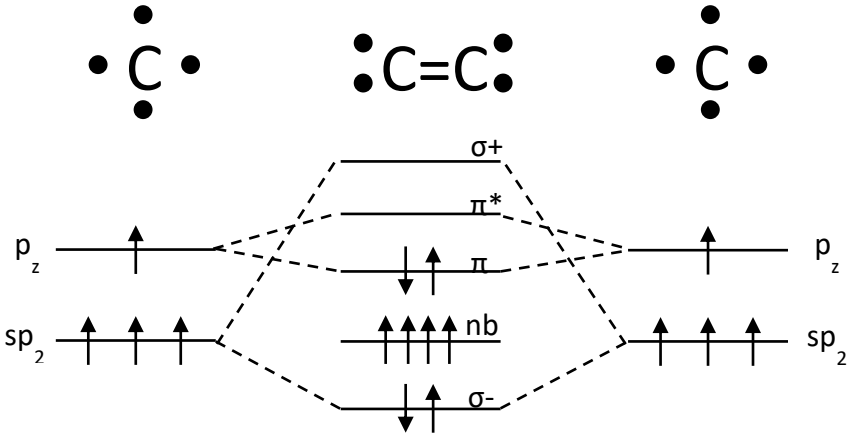

Figure I.6: Orbital splitting when two carbons form a double bond

C. Metal-Semiconductor contact

The current flow between a metal and a semiconductor has been described by Schottky in 1938.[23] His explanation defined the Schottky rectifying barrier and it involved the matching of the metal and organic semiconductor Fermi levels.

Named after the Italian physicist Fermi, the Fermi level (E_f) is defined as the highest occupied orbital at absolute zero,[21] where no electron will have enough energy to be promoted to any higher energy level.

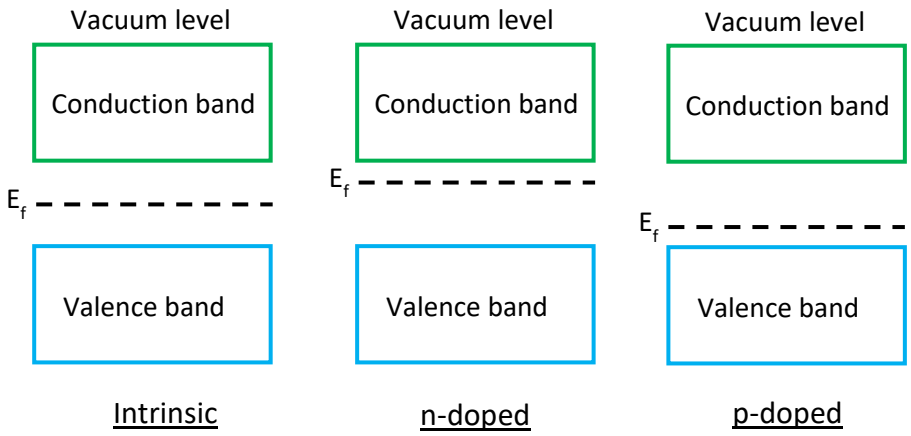

Figure I.7: Fermi level and semiconductor doping

In semiconductors, the Fermi level is described as the distribution of electrons in a given material. In an intrinsic semiconductor, the Fermi level is usually considered to be in the middle of the band gap, as the electrons are evenly distributed. Through an impurity or a defect, semiconductors can be doped. For example, an impurity can lead to an increase of electrons in the material. The distribution of electrons is altered and there is a greater probability of finding electrons in the conduction band. The Fermi level is therefore considered closer to the conduction band. In this case, the semiconductor is then said to be n-doped. In the case of hole doping, the semiconductor is called p-doped. The population of electrons in the conduction band is reduced and the Fermi level is considered closer to the valence band. Figure I.7 illustrates the notion of Fermi level and doping in semiconductors.

This notion of Fermi level become important when organic materials are placed in contact with a metal. Indeed, in order to inject charges (electrons and holes) effectively from the metal to the organic material (or reverse) it is necessary for these

two levels to be aligned. However, when taken separately the Fermi level of the organic material is rarely of the same value as the Fermi level of the metal.

Before continuing, it is important to define the relevant terms. The work function ($Ø_{m,}$ for metals and $Ø_{sm}$ for semiconductor) is defined as the minimum energy necessary to move an electron from the Fermi level to a state of rest in the free space outside the surface of the metal or semiconductor (vacuum).[23] Since there is no electrons located on the Fermi level in a semiconductor (since it is in the band gap), it is necessary to introduce the notion of electron affinity (χ). It is defined as the energy to promote an electron from the bottom of the conduction band to the vacuum.

If we consider a semiconductor that is more electron-rich (n-type) than the metal, the electrons with higher energy in the conduction band of the semiconductor, will transfer from the semiconductor to the metal as it is a more energetically stable state (lower energy). This movement of electrons will create a depletion layer at the interface of the two materials with a majority of holes present. This depletion layer is also called a space charge layer. When electrons are removed from the n-type semiconductor, the Fermi level is lowered down, therefore in the depletion layer the semiconductor Fermi level (E_{fsm}) is lower than in the rest of the semiconductor. Once the equilibrium is reached, all of the Fermi levels (Metal, depletion layer and semiconductor) are aligned. Since the distance from the Fermi level to the vacuum ($Ø_{sm}$) always stay the same, a bending of the different energy levels is observed at the junction between metal and semiconductor (Figure I.8). As the two conduction bands are close to each other, there is no favourable conditions anymore for the electrons to migrate from the semiconductor to the metal (hence the equilibrium state). Additionally, to migrate the electrons need to pass a barrier (eV_0), called the built-in potential, and the electrons that migrate from the metal to the semiconductors also have to overcome the Schottky barrier ($Ø_B$). This type of contact is called a Schottky contact or rectifying contact.[23] Here we only present the case of a semiconductor more electron rich than the metal but a similar process occurs if the

metal is more electron rich. Instead of a depletion layer, an accumulation of electrons occurs at the metal-semiconductor interface.

For the rare cases where the two Fermi levels are matched, there is no bending of the energy level. This type of contact is named an ohmic contact.

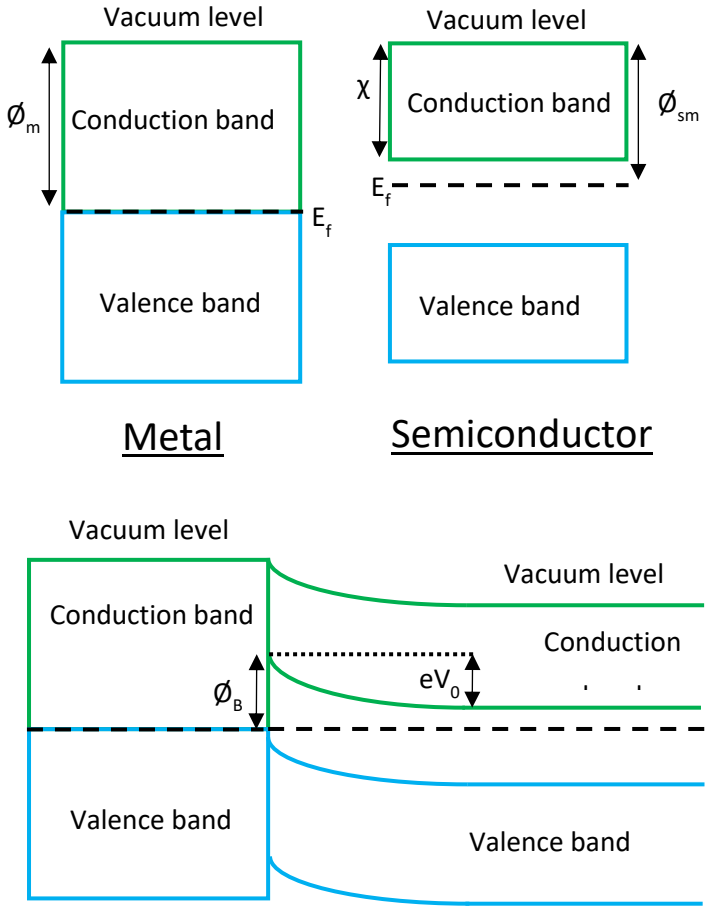

Figure I.8: Metal and semiconductor contact

III. OLED architecture and operation

Organic light emitting diodes exist under numerous architectures. In its simplest form, OLEDs are composed of one emissive material (EM), made of an organic material with π-conjugated bonds, sandwiched between two electrodes (anode and cathode), deposited on a substrate (flexible or rigid). At least one of the electrodes must be transparent.

The most common type of OLED is called bottom emitting. The bottom electrode, which is transparent in this case, is deposited on a transparent substrate,

the EM is deposited on top of it and the top electrode completes the device. Another existing configuration is top emitting. This time the top electrode has to be

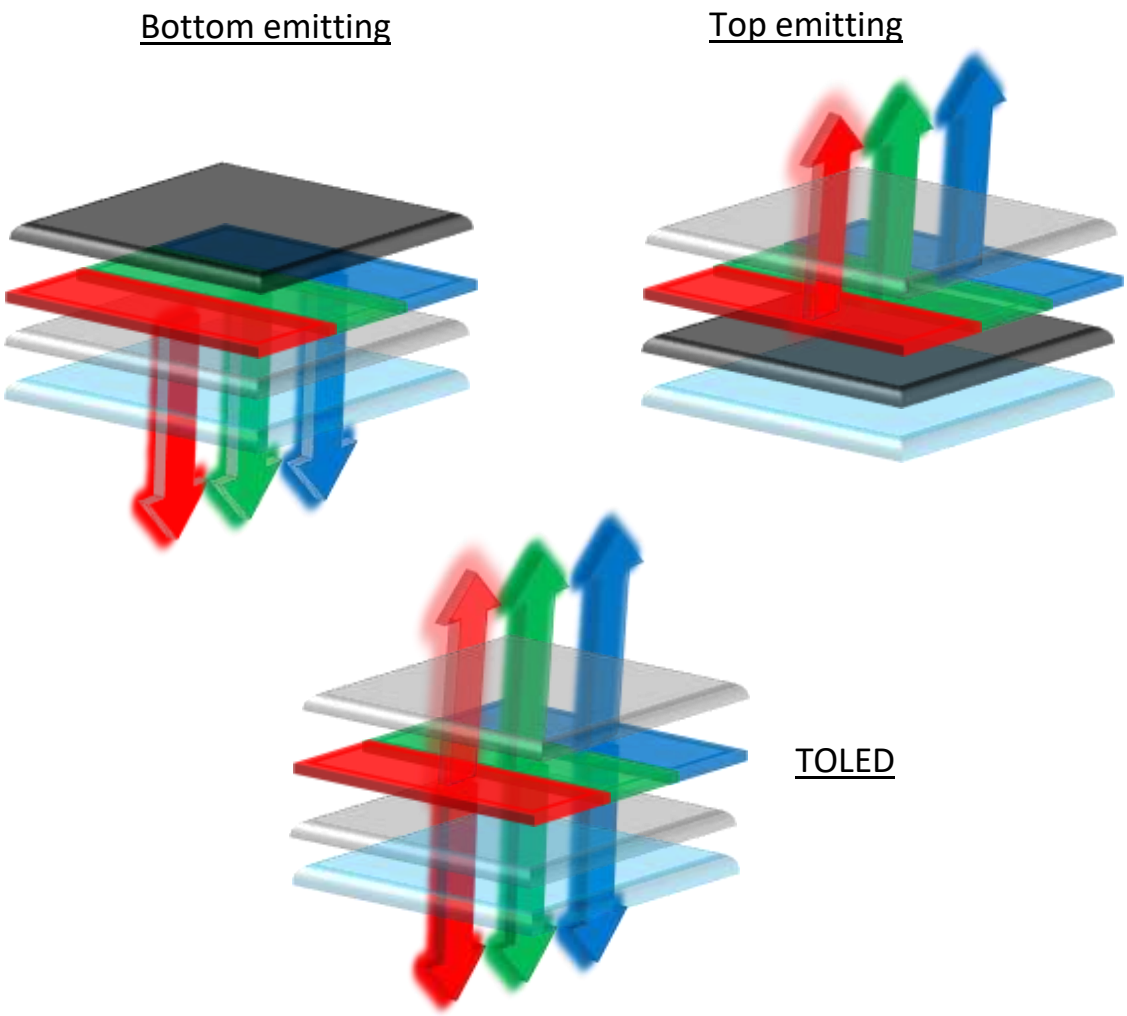

Figure I.9: Different OLED configurations

transparent and the substrate in this case can be opaque. The emission of the light comes from the top of the device. In both cases the non-transparent electrode is reflective.[24] In some cases however, where both electrodes are transparent, the device is called a transparent OLED (TOLED) and the emission comes from both sides, as presented in Figure I.9.

The device is said to be in a conventional architecture when the anode is the bottom electrode and the cathode the top electrode. However, devices can also be

in an inverted architecture, where the cathode is the bottom electrode and the anode is on top.

In order to be efficient the emissive material must satisfy several criteria. Firstly, the material needs to have a balanced hole and electron mobility. If the charges are unbalanced in the emissive material, then an accumulation of one of the carriers occurs which will lead to a reduction in performance. Additionally, the HOMO and LUMO of the EM have to be close to the work function of the anode and cathode respectively, in order to limit the energy barriers. Of course, the EM also must be a good emitter and have a good stability towards heat, oxygen and humidity. As it can be challenging to synthesise a compound with all these qualities, it is very common to have much more complex architecture to improve stability and performance (Figure I.10).

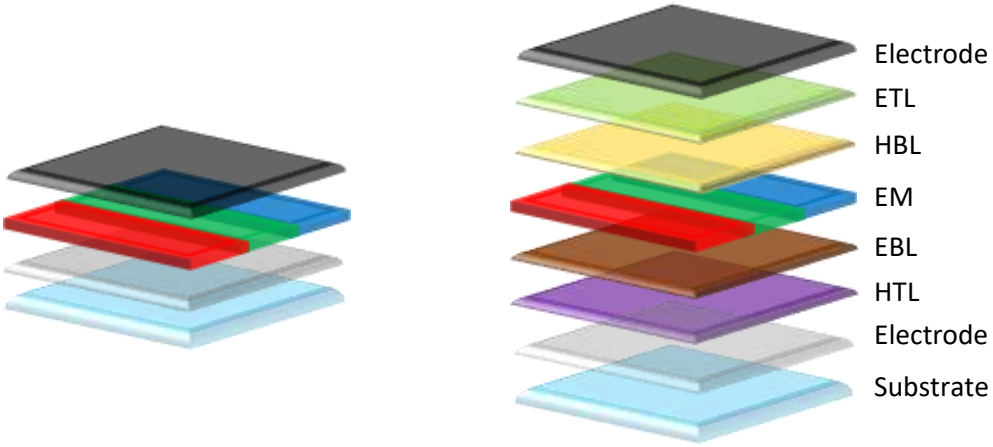

Figure I.10: Complexification of OLED architecture

To improve the hole or electron mobility in the emissive layer, hole transport layers (HTL) and electron transport layers (ETL) can be added between the anode and the EM or between the EM and the cathode, respectively. Another way to improve the efficiency is to increase the probability of recombination in the EM. To achieve this, it is necessary to stop the carriers from going through the EM to the electrode directly. These additional blocking layers are called hole blocking layers (HBL) and electron-blocking layers (EBL). For the HBL, there should be a large electronic energy

gap between the HOMO of the EM and the HOMO of the HBL to prevent hole leakage. Similarly for EBL there should be a large energy gap between the LUMO of the EM and the LUMO of the EBL to prevent electron leakage.[24] The complexity of the architecture varies according to the emissive material used as well as the electrodes. One device can be composed of all these extra layers put together.

Whichever architecture is chosen, all OLEDs work according to the same principle (Figure I.11). When a potential difference between the two electrodes is applied, in such a way that the anode has an electrical potential more positive than the cathode, electrons are injected into the cathode and at the same time on the anode side electrons are extracted from the layer in close contact, leaving electron holes. The electrons and the holes are then transported to the emissive material, where an exciton can be formed. An exciton is defined as a bound state between an electron and a hole. When the exciton relaxes, it will emit light. The colour of the emitted light is dependent on the HOMO-LUMO gap of the emissive material.

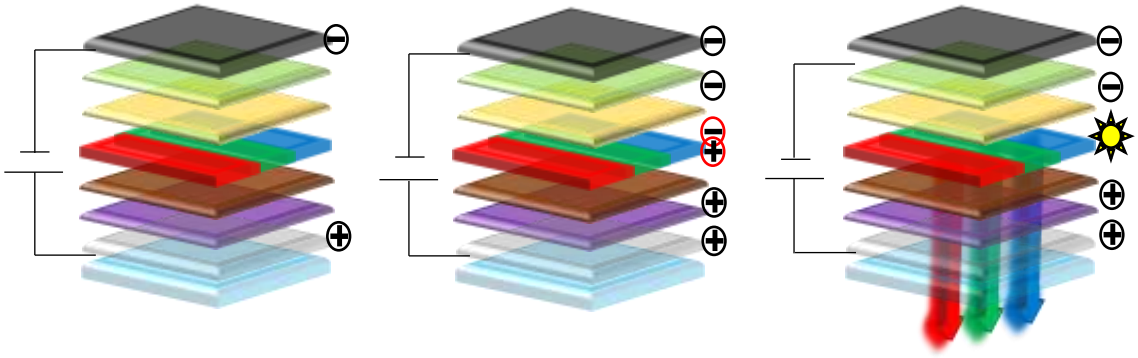

Figure I.11: Scheme of the electroluminescence process in OLED

For the anode, metals with a high work function are usually required as most EM have a HOMO around 5-6 eV. A large variety of these metals exists however since the most common architecture is “bottom emitting” OLEDs, the chosen metal has to also be transparent in the emission region. Indeed, any absorption of the light by the electrode will result in a drop in the device luminance. The most commonly used anode metal is indium tin oxide (ITO).

On the other side, the cathode needs low work function metals (Calcium, Lithium fluoride, Caesium carbonate). Indeed, most emissive layers have a LUMO around 2-3 eV. Calcium or barium are the most commonly used cathode in bottom emitting OLEDs. However, their low work function makes them very sensitive to oxygen degradation. In such cases, an additional metal is usually added on top of the electrode and is used as a protective barrier to prevent such degradation. The most commonly used is aluminium. The latter can also be oxidised, however it has been demonstrated that on a 20 nm layer of pure aluminium the oxidation and formation of aluminium oxide saturate after reaching about 4 nm deep in the layer.[25] The newly formed aluminium oxide is impermeable to further oxygen diffusion. Therefore, the deposition of a thick layer of aluminium (100 nm by example) is sufficient to protect metals such as calcium or barium from oxygen degradation.

IV. Deposition techniques

The deposition technique for OLEDs are categorised in two main processes: “dry” processes, for example thermal evaporation, and “wet” processes, which include any deposition techniques requiring the use of solvents (spin coating, inject printing, blade coating or drop casting).

Widely used in the processing of inorganic semiconductors, vacuum thermal evaporation (VTE) is the most conventional way to deposit organic semiconductors onto a substrate. Powders, pellets or wires of a material are placed into a crucible that is in contact with a conducting wire. In some cases, such as the evaporation of aluminium, the metal can be directly put in contact with the wire. A current is applied to the wire in order to create a resistive heating process. Once the required temperature is reached, the material will start to be evaporated. In order to avoid any collision or reaction with any other particles, all processes occur under high vacuum (10^{-5} to 10^{-6} mbar). In most cases, a “bottom up” geometry is used, where the material is positioned under the substrate. This geometry prevents the spilling of the source material out of the crucible. It also avoids contamination of the substrate

by the dust created through flaking of previously evaporated residual material. The thickness is measured by a thickness monitor positioned near the substrate.

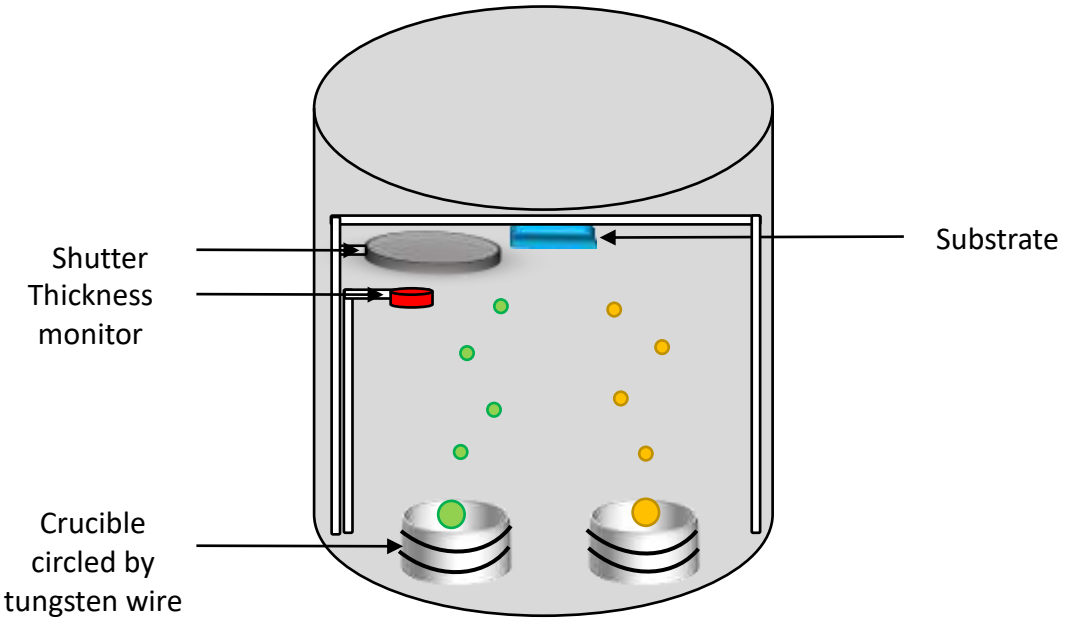

Figure I.12: Scheme of the thermal evaporator used in this thesis

This technique presents the great advantage of very accurate control of the thickness of the deposited layer (precision of the order of a few angstroms) and the deposition of a uniform film. Additionally, by using a shadow mask (fine metal stencil sitting atop the surface) it is possible to deposit the material in an extremely precise location and in an uniform pattern[24]. VTE also offers great flexibility on the design of the electronic device architecture by allowing the deposition of an unlimited number of layers. As it is a "dry-process" (no solvents are used), there is no risk of dissolution of the previously deposited layers.

On the contrary, the first limitation of this technique is the molecular weight of the molecules. Indeed, if VTE is perfectly adapted for small molecules (under 1 000 $g.mol^{-1}$), such as oligomers, fullerenes and phthalocyanines, for higher molecular weight molecules (conjugated polymers), the heating process induces thermal dissociation in the molecules before reaching the evaporation temperature. The molecular weight limitation for VTE can vary according to the molecules but it is usually between 1 000 and 2 000 $g.mol^{-1}$.[26] Another major drawback of VTE is the

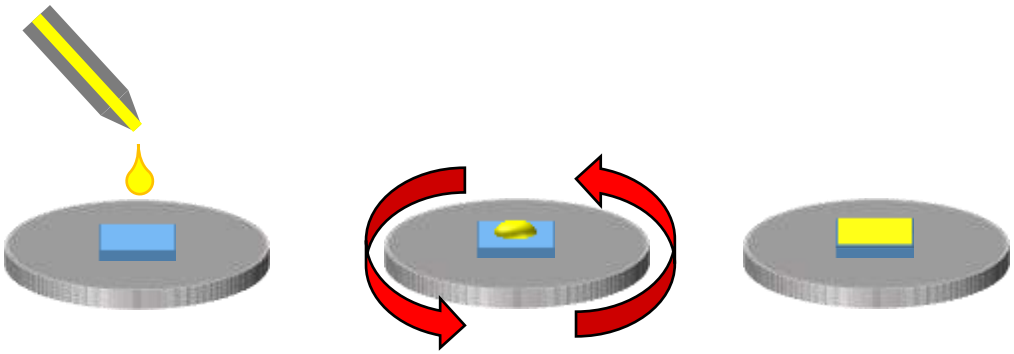

Figure I.13: Illustration of the spin-coating process

waste of material, as 70% to 80%[7] can be lost during the evaporation. Indeed, a large amount of product will cover up the walls of the vacuum chamber or the shadow mask.

Recently there has been a large focus in both academia and industry on the development of "wet" processes, in order to reduce the production cost of OLEDs.

Multiple "wet" processes exist: blade coating, 3D printing, drop casting, spin-coating *etc*. The latter is the main technique used in this work. A Few drops of a solution, containing the desired material, are depositing onto the substrate and the spin-coater undergoes a rapid acceleration until the desired speed. Part of the solution is expelled from the substrate whilst the rest, after solvent evaporation, forms a thin film. This method of deposition is a quick and easy way to obtain thin films of materials. The thickness of the film depends on the interface between the deposited material and the substrate or the under layer, the viscosity of the solution and wettability of the substrate.

Solution processing methods offer the main advantage of being possible under ambient conditions (there is no need to create a vacuum before deposition or use high temperatures) allowing a high-speed deposition over a large area, which drastically reduces the manufacturing cost of the deposition. Other advantages include a reduced loss of material compared to VTE, the possibility to blend one material with another to obtain different properties.

However, with most solution processing methods it is very difficult to fabricate a specific pattern on the device. 3D ink-jet printing is one of the few solution

processing methods that allows an accurate deposition of the material.[24,27] 3D ink-jet printing consists of drawing the same pattern over and over again on the substrate until it forms a solid object using inks made of polymers.[28,29] In essence it works in the same way as an ink-jet printer that prints the same letter repetitively, piling up layers of ink one on top of each other. Nozzles are used in the printer to have an accurate control of the pattern. This process is quite fast as an OLED phone screen can be printed in few seconds.[30] However, ink-jet printing requires additional demands on the material characteristics compared to the common solution processing.

Another disadvantage of "wet" processes is the extreme difficulty to develop complex device architectures. Indeed, the use of solvents to solubilise the material before deposition induces a possibility of damaging the underlying layers. This drawback causes a significant problem for the use of small molecules, which usually require multilayer devices for efficient performance. To resolve this issue it is possible to use crosslinking polymers,[31,32] which become insoluble after treatment allowing for "wet" process deposition without risk. Another way is to change solvent for each layer and make sure it does not damage the under layers (orthogonal processing).[33] A final possibility is to functionalise the molecules or blend them with one another in order to achieve the desired properties.[31] However, this last technique could lead to some compromise where one property will be traded off against another.

V. OLED Materials

A. Emissive layer

The main requirements for OLED emissive materials are high photoluminescence quantum yield in the solid state, balanced charge carrier mobility, good film forming properties, good colour purity and good stability.[24] As the HOMO-LUMO energy gap influences the colour of the light emission, it is important to control its size. Most emissive materials will emit at a wavelength include in the range of the visible spectrum (380 nm – 750 nm or 1.65 – 3.26 eV), however it is possible to find IR and UV emitting OLED materials.[31] In order to obtain efficient

materials, the electronic barrier between the HOMO or LUMO of the material and the electrodes should be minimal. Commonly, the HOMO of the material is around 5-6 eV in order to align with the work function of ITO whereas the LUMO energy is often around 2-3 eV, in order to align well with a low work function metal, such as calcium or magnesium.[24]

The majority of emissive materials can be separated into two groups: small molecules (which also include oligomers) and polymers.[34] Polymers are mainly deposited via "wet" processes, as techniques like VTE are not suitable. Small molecules were initially mainly deposited *via* thermal evaporation, however this trend seems to have changed and "wet" processes are more and more commonly used for small molecules. The latter are usually used in multilayer OLEDs, as they often require electron/hole transport/blocking layer whilst polymers are mostly used in much simpler OLED structures.

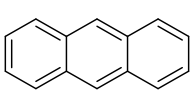

Anthracene

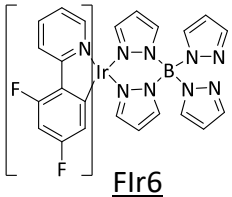

FIr6

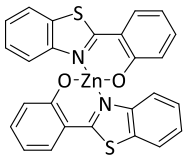

$Zn(BTZ)_2$

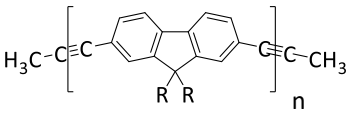

R= $CH_2(CH_2)_{10}CH_3$

Poly[9,9-didodecylfluroenyl-2,7-yleneethylnylene]

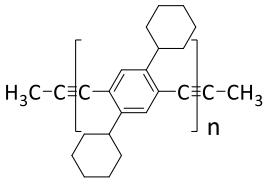

Poly(2,5-dicyclohexylphenylene-1,4-ethynylene)

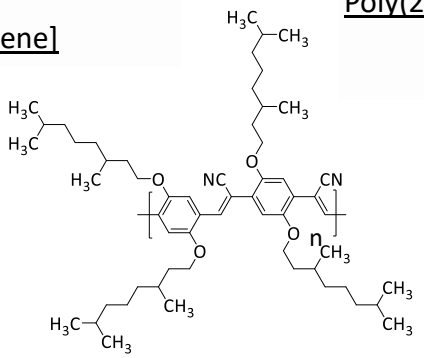

Poly(2,5-di(3,7-dimethyloctyloxy)cyanoterephthalylidene)

Figure I.14: Examples of small molecules and polymers light emitting materials used in OLEDs

In 1990, the first electroluminescent polymer, poly(para-phenylene vinylene), was reported.[35] Ten years later, Professors Alan Heeger, Alan MacDiarmid, and Hideki Shirakawa won the Nobel Prize of chemistry for their research on doped polyacetylene and their ability to conduct electricity.[31] Nowadays, conjugated polymers are mainly used for OLEDs as the delocalized π-electron system of the sp^2 carbons in the main chain can result in high electron and hole mobility.[34] Some examples of polymeric emissive materials are polyarylenes, polyheteroarylenes, polyacetylenes, polyfluorene, poly-p-phenylene and polyphenylenvinylene (PPV). The latter is the most common family of polymers used as yellow-green emitters (and sometimes as red emitters).[31] As mentioned previously, device architectures are becoming increasingly complex, and in this aspect, cross-linked polymers offer interesting properties. Indeed, one of the main challenges is to combine complex OLED architectures with solution processing methods, which requires deposition of multiple layers without dissolving adjacent layers. Cross-linkable polymers can undergo thermal, photonic or chemical treatment to render the layer insoluble after deposition, which allows the deposition of another layer on top of the cross-linked polymer whilst avoiding interlayer mixing.[36,37]

Although small molecules tend to have a lower mobility,[38] they have several advantages over polymers. They usually offer a better batch-to-batch reproducibility, and they can be more easily functionalised and optimised.

OLED emissive materials are also characterised by their emission process. Indeed, after electron excitation from the ground state (S_0) to the excited state (S_1), three types of radiative decay are recognised for OLED emissive materials: fluorescence, phosphorescence and thermally activated delay fluorescence (TADF) (Figure I.15).

Fluorescence results in the emission of light from the direct relaxation of an electron from its excited state (S_1). These materials demonstrate great lifetime, high colour purity of electroluminescence and can usually by manufactured at low cost. However, their efficiency is limited, as triplet excitons are not utilised. Upon

excitation, two types of excitons can be formed: singlet (S_1) and triplet (T_1), the relative probability of formation for each of them is 25% and 75%, respectively.[39,40] In fluorescent molecules, the energetic difference between singlet and triplet state is relatively large and their intersystem crossing (ISC) and reverse intersystem crossing (RISC) are relatively weak. Hence, any transition triplet to singlet or reverse is forbidden and therefore unlikely, thus limiting their internal quantum efficiency to 25%. Probably the most well-known fluorescent material in OLED devices is Alq_3, one of the two components used by Tang and Van Slyke in the first efficient OLED.

On the contrary, phosphorescent materials can emit at an internal quantum efficiency up to 100%. Indeed, if they have a rather large triplet-singlet energy gap, their ISC is very strong. Electrons can then be transferred from S_1 to T_1. Although the transition T_1-S_0 is forbidden, it is still possible. The electron will have to change its spin orientation before relaxation (spin orbit coupling), explaining why phosphorescent material demonstrated longer lifetime. This type of material usually exhibits high efficiency and good luminance. However, most emissive materials are based on metal complexes, such as iridium, copper, platinum or osmium, which, in addition to being more toxic than materials use for fluorescent molecules, also increase the fabrication cost. Furthermore, they can also suffer from triplet-triplet annihilation at high current. A good example of a phosphorescent material is iridium-tris-(2-phenylpyridine) ($Irppy_3$), a highly efficient green emitter.[41]

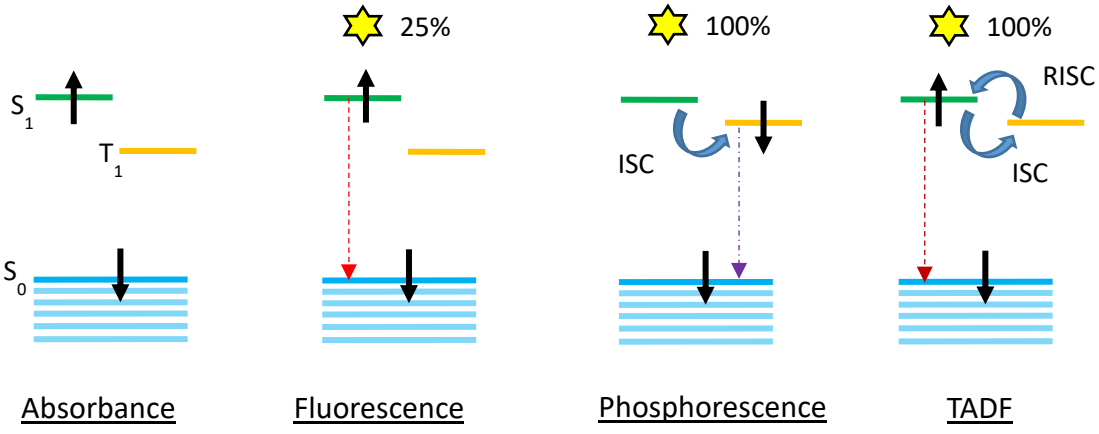

Figure I.15: Electron radiative decay mechanisms

TADF compounds are the latest class of materials studied in OLEDs. Although the process has been known since 1962,[42] the phenomena only started to show potential for OLED materials around 2010.[43] In contrast to the other two mechanisms, TADF materials should have a small T_1-S_1 energy gap. As before, the direct transition of T_1-S_0 is still forbidden, however the small T_1-S_1 energy gap allow electrons to go from the triplet state (T_1) to the excited singlet state (S_1), if the thermal energy is sufficient, through RISC. From S_1, the electrons can relax through a fluorescence mechanism. In theory, TADF materials should be able to utilise 100% of the formed excitons for emission, without any heavy metal involved. However, TADF materials still face major challenges, especially in term of lifetime. A good example of a TADF material is tetrakis-N-carbazoyl-isophthalonitrile (4CzIPN).[44]

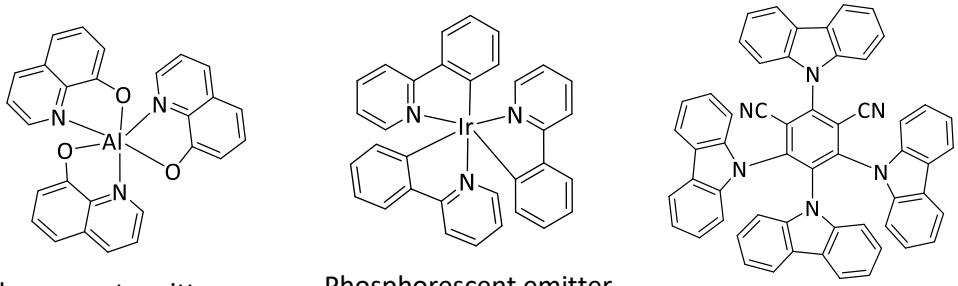

Fluorescent emitter

Alq_3

Phosphorescent emitter

$Irpp_3$

TADF emitter

4CzIPN

Figure I.16: Examples of a fluorescent, a phosphorescent and a TADF light emitters for OLED

B. Charge transporting and blocking layers

One of the major challenges in optimising the emissive layer is to obtain a high and balanced charge transport. In order to improve this, extra-layers are usually used. For example, in their study Rhee *et al.*[45] compared the impact of different electron transport/blocking materials on their device performances. They were able to improve the exciton recombination by simultaneously improving the electron mobility (in this case the emissive material was hole dominant) and the carrier accumulation at the interface emissive layer – electron transport/blocking layer through the addition of an extra-layer.

There are a range of extra-layers commonly used in OLEDs: hole transport layers (HTL), electron transport layers (ETL), hole blocking layers (HBL), electron blocking layers (EBL), hole injection layers (HIL) and electron injection layers (EIL). The transport layers increase the mobility of the charges, while the blocking layers will confine the charges to the desired recombination zone, and the injection layers will usually improve the contact between the electrode and the other organic layer. Figure I.17 present a sample of different extra layers. While some materials will only assume one of these functions, such as TAPC, TCTA or CBP that are exclusively HTL, several materials will combine a few of them. For example, mCP combines hole transport and hole injection properties. A number of ETL will often combine factors such as HBL, for example TPBi, BCP, BPhen or $Bepp_2$. However, the properties of such materials can also be dictated by the other layers present in the OLED (electrodes, emissive layers, other additional layers,…).[46] If TPBi (HOMO at 6.0 eV) is used with Super-Yellow (HOMO around 5.2 eV), it will be a good HBL, as the mismatch between both their HOMO levels is sufficient. However, if it is used with F8BT (HOMO around 5.9 eV), another commercially available emissive material, TPBi would be a poor HBL.

Since every individual material is different from each other and can assume a different function, it is possible to make general observations:

- (i) The materials positioned between the anode and the EM will usually possess a HOMO close to 4-5 eV in order to match the work function of ITO, the most common anode used in OLED. Similarly, the material between the cathode and the EM will have a LUMO around 2-3 eV in order to match with the work function of common electrodes like calcium or barium. Obviously, it is also important to consider the HOMO-LUMO gap of the emissive material as well when designing/choosing an extra-layer material.
- (ii) A high band gap and/or unipolar mobility are usually required to reduce the probability of recombination in the extra-layer.

- (iii) These materials should also be thermally stable to realise a long operational and efficient device even under the joule heating effect.
- (iv) They should be easily processable either by “dry” processes or by “wet” processes.
- (v) An amorphous morphology will avoid light scattering and crystallisation-induced degradation.[7]

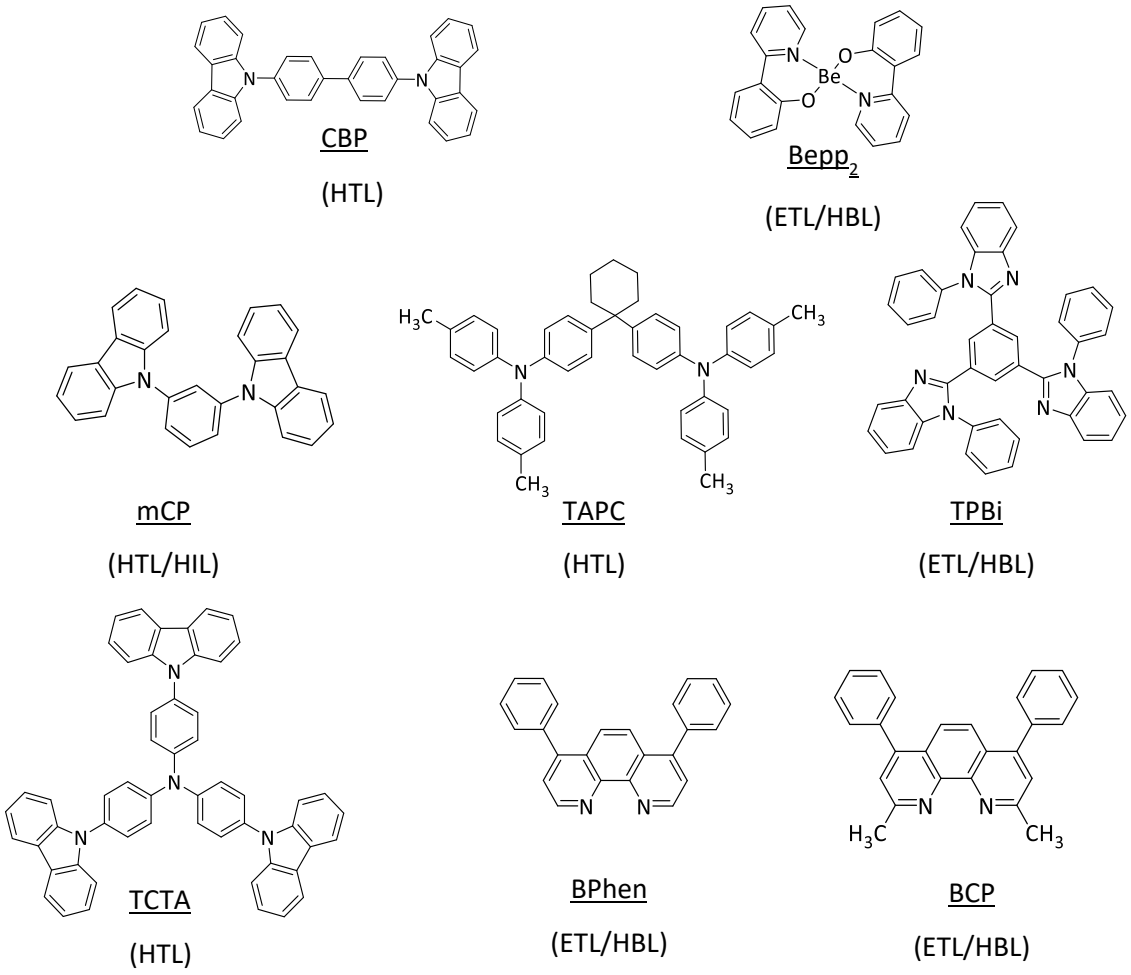

Figure I.17: Molecular structure of charge transport material used in OLED

VI. Bibliography

1 M. Faraday, Fourth Series, *Philos. Trans. R. Soc. London*, 1833, **123**, 507–522.

2 L. Łukasiak and A. Jakubowski, *J. Telecommun. Inf. Technol.*, 2010, **1**, 3–9.

3 A. Bernanose, M. Comte and P. Vouaux, *J. Chim. Phys.*, 1953, **50**, 64–68.

4 W. Helfrich and W. G. Schneider, *Phys. Rev. Lett.*, 1965, **14**, 229–231.

5 C. W. Tang and S. A. Vanslyke, *Appl. Phys. Lett.*, 1987, **51**, 913–915.

6 R. Liu, PhD thesis, Iowa State University, 2012.

7 J.-H. Jou, S. Kumar, A. Agrawal, T.-H. Li and S. Sahoo, *J. Mater. Chem. C*, 2015, **3**, 2974–3002.

8 OLED history: A 'guided tour' of OLED highlights from invention to application | OLED-Info, https://www.oled-info.com/history, (accessed 7 February 2018).

9 R. Mertens, LGD brings a rollable 65" OLED TV to CES 2018 | OLED-Info, https://www.oled-info.com/lgd-brings-rollable-65-oled-tv-ces-2018, (accessed 7 July 2018).

10 J. Kido, K. Hongawa, K. Okuyama and K. Nagai, *Appl. Phys. Lett.*, 1994, **64**, 815–817.

11 E. Taylor-shaw, E. Angioni, N. J. Findlay, B. Breig, A. R. Inigo, J. Bruckbauer, D. J. Wallis, J. Skabara and R. W. Martin, *J. Mater. Chem. C*, 2016, **4**, 11499–11507.

12 N. J. Findlay, J. Bruckbauer, A. R. Inigo, B. Breig, S. Arumugam, D. J. Wallis, R. W. Martin and P. J. Skabara, *Adv. Mater.*, 2014, **26**, 7290–7294.

13 M. Chapran, E. Angioni, N. J. Findlay, B. Breig, V. Cherpak, P. Stakhira, T. Tuttle, D. Volyniuk, J. V Grazulevicius, Y. A. Nastishin, O. D. Lavrentovich and P. J. Skabara, *ACS Appl. Mater. Interfaces*, 2017, **9**, 4750–4757.

14 K. T. Kamtekar, A. P. Monkman and M. R. Bryce, *Adv. Mater.*, 2010, **22**, 572–582.

15 F. So, J. Kido and P. Burrows, *MRS Bull.*, 2008, **33**, 663–669.

16 IKEA launches its first OLED lamp, the Vitsand chandelier | OLED-Info, https://www.oled-info.com/ikea-launches-its-first-oled-lamp-7-panel-

vitsand, (accessed 7 July 2018).

17 Samsung launches the 7.7" Super AMOLED tablet and the 5.3" HD Super AMOLED phone | OLED-Info, https://www.oled-info.com/samsung-launches-77-super-amoled-tablet-and-53-hd-super-amoled-phone, (accessed 7 July 2018).

18 A. H. Wilson, *Proc. R. Soc. A Math. Phys. Eng. Sci.*, 1931, **133**, 458–491.

19 A. H. Wilson, *Proc. R. Soc. A Math. Phys. Eng. Sci.*, 1931, **134**, 277–287.

20 P. Stallinga, in *Electrical Characterization of Organic Electronic Materials and Devices*, John Wiley & Sons, 2009, 1-45.

21 C. Housecroft and A. Sharpe, in *Inorganic Chemistry*, Pearson Ed., 2005, 141–143.

22 H. Naarmann, in *Ullmann's Encyclopedia of Industrial Chemistry*, Wiley-VCH Verlag GmbH & Co. KGaA, Weinheim, Germany, 2000, 295–311.

23 B. J. Baliga, in *Fundamentals of Power Semiconductor Devices*, Springer US, Boston, MA, 2008, 167-201.

24 B. Geffroy, P. le Roy and C. Prat, *Polym. Int.*, 2006, **55**, 572–582.

25 T. Campbell, R. K. Kalia, A. Nakano, P. Vashishta, S. Ogata and S. Rodgers, *Phys. Rev. Lett.*, 1999, **82**, 4866–4869.

26 P. Kovacik, PhD thesis, University of Oxford, 2012.

27 S. Xia, K.-O. Cheon, J. J. Brooks, M. Rothman, T. Ngo, P. Hett, R. C. Kwong, M. Inbasekaran, J. J. Brown, T. Sonoyama, M. Ito, S. Seki and S. Miyashita, *J. Soc. Inf. Disp.*, 2009, **17**, 167–172.

28 A. Islam, M. Rabbani, M. H. Bappy, M. A. R. Miah and N. Sakib, in A review on fabrication process of organic light emitting diodes, *2013 Int. Conf. Informatics, Electron. Vis.*, 2013, 1–5.

29 T. Sonoyama, J. Brooks, S. I. D. Member, K. Cheon, M. Inbasekaran, J. J. Brown and S. I. D. Member, *J. Soc. Inf. Disp.*, 2008, **16**, 1229–1236.

30 S. R. Forrest, *Nature*, 2004, **428**, 911–918.

31 A. C. Grimsdale, K. Leok Chan, R. E. Martin, P. G. Jokisz and A. B. Holmes, *Chem.*

Rev., 2009, **109**, 897–1091.

32 O. Nuyken, S. Jungermann, V. Wiederhirn, E. Bacher and K. Meerholz, 2006, **824**, 811–824.

33 A. R. Brown, N. C. Greenham, J. H. Burroughes, D. D. C. Bradley, R. H. Friend, P. L. Burn, A. Kraft and A. B. Holmes, *Chem. Phys. Lett.*, 1992, **200**, 46–54.

34 C. Sekine, Y. Tsubata, T. Yamada, M. Kitano and S. Doi, *Sci. Technol. Adv. Mater.*, 2014, **15**, 1-15.

35 J. H. Burroughes, D. D. C. Bradley, A. R. Brown, R. N. Marks, K. Mackay, R. H. Friend, P. L. Burns and A. B. Holmes, *Nature*, 1990, **347**, 539–541.

36 M. C. Gather, A. Köhnen, A. Falcou, H. Becker and K. Meerholz, *Adv. Funct. Mater.*, 2007, **17**, 191–200.

37 C. A. Zuniga, S. Barlow and S. R. Marder, *Chem. Mater.*, 2011, **23**, 658–681.

38 S. Forrest, P. Burrows and M. Thompson, *IEEE Spectr.*, 2000, **37**, 29–34.

39 R. H. Friend, R. W. Gymer, A. B. Holmes, J. H. Burroughes, R. N. Marks, C. Taliani, D. D. C. Bradley, D. A. Dos Santos, J. L. Brédas, M. Lögdlund and W. R. Salaneck, *Nature*, 1999, **397**, 121–128.

40 L. J. Rothberg and A. J. Lovinger, *J. Mater. Res.*, 1996, **11**, 3174–3187.

41 M. A. Baldo, S. Lamansky, P. E. Burrows, M. E. Thompson and S. R. Forrest, *Appl. Phys. Lett.*, 1999, **75**, 4–6.

42 C. A. Parker and C. G. Hatchard, *J. Phys. Chem.*, 1962, **66**, 2506–2511.

43 D. Volz, *J. Photonics Energy*, 2016, **6**, 1-13.

44 J. W. Sun, J.-H. Lee, C.-K. Moon, K.-H. Kim, H. Shin and J.-J. Kim, *Adv. Mater.*, 2014, **26**, 5684–5688.

45 S. H. Rhee, K. B. Nam, C. S. Kim, M. Song, W. Cho, S.-H. Jin and S. Y. Ryu, *ECS Solid State Lett.*, 2014, **3**, 19–22.

46 A. P. Kulkarni, C. J. Tonzola, A. Babel and S. A. Jenekhe, *Chem. Mater.*, 2004, **16**, 4556–4573.

Chapter II: OLED optimisation and influencing factors

I. Introduction

Once freshly synthesised and purified, the OLED performance of a new emissive material can be studied. First, the new emitter is placed in a simple device architecture in order to register its basic performance. Then, one-by-one, different parameters for this material (e.g., concentration, temperature, rate of deposition for spin-coating) are varied and the impact of each on the device performance recorded. During this phase of optimisation, the device architecture will generally evolve too.

The main interest for this study is to examine different parameters and understand their impact on device performance. For that a well-known commercial material, PDY-132, also known as Super-Yellow (sold by Merck), was used as an emissive material. Figure II.1 presents the molecular structure of Super-Yellow (SY).

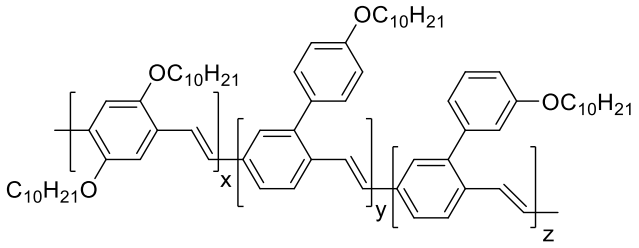

Figure II.1: Molecular structure of Super-Yellow.

SY is a member of the poly(para-phenylene vinylene) (PPV) polymer family. PPV was the first polymer used as a light emitting polymer in OLED.[1] However, when unsubstituted this polymer is insoluble and therefore not suitable for deposition by solution process. Super-Yellow possesses multiple substituents that provide good solubility in common solvents, such as chloroform or toluene. It presents a broad green-yellow emission spectrum. Although SY was extensively studied in recent years,[2-19] its reported performances varied extensively. For example, the current efficiency of the devices made with Super-Yellow can go from 0.5 cd/A[6] to 27 cd/A[14] according to the chosen active layer parameters and/or to the device architecture.

However, Merck reports the maximum current efficiency for its material at 11 cd/A in a simple architecture (ITO/PEDOT:PSS/SY/Ba/Al).[20]

II. Photoluminescence

To measure the photoluminescence quantum yield (PLQY) of a material, a monochromatic laser beam is passed through the material and the ratio between the total emitted photons to the total absorbed photons is measured. Such measurements are extremely useful for emissive materials as it indicates the potential efficiency of a compound. For example, Taylor-Shaw *et al.*[21] explained the large difference of luminous efficacy between their $(TPA\text{-}Flu)_2BT$ (40 lm/W) and their $(TPA\text{-}Flu)_2BTBT$ (10 lm/W) through comparison of their PLQY values (61% and 17%, respectively). PLQY is a measurement not useful in OLED materials but also for organic down converters[22] and organic lasing materials[23].

In 1997, J.C de Mello *et al.*[24] demonstrated a method allowing the PLQY measurement of any material irrespective of how the sample was prepared (powder, thin film or solution). This technique requires inducing photoluminescence *via* a monochromatic laser beam while the material is placed in an integrating sphere. The resulting light emission is measured with a CCD spectrometer linked to the sphere by an optical fibre. The laser beam wavelength is chosen to match the maximum absorbance wavelength of the emissive material. A thin film of Super-Yellow has a maximum absorbance at 444 nm.

Three measurements are necessary and are represented in Figure II.2. In the first experiment (experiment a) the integrating sphere is empty, the laser beam hits the back of the sphere directly, and the laser light is the only light detected by the spectrometer. For the other two experiments (experiments b and c), a sample is placed inside the integrating sphere. The solution sample consists of Super-Yellow dissolved in toluene (5 mg/ml). For the powder sample, the material is sandwiched between two glass slides. For the thin film sample, the emitting material is deposited by spin-coating (5 mg/ml solution in toluene at 800 rpm for 60 s) on a glass substrate.

In the second experiment (experiment b), the sample is placed in the integrating sphere in a way that it does not enter in direct contact with the laser beam. Finally, in experiment (c) the laser beam is directed on to the sample. Typically, the sample is positioned at a certain angle (around 70° to 90°) compared to the laser beam in order to avoid the reflective light escaping the sphere through the laser entrance hole. For each experiment, an emission spectrum from 300 to 800 nm is registered.

In experiment c, the absorbed light is composed of two variables. A fraction *A*, which is the laser beam light directly absorbed by the material, and a fraction α, which corresponds to the initially non-absorbed light which is scattered on the wall of the sphere and subsequently absorbed by the material. The fraction A can be measured in experiment b. Therefore, A is equal to:

$$A = (1 - \frac{Lc}{Lb})$$

With L the area under the laser profile curve of the corresponding experiment (b or c). It is proportional to the amount of unabsorbed light.

The PLQY, which is equal to the number of photons emitted divided by the number of photons absorbed, was demonstrated to be equal to:

$$PLQY = \frac{Pc \ - \ (1 - A) \ \times \ Pb}{La \ \times \ A}$$

With P the area under the emission curve of the corresponding experiment (b or c). It is proportional to the amount of emitted light.

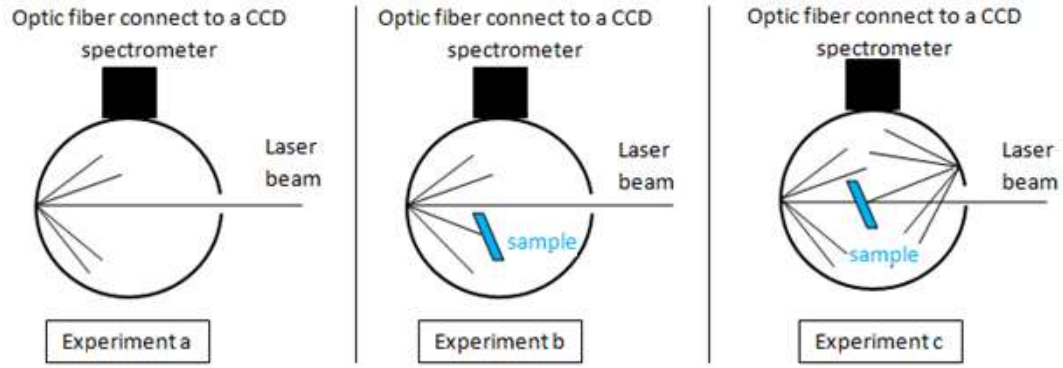

Figure II.2: Diagram representing the three experiments necessary for PLQY measurement

The measured PLQY values for Super-Yellow in the solid state and the solution state are shown in Table II.1.

Table II.1: PLQY values for Super-Yellow

	PLQY measured	PLQY (Literature[25])
Powder	26.2%	X
Solution	58.9%	69% ± 3%
Thin Film	12.7%	17% ± 1%

In the solution state, a PLQY of 58.9% was measured, while this value is reduced to 26.2% (powder) and 12.7% (thin film) in the solid state. This phenomenon is often observed for different materials[26] and it is usually credited to the formation of less emissive aggregates in the solid state.[27] The formation of aggregates leads to an increase in interactions between the polymer chains resulting in a quenching of the fluorescence.[28] The latter phenomenon is clearly visible on Figure II.3 (left), where the fluorescence in solution is a few order of magnitude higher than in solid state.

Our results are generally lower than the one present by Snedden *et al.*[25] This difference between the values we measured and the literature ones are explained by the different sample preparations. By example, they used a solution at 3 mg/ml in ρ-xylene where we used a solution at 5 mg/ml in toluene. The larger difference observed in solution is also due to their use of comparative method for measurement when we use an absolute method. Overall, the values from literature and ours are different quantitatively, but they do follow a similar trend and the same aggregates induced fluorescence quenching is observed in both set of results.

The normalised intensity spectra show a bathochromic shift from solution to powder, the thin film spectrum offering an intermediate shift. This type of shift is often observed and is usually attributed to a more intense packing in crushed powder state compare to solution.

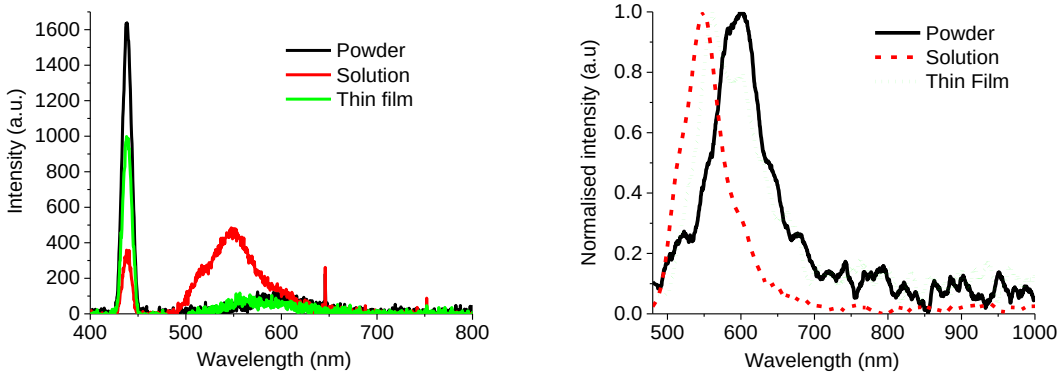

Figure II.3: Excitation and emission spectra obtained from PLQY measurement for SY (left). Normalised intensity spectra of the SY fluorescence (Right).

III. Active layer optimisation

A. Thickness and solution concentration

The characteristics of OLEDs are directly influenced by the thickness of their emissive layers.[29] Indeed, with a very thin layer a higher current is expected, usually due to a lower overall ohmic resistance. These two parameters (lower resistance and higher current) will lead to a lower turn on voltage but will also make the devices more sensitive to degradation. A thin layer is also more susceptible to pinholes, which can provide a parasitic current pathway through an anode-cathode contact. On the other hand, a thicker layer will not have this issue of pinholes but will have a higher overall resistance resulting in less current passing through and therefore limiting the luminance.[30]

This explains the importance of finding the optimum thickness in the early stage of device optimisation and finding the balance between a thin enough layer to have high current and a thick enough layer to avoid pinholes and deterioration of the device. As the emissive layer in this work is solution processed, the easiest way to alter the thickness is to vary the concentration of the solution while keeping the same spin-coating parameters.[31]

A simple conventional architecture was chosen for these first devices. ITO/PEDOT:PSS/SY/Ca/Al. PEDOT:PSS was chosen for its good performance as a hole

transport layer, but also because it provides a smoother surface than ITO and hence a better contact with the organic emissive layer. Toluene was used as a solvent for the Super-Yellow solution preparations. It is worth noting that solutions prepared with a concentration of over 6 mg/ml were too viscous to be deposited properly by spin-coating. The different specifications for the fabrication and the details of the thickness measurements by AFM can be found in the experimental (chapter VI). The results are shown in Table II.2. The values presented on this table, as well as the next ones, are an average over 6 to 8 measurements.

The optimum thickness for our devices is 100 nm, formed when deposited from a 5 mg/ml solution. The maximum current efficiency obtained is 8.10 cd/A at 3 000 cd/m^2 (7.5 cd/A at 10 000 cd/m^2) with a maximum luminance of 59 266 cd/m^2 at 10.5 V and a turn on voltage of 2.5 V.

Table II.2: Impact of SY emissive layer thickness on OLED performance

Concentration (mg/ml)	Thickness (nm)	Current efficiency (cd/A)[a]	Maximum Luminance (cd/m^2)[a]	Turn on voltage (V)[b]
4	80	5.25 (4.4)	46 866 (7.6)	2.3
5	100	8.10 (6.2)	59 266 (10.5)	2.5
6	115	4.58 (9.3)	1 246 (12)	3.2

[a] *values in parentheses indicate the operating voltage at which values were recorded (in Volts);* [b] recorded at a luminance of 1 cd/m^2

The impact of concentration on layer thickness is clearly visible in Figure II.4. As mentioned earlier, an increase in the thickness of the layer will have the main effect of reducing the current flow *via* an increased resistance. The change in resistance is visible through the operating voltage and the turn on voltage. Both of these values are rising with increased thickness, proof of a higher barrier for the current to pass to obtain the optimum performance. Soon after reaching the optimum performance, the devices with the 80 nm active layer were short-circuiting. This phenomenon was not observed for the other two thicknesses. Therefore, we can

make the hypothesis that the higher current passing through the material causes degradation of the active layer. In this case, the increased resistance is beneficial to the device. However, at thicknesses over 100 nm the current flow becomes so low that the luminance is drastically reduced.

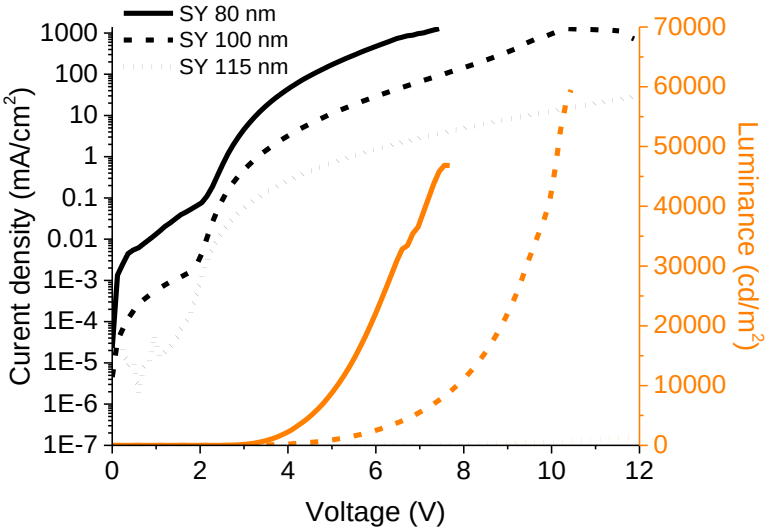

Figure II.4: Current density and luminance versus voltage for SY at different thickness

B. Annealing

Annealing consists of heating the active layer, usually on a hot plate, after its deposition.[32] Annealing can be used for multiple reasons, although the two principal reasons are to remove residual traces of solvent after spin-coating (notably for water-based molecules like PEDOT:PSS) and to change the morphology or organisation of the polymers and/or small molecules. By example, to induce crosslinking of polymers to make them insoluble and favour the deposition of subsequent layers on top by solution processing.[9]

The same device architecture as the previous study was used with a SY concentration of 5 mg/ml. The annealing temperatures were 60°C, 80°C, 100°C and 120°C. The films were annealed for 20 min on a hot plate, inside the glove box, and then cooled down to room temperature before the cathode deposition.

Out of the different parameters presented here, the current efficiency is the most affected by the changes of temperature. Indeed, for each increase of 20°C the efficiency is reduced by 0.1 cd/A, except at 120°C where the reduction is of 0.3 cd/A. Initially, the luminance also decrease, however for any temperatures over 60°C, it seems to stabilise around 57 200 cd/m^2, thus a total loss of luminance of only 3%. The relatively low variations observed in this study could come from small thermal degradations of the emissive layer.[33]

However, the stability of the turn on voltage and the relative stability of the operating voltage suggest that no important morphological changes happened upon annealing. This hypothesis is in agreement with the AFM measurement made on different SY annealed thin films by Burns *et al*.[33], where they demonstrated that the roughness of the film is barely impacted by the increase of temperature and the RMS roughness remains in the range of 0.5 to 1.0 nm.

Therefore, with a loss of only 3% of its luminance and no important morphological changes observed, Super-Yellow can be considered as a relatively stable material under heating. Besides the higher performances exhibit without any annealing means that the optimum configuration for future devices does not require any annealing of the active layer after deposition, which is a positive point as it limits the number of fabrications steps.

Table II.3: Annealing study on SY OLED

Annealing temperature (°C)	Current efficiency (cd/A)[a]	Luminance (cd/m^2)[a]	Turn on voltage (V)[b]
No annealing	8.10 (5.4)	59 173 (9.3)	2.4
60	7.94 (5.5)	56 120 (9.2)	2.4
80	7.81 (5.5)	57 213 (9.6)	2.4
100	7.76 (5.6)	57 200 (9.3)	2.4
120	7.47 (5.4)	57 240 (9.3)	2.4

[a] *In brackets the operating voltage at which values were recorded (in Volts);* [b] recorded for a luminance of 1cd/m^2

C. Spin-speed

Spin-speed can have an important impact on the spin-coated thin film. The rotational speed set up for the deposition will affect the degree of centrifugal force applied to the material. This force is one of the factors, alongside the solvent volatility, that will decide the solvent evaporation rate[34] and afford significant morphological changes. For example, in their study, DeLongchamp *et al.*[35] demonstrated the impact of spin-speed on the orientation of P3HT when spin-coated. The polymer passed from an edge on to a plane on orientation when the spin-speed is higher than 1 000 rpm. A faster solvent evaporation rate pushed the polymers toward a less equilibrated structure. The morphological changes however where not visible on AFM pictures and were attributed to microstructural changes.

It was shown earlier that the solution concentration could have a huge impact on the device performance. Since the solvent evaporation rate will increase with increased spin-speed, the viscosity of the film will too. Therefore changing the spin-speed can also have an effect on the film thickness.[36–38]

Since spin-speed affected two parameters at once, it is more difficult to determine with accuracy which one is influencing device performance.

In this study, the spin-speed was varied by steps of 200 rpm. The other parameters (solution concentration and annealing), as well as the device architecture, were kept the same. The results are shown in Table II.4.

Table II.4: Spin-speed study on SY OLED

Spin-speed (rpm)	Current efficiency (cd/A)[a]	Luminance (cd/m^2)[a]	Turn on voltage (V)[b]
800	8.11 (6.1)	59 123 (10.6)	2.5
1 000	8.53 (5.5)	63 374 (9.6)	2.4
1 200	8.98 (5.1)	65 282 (9.8)	2.4
1 400	9.40 (5.2)	66 456 (9.7)	2.3
1 600	7.67 (6.1)	59 586 (10.1)	2.6
1 800	7.35 (6.1)	57 017 (9.8)	2.6

[a] *In brackets the operating voltage at which values were recorded (in Volts);* [b] recorded for a luminance of 1 cd/m^2

A variation in the spin-speed show a significant influence on the device performance with a 1.3 cd/A increase at the optimum speed compared to the reference. The optimum spin-speed, with a Super-Yellow solution concentration of 5 mg/ml, for our devices is 1 400 rpm. The maximum current efficiency obtain is 9.40 cd/A at 2 234 cd/m^2 (8.4 cd/A at 10 000 cd/m^2) with a maximum luminance of 66 456 cd/m^2 at 9.7 V and a 2.3 V turn on voltage. Increasing the spin-speed leads to improved current efficiency but also contributes to a slight increase in the maximum luminance.

The Super-Yellow thickness at two different spin-speeds (800 and 1 400 rpm) was studied to judge the impact of changing the spin-speed. At 800 rpm the film was 100 nm thick, while when spun at 1 400 rpm it was only measured at 80 nm. The increase in spin-speed leads to more solution spinning off the substrates edges, which result in a thinner film. Earlier, a 4 mg/ml solution was also measured at 80 nm thick. However, its OLEDs performances were lower. Increasing the spin-speed, did not just reduced the thickness but also spread the active layer more uniformly.[39] As a result, the recombination process can happened more effectively, since more charges are transported to the recombination zone. Therefore, despites similar thickness the device spin-cast at 1 400 rpm exhibit better performances thanks to a better repartition of the material on PEDOT:PSS.

IV. Device architecture

A. Inverted architecture

In the large amount of research carried out on Super-Yellow, a number of studies[11,14,19] report the use of an inverted architecture in order to obtain improved performance.

In an inverted architecture OLED, ITO becomes the electron donating electrode. However, this can be problematic as it is necessary to lower the ITO work function before the deposition of the emissive material. Indeed, without doing this, a large energy barrier will separate the ITO work function (4.7 eV) and the LUMO of

the emissive material (around 2.7 eV for Super-Yellow), resulting in inefficient devices. One way to overcome this problem is to use modification layers.

The combination of Zinc oxide (ZnO) and polyethyleneimine (PEI) are well known modification layers in organic electronics.[11,40–45] ZnO is largely used in organic electronics thanks to its good electron transport properties, air stability and because as a film it is transparent to visible light.[11] The deposition of ZnO is performed according to the method developed by Bruyn *et al.*.[46] Hence, zinc acetylacetonate hydrate ($Zn(acac)_2$, Sigma-Aldrich) was dissolved in ethanol (20 mg/mL concentration) and stirred for 24 h at 50 °C. Next, the solution was filtered through a 0.2 µm polytetrafluoroethylene (PTFE) filter, to remove precursor aggregates. The solution was then spin-coated on top of ITO at 2 000 rpm for 45 seconds before being annealed at 120°C for 30 seconds in ambient conditions. This thin layer of zinc oxide can reduce the work function of ITO by up to 0.6 - 1 eV.[41,42] However, a work function between 4.1 and 3.7 eV is still too high for SY material. Additionally, Sungho Woo *et al.*[41] demonstrated that the roughness of zinc oxide could decrease the performance of the device. Therefore, a second surface modification layer is usually deposited on top of the metal oxide.

Commonly polyethyleneimine (PEI) is used to further reduce the electrode work function and allow a better contact with the emissive layer. With electron affinity and ionization potential energy values of 0.3 eV and 6.5 eV respectively (band gap of 6.2 eV), PEI should act as an insulating layer.[47] However, it was demonstrated that the amine groups in the PEI backbone can protonate and adsorb on to the underlying surface, resulting in the formation of an interfacial dipole. This dipole induces a vacuum level shift leading to a reduction of the work function of the electrode.[42,48,49] Zhou *et al.*[47] describes a simple way to make and depose PEI on ZnO. The PEI is dissolved in 2-methoxyethanol solution (Sigma-Aldrich) before being spin-coated, on top of ZnO, at 5 000 rpm for 50s. The samples are then annealed at 100°C for 10 min and then rinsed with 2-methoxyethanol to remove any PEI surplus.

On top of their properties to reduce the work function and act as an electron transport layer, the combination of these two layers has demonstrated an increased stability to ambient air and a good thermal stability (up to 150-190°C)[47] compared to conventional architecture devices and electrodes made with calcium.

On top of the active material, a layer made of molybdenum trioxide is deposited to act as a hole transport layer and help the contact with the top electrode (100 nm of aluminium). The architecture of these devices is therefore ITO/ZnO/PEI/SY/MoO_3/Al, as shown in Figure II.5.

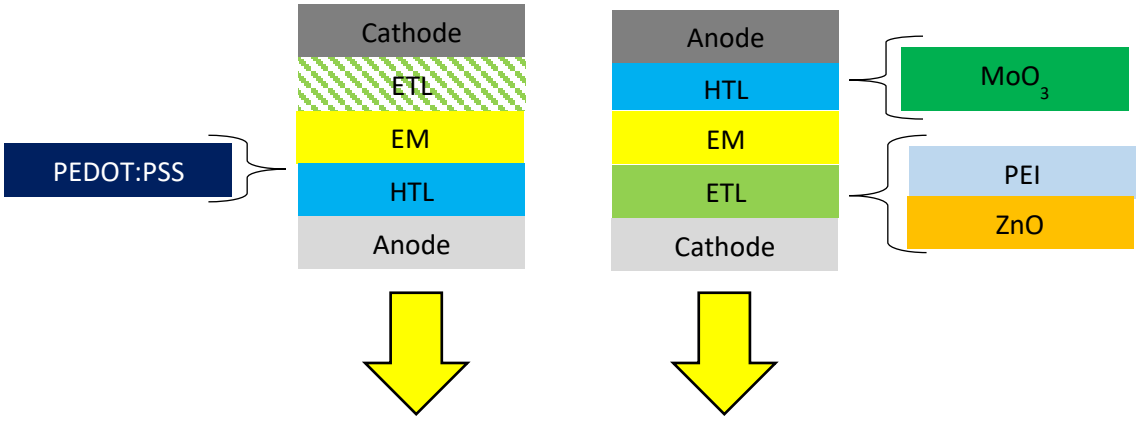

Figure II.5: Conventional and inverted OLED architecture

B. Molybdenum trioxide

The addition of a HTL between the active layer and the electrode is important. Indeed, the devices without a HTL demonstrated lower performances when compare to devices with a HTL.[50] If the most popular HTL in a conventional OLED is PEDOT:PSS, in an inverted architecture its low wettability leads to a poor morphology when deposited on top of an active layer. Therefore, other HTLs are investigated.

Metal oxides, such as molybdenum-oxide (MoO_3), vanadium- oxide (V_2O_5) and tungsten-oxide (WO_3), offer a great alternative to PEDOT:PSS. MoO_3 has been studied due to its easy thermal deposition, low contamination and intrinsic stability, as well as its work function matching the HOMO of a majority of organic emissive materials (5.3 eV).[51–53] The large number of studies featuring MoO_3 is also due to its versatility. Indeed, it is used in OLEDs as well as in OPVs, in conventional architecture (sometimes

mixed with PEDOT:PSS)[12,5412,54] or in an inverted architecture. Additionally, molybdenum oxide offers the possibility to be solution processed[55] *via* precursor materials, but this will be discussed later in this chapter. Often, the addition of molybdenum oxide between the electrode and the active layer has been proven to reduce the operating voltage, as well as improve the device efficiency and lifetime.[52,56]

Since the HTL is thermally evaporated, the control over its thickness is straightforward and precise. Thicknesses of 5, 10 and 20 nm were studied. The results are shown in Table II.5.

Table II.5: MoO_3 thickness impact on the OLED performances

Type of Architecture	MoO_3 Thickness (nm)	Current efficiency (cd/A)[a]	Luminance (cd/m^2)[a]	Turn on voltage (V)[b]
Conventional	X	9.40 (5.2)	66 456 (9.7)	2.3
Inverted	5	9.20 (7.0)	45 506 (11)	3.4
	10	9.51 (7.2)	38 054 (11)	3.3
	20	7.02 (9.8)	30 379 (12)	4.3

[a]*In brackets the operating voltage at which values were recorded (in Volts);* [b] recorded for a luminance of 1 cd/m^2

The devices with a HTL of 5 nm exhibit the highest luminance with a value of 45 506 cd/m^2. However, devices with a 10 nm layer of molybdenum trioxide exhibit a better current efficiency of 9.51 cd/A compared to 9.20 cd/A with a thickness of 5 nm. If the devices with a 5 nm HTL present a lower current efficiency, despites a higher luminance, it is because of a higher current flowing through the device.

When the thickness of the layer is further increased, the luminance is reduced and so is the current efficiency. The turn on voltage, which previously remained around 3.4 V, increased to 4.3 V. Consequently, a thickness over 10 nm is harmful to the devices performances.

The higher turn on voltage and operating voltage indicates a less favourable charge injection into the active layer, which can be expected as the device architecture was complicated. Furthermore, the addition of layers at the electron injection to lower down the ITO work function also implied an increased number of electronic barriers and a poorer energy level arrangement, inevitably slowing down the electron injection.

The similar current efficiency obtained with the inverted architecture and the conventional one testify of a maintained recombination rate, despites of the luminance drop. It is not the first time that the latter phenomenon is observed. Indeed, Hofle *et al.*[19] experienced a luminance reduction from 8 600 to 5 900 cd/m^2 in their devices when passing from a conventional to an inverted architecture, however, no explanation was given for this luminance drop. Such an occurrence usually symbolised that a fewer number of charges are able to reach the active layer. The reasons for this however can be numerous (morphology, charges mobilities, an increased number of energy level mismatch…) and a deeper study should be carried out to narrow it.

C. Molybdenum bronzes

The inverted architecture OLEDs, presented earlier, showed similar results compare to conventional OLEDs, however they require the deposition of molybdenum via thermal evaporation. In the longer term it may be important to find an alternative to the thermally evaporated MoO_3 layer. As spin-coating PEDOT:PSS on top of an organic layer is challenging, an alternative can be a solution processed molybdenum layer.

Solution processable molybdenum oxide has been intensively studied over the past years. Fu *et al.*[51] and Zhang *et al.*[57] both presented OLEDs with solution-processable molybdenum oxide but both used a significant amount of acid solution (hydrogen peroxide or acetic acid). This excess acid can be harmful for the device and damage the underlying layers. Additionally, most of these techniques require high temperature annealing after deposition, which is not compatible with most emissive

materials. However, Li *et al.*[58,59] and Soultati *et al.*[60] demonstrated the potential of molybdenum bronze (HMoOx) in organic electronics.

The formulation of the molybdenum bronze is straightforward. Pure molybdenum powder (0.2 g, Sigma-Aldrich) is first dispersed in ethanol (20 ml) by ultrasonication followed by the addition of, a small amount of 30% (w/w) hydrogen peroxide (0.7 ml). Ethanol is used to control the oxidation rate of molybdenum by hydrogen peroxide. The solution is left stirring for 20 hours. Next, the solution changes from grey to dark blue, which is attributed to H^+ insertion into the metal oxide lattice and then the reduction of a metal element (Mo^{6+}) to lower oxidation states (Mo^{5+}, Mo^{4+}), forming hydrogen molybdenum bronzes (HMoOx).

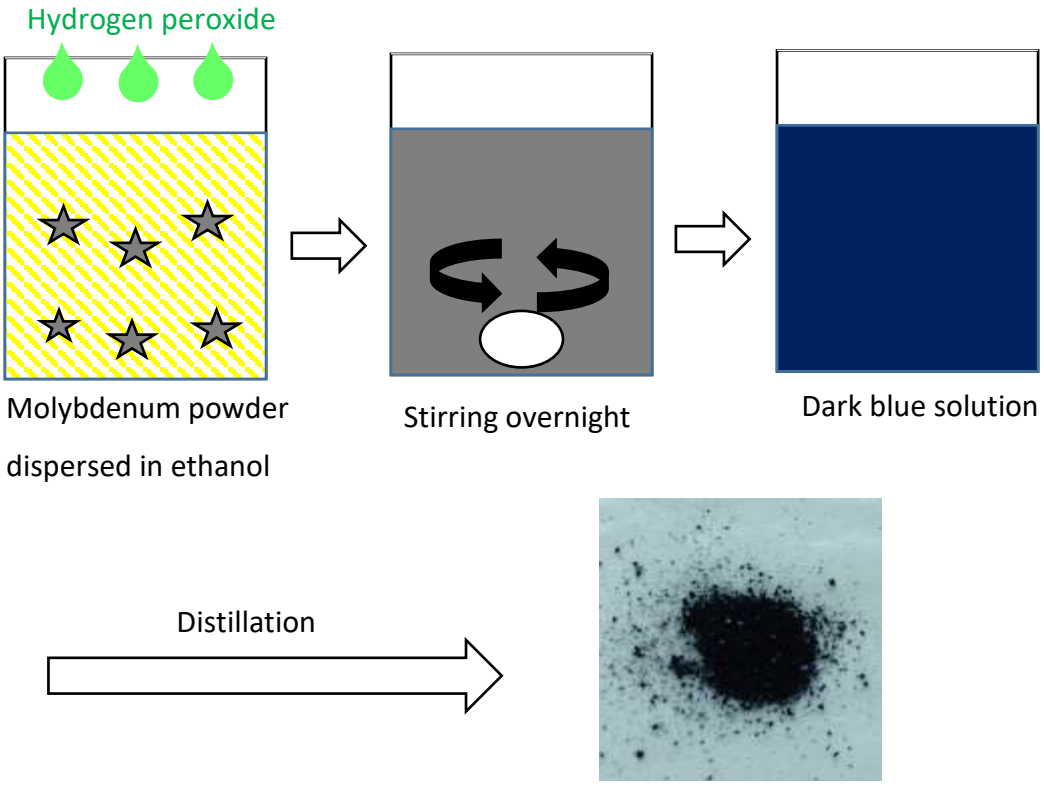

Figure II.6: Fabrication process of the molybdenum bronzes

In order to obtain a powder and to remove the harmful solvent (H_2O_2), the solution was distilled. First, the solution was heated at 110°C, approximately the boiling point of 30% hydrogen peroxide.[61] However, at this temperature water is also evaporating and the H_2O_2 concentration can therefore increase. The boiling point of hydrogen peroxide increases with increasing concentration and can reach 150°C at

100% therefore the temperature was slowly increased. At 130°C, all solvent had evaporated and a dark blue powder was obtained. Figure II.6 summarize the formulation process.

Five different solvents were studied to dissolve the powder: water, acetone, isopropanol (IPA), ethanol and acetonitrile. These solvents were chosen because they will not dissolve the SY layer. One milligram of powder was dissolved in about 0.5 ml of solvent. Only water dissolved the molybdenum bronze directly. To help the dissolution the solutions were stirring at 40°C on a hot plate for two minutes. Both ethanol and IPA dissolved the powder after heat treatment. Immediately after the treatment, the solutions of acetone and acetonitrile turn dark blue, though the molybdenum bronzes were only in suspension in the solvent. Quickly after removing the solutions from the heat, the powder precipitated again. Therefore, only the solutions in ethanol, IPA and water were suitable to dissolve the molybdenum bronze.

In order to avoid potential humidity, which could harm the lifetime of our devices, the use of water as a solvent was ruled out. Both IPA and ethanol could have been used for this series of tests and we chose to use ethanol as it presents the lowest boiling point of the two.

Four different concentration were studied: 1 mg/ml, 3 mg/ml, 5 mg/ml and 7 mg/ml. The solutions were spin-coated on top of the SY layer at 3 000 rpm for 60 s. Devices without HMoOx were also made for comparison.

If devices without any molybdenum oxide shown no light emission, the insertion of a very thin layer (1 mg/ml) of our HTL is enough to observe luminance, proving the importance of an HTL in this architecture. However, the performances with such a layer are extremely low (luminance under 250 cd/m^2 and a current efficiency of 3.0 cd/A). When the thickness is increased, the device performance also increases. For example, the devices exhibit current efficiencies up to 7.4 cd/A with a 3 mg/ml, 5.7 cd/A with 5 mg/ml and 6.1 cd/A with 7 mg/ml. The lower current efficiency observed with the 5 mg/ml solution compare to the 3 mg/ml, is due to a

lower luminance despite a similar current density. On the contrary, the devices with a 7 mg/ml solution exhibit similar luminance to the ones with a 3 mg/ml solution but with a higher current density.

Overall, the performances obtained with the HMoOx solution-processed layers are lower than the devices made using an evaporated layer of MoO_3. This phenomenon is, at least in great part, due to a lower current flowing in the devices, symbol of a decreased hole transport properties compare to the thermally evaporated molybdenum.

Molybdenum bronze post deposition treatments have been demonstrated to improve the device performances. Li *et al*.[59] studied HMoOx in OPV and demonstrated that after exposing the film to a certain pressure (10 min at 10 Pa) the work function of the bronzes can be lower down (5.7 eV to 5.4 eV). The resulting devices present better charge extraction and therefore better performance. Such treatment applied to our bronzes could improve the charge injection, and to some extent their transport, *via* the reduction of the energy gap between HMoOx and the top electrode. Other possibilities involve the insertion of caesium or silver nanoparticles into the bronzes or post deposition annealing to enhance their performance.[58,59] This latter option however can be difficult when the bronzes are deposited on top of other layers, as the annealing treatment could damage them.

If the molybdenum bronzes did not reach the values obtained with the evaporated molybdenum oxide, they still hold a certain potential for all solution process inverted OLEDs.

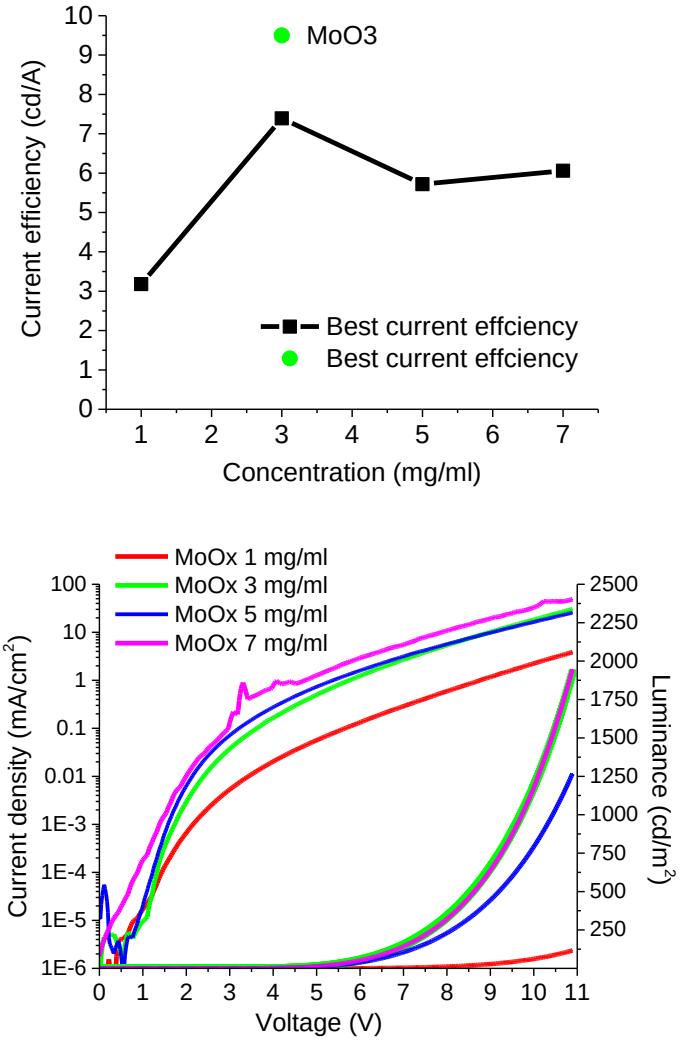

Figure II.7: Current efficiency in relation to the molybdenum bronze concentration (top). Current density and Luminance versus voltage for the devices with HMoOx (bottom)

D. PEI concentration

As mentioned earlier, polyethyleneimine is used in addition to zinc oxide to lower the work function of ITO, so it can inject electrons more efficiently into the device. Stolz *et al.*[6] demonstrated the importance of the PEI thickness on the work function modification of a silver electrode. In their work, they demonstrated an initial reduction of the silver work function from 4.6 eV for silver alone to 3.5 eV with a 1.7 nm thick layer of PEI, however the work function modification saturated after 5 nm

of PEI at around 3.15 eV. Such modification of the work function has a direct impact on the device performances.

In this study, the device architecture is kept the same as before (ITO/ZnO/PEI/SY/MoO_3/Al), however here the PEI thickness is varied in order to study its influence on the device performances.

Polyethyleneimine (Alfa Aesar, Mw: 1800) was dissolved in 2-methoxyethanol at concentrations of 2, 4, 6 and 10 mg/ml (approximately 0.2, 0.4, 0.6 and 1%wt). These concentrations correspond to thickness between 4 and 12 nm.[6]

Table II.6: Results for PEI concentration test

PEI concentration	Current efficiency (cd/A)[a]	Luminance (cd/m^2)[a]	Turn on voltage (V)[b]
2 mg/ml	9.55 (7.7)	48 651 (11)	3.2
4 mg/ml	9.51 (7.2)	39 929 (11)	3.2
6 mg/ml	9.65 (7.4)	43 379 (11)	3.4
10 mg/ml	8.82 (7.4)	35 052 (12)	3.5

[a] *In brackets the operating voltage at which values were recorded (in Volts);* [b] recorded for a luminance of $1cd/m^2$

Up to 6 mg/ml, the impact of PEI thickness on the device performance is minimal overall. The current efficiency does not vary significantly. The turn on voltage is the same for 2 and 4 mg/ml and is only slightly increased for 6 mg/ml. The luminance varied more between the different concentrations but without a specific trend. At concentrations over 6 mg/ml, the current efficiency dropped with the luminance while the turn on voltage continued increasing.

In summary, a PEI concentration between 2 to 6 mg/ml will ensure the best device performances. Over 6 mg/ml, the balance between the PEI insulating nature and its properties to reduce work function, and improving the transport and injection of negative charges, is tilted towards the insulating effect.

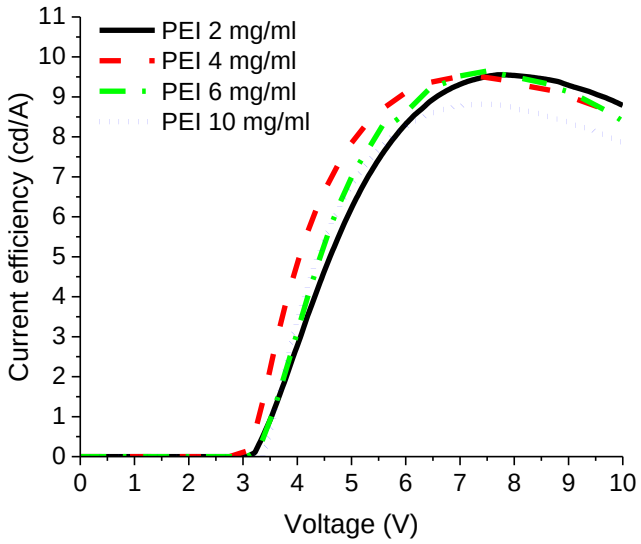

Figure II.8: Variation of PEI thickness and impact on the current efficiency

E. PEI molecular weight

Courtright *et al.*[42] studied the influence of PEI molecular weight (Mw) on OPV device performance. They noticed a relation between the Mw and the work function of the ITO/ZnO electrode. Indeed, they showed that it could be tuned. For example, PEI with a molecular weight of 2 000 g mol^{-1} spin-coated on top of a zinc oxide layer will modify the electrode work function to 2.97 eV, however if the molecular weight is reduced to 800 g mol^{-1} the work function can be further reduced to 2.75 eV. Such a low work function aligns almost perfectly with the Super-Yellow LUMO of 2.7 eV and it was previously highlighted that a lowering of the energetic barrier between the modification layer and the emissive layer would lead to better electron injection. However, Courtright *et al.* also demonstrated that a low molecular weight would affect negatively the stability of the devices over time. Indeed, OPV devices made with a 750k g mol^{-1} PEI layer showed only a 13.6% reduction in performances after 3 months, whereas when 800 g mol^{-1} PEI was used, the performance was reduced at up to 31.9% in the same period, with an immediate drop of 25 % of their performances in the first 15 days.

To study the impact of molecular weight on device performance, a device with an 800 g/mol polyethyleneimine (Sigma-Aldrich) was made and compared to previous devices with a 1 800 g/mol polyethyleneimine (Alfa Aesar). PEI concentration was kept at 6 mg/ml and spin-coated at 5 000 rpm for 60s.

Table II.7: Impact of the molecular weight of PEI on OLED performances

PEI Mw	Current efficiency (cd/A)[a]	Luminance (cd/m^2)[a]	Turn on voltage (V)[b]
1 800 (Alfa Aesar)	9.80 (7.3)	38 510 (11)	3.2
800 (Sigma-Aldrich)	10.02 (6.1)	35 853 (10.1)	2.6

[a] *In brackets the operating voltage at which values were recorded (in Volts);* [b] recorded for a luminance of 1cd/m^2

Reducing the molecular weight of PEI had the expected effect on the electron injection. The turn on voltage and operating voltages were decreased. Additionally, changing PEI also induced an increase in the current efficiency, which now reach 10.02 cd/A. However, the luminance is reduced compare to the devices with a high molecular weight PEI. The current is a good example of both these phenomena. Indeed, if the first devices with a low Mw PEI do reach higher values at lower voltage, due to better charge injection, they are not able to sustain current higher than 830 mA/cm^2, whereas higher Mw PEI sustained a current higher than a 1 000 mA/cm^2.

Therefore, when using insulating polymers, such as PEI, as electron transport/injection material great care should be given to both the thickness of the layer and the molecular weight of the chosen polymer. Indeed, if a variation in the thickness could lead to a partial insulation of the device from the electrode, a variation in the molecular weight will affect the charge injection.

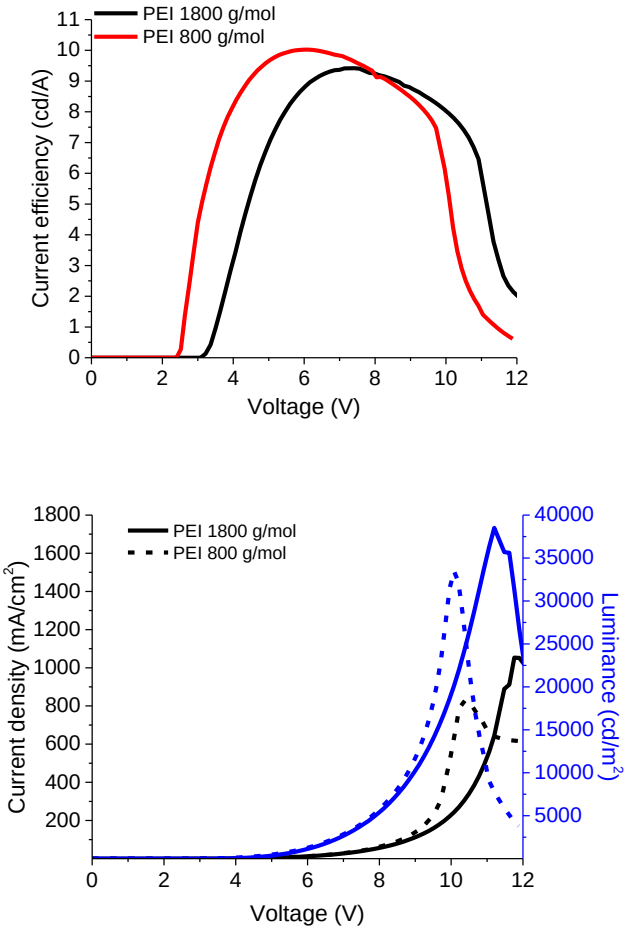

Figure II.9: Current efficiency versus voltage (left) and Current density and luminance versus voltage for different Mw PEI.

V. Conclusion

The fabrication of any efficient organic light emitting diodes requires the consideration of numerous parameters. The first of them is usually PLQY, as it is a requirement to characterise any new emissive material. While this gives an indication on the potential efficiency of a new material, it does not give any quantitative values as to the future performances of this material in a device.

Overall, the active layer thickness appears as the main influence on devices performances. Therefore, a special interest should always be focus on finding the optimum thickness and it should always be one of the first steps of device optimisation. When the emitter is deposited by spin-coating, the easiest way to

modify the layer thickness is to vary the solution concentration. In this study, a variation of 1 mg/ml in the solutions lead to a difference of 15 to 20 nm. A disparity large enough to increase the current efficiency of our devices from 5.25 to 8.10 cd/A. A spin-speed study can be a good complement to a thickness study. Indeed, with a variation of speed the thickness of the layer can be further optimised and a better film uniformity can be achieved.

If an annealing test does not always prove successful in improving the device performances, it still provides important information on the heat resistance of the device. In this aspect, such a test should always be carried out on new emissive material. The heat resistance of a device can be a crucial point when choosing the best materials for OLED. Indeed, not only will the devices most likely undergo self-heating during operation, but also the device itself could be exposed to a heat source, such as ray of sunlight by example.

In a conventional architecture, ITO/PEDOT:PSS/SY/Ca/Al, Super-yellow was demonstrated to perform best when deposited from a solution with a concentration of 5 mg/ml in toluene at a spin-speed of 1400 rpm for 60 s. No post annealing is necessary. Such devices demonstrated a current efficiency of 9.40 cd/A at 2234 cd/m^2 (8.4 cd/A at 10 000 cd/m^2) with a luminance of 66 456 cd/m^2 at 9.7 V and a 2.3 V turn on voltage.

A change in the device architecture allow us to study other layers alongside the emissive layer. Indeed, by switching to an inverted architecture, replacing the previous HTL by MoO_3 and by adding a combination of EIL and ETL (ZnO/PEI), it was possible to study the influence of the modification of such layers on devices performance. By analogy to the optimisation of the active layer, the thickness control of molybdenum layer and PEI is important. However, in the case of PEI the thickness is not the only important parameter to consider. Indeed, the molecular weight of the latter can also affect the device performance. The use of a more complex architecture requires a more complex optimisation, as each layer has to be optimised one by one and each is highly important when trying to obtain the best performance.

Using an inverted architecture, ITO/ZnO/PEI/SY/MoO_3/Al, the devices exhibited a current efficiency of 10.02 cd/A at 1466 cd/m^2 (8.7 cd/A at 10 000 cd/m^2) with a luminance of 35 853 cd/m^2 at 10.1 V and a 2.6 V turn on voltage.

In this architecture, however the HTL layer was thermally evaporated. As an alternative, molybdenum bronze was proposed instead. Molybdenum bronze is relatively easy to formulate and is soluble in solvents (IPA, ethanol and water) that will not damage the active layer. Devices exhibited a maximum current efficiency of 7.4 cd/A. Despite demonstrating a lower performance than their thermally evaporated homologues, these results are still promising. Indeed, it was demonstrated than post deposition treatment, such as vacuum treatment[59] or annealing[58,60] can have beneficial effect on the film morphology. As the bronzes are deposited on top of the active layer, great care will have to be taken when studying possible post treatment.

VI. Bibliography

1 J. H. Burroughes, D. D. C. Bradley, A. R. Brown, R. N. Marks, K. Mackay, R. H. Friend, P. L. Burns and A. B. Holmes, *Nature*, 1990, **347**, 539–541.

2 S. R. Tseng, Y. S. Chen, H. F. Meng, H. C. Lai, C. H. Yeh, S. F. Horng, H. H. Liao and C. S. Hsu, *Synth. Met.*, 2009, **159**, 137–141.

3 J. Lee, H. Youn and M. Yang, *Org. Electron. physics, Mater. Appl.*, 2015, **22**, 81–85.

4 H. J. Bolink, E. Coronado, J. Orozco and M. Sessolo, *Adv. Mater.*, 2009, **21**, 79–82.

5 H. Youn and M. Yang, *Appl. Phys. Lett.*, 2010, **97**, 1–4.

6 S. Stolz, M. Petzoldt, S. Duck, M. Sendner, U. H. F. Bunz, U. Lemmer, M. Hamburger and G. Hernandez-Sosa, *ACS Appl. Mater. Interfaces*, 2016, **8**, 12959–12967.

7 J. H. Youn, S. J. Baek, H. P. Kim, D. H. Nam, Y. Lee, J. G. Lee and J. Jang, *J. Mater. Chem. C*, 2013, **1**, 3250–3254.

8 H. Lee, Y. Kwon and C. Lee, *J. Soc. Inf. Disp.*, 2012, **20**, 640–645.

9 A. Köhnen, M. Irion, M. C. Gather, N. Rehmann, P. Zacharias and K. Meerholz, *J. Mater. Chem.*, 2010, **20**, 3301.

10 J. Liu, T.-F. Guo and Y. Yang, *J. Appl. Phys.*, 2002, **91**, 1595.

11 Y. H. Kim, T. H. Han, H. Cho, S. Y. Min, C. L. Lee and T. W. Lee, *Adv. Funct. Mater.*, 2014, **24**, 3808–3814.

12 Y. Kwon, Y. Kim, H. Lee, C. Lee and J. Kwak, *Org. Electron. physics, Mater. Appl.*, 2014, **15**, 1083–1087.

13 S. Höfle, A. Schienle, C. Bernhard, M. Bruns, U. Lemmer and A. Colsmann, *Adv. Mater.*, 2014, **26**, 5155–5159.

14 M. U. Hassan, Y. C. Liu, K. U. Hasan, H. Butt, J. F. Chang and R. H. Friend, *Appl. Mater. Today*, 2015, **1**, 45–51.

15 S. Höfle, C. Bernhard, M. Bruns, C. Kübel, T. Scherer, U. Lemmer and A. Colsmann, *ACS Appl. Mater. Interfaces*, 2015, **7**, 8132–8137.

16 S.-J. Ko, H. Choi, W. Lee, T. Kim, B. R. Lee, J.-W. Jung, J.-R. Jeong, M. H. Song, J. C. Lee, H. Y. Woo and J. Y. Kim, *Energy Environ. Sci.*, 2013, **6**, 1949.

17 S. J. Cha, S. N. Cho, W. H. Lee, H. S. Chung, I. N. Kang and M. C. Suh, *Macromol. Rapid Commun.*, 2014, **35**, 807–812.

18 C. Y. Bin Ng, K. H. Yeoh, T. J. Whitcher, N. A. Talik, K. L. Woon, T. Saisopa, H. Nakajima, R. Supruangnet and P. Songsiriritthigul, *J. Phys. D. Appl. Phys.*, 2014, **47**, 015106.

19 S. Hofle, A. Schienle, M. Bruns, U. Lemmer and A. Colsmann, *Adv. Mater.*, 2014, **26**, 2750–2754.

20 PDY-132, https://www.merckgroup.com/content/dam/web/corporate/non-images/business-specifics/performance-materials/Optoelectronics/global/Datasheet-Livilux-PDY-132-Super-Yellow-EN.pdf, (accessed 4 July 2018).

21 E. Taylor-Shaw, E. Angioni, N. J. Findlay, B. Breig, A. R. Inigo, J. Bruckbauer, D. J. Wallis, P. J. Skabara and R. W. Martin, *J. Mater. Chem. C*, 2016, **4**, 11499–11507.

22 N. J. Findlay, J. Bruckbauer, A. R. Inigo, B. Breig, S. Arumugam, D. J. Wallis, R. W. Martin and P. J. Skabara, *Adv. Mater.*, 2014, **26**, 7290–7294.

23 C. Orofino, C. Foucher, F. Farrell, N. J. Findlay, B. Breig, A. L. Kanibolotsky, B. Guilhabert, F. Vilela, N. Laurand, M. D. Dawson and P. J. Skabara, *J. Polym. Sci. Part A Polym. Chem.*, 2017, **55**, 734–746.

24 J. C. de Mello, F. H. Wittmann and R. H. Friend, *Adv. Mater.*, 1997, **9**, 230–232.

25 E. W. Snedden, L. A. Cury, K. N. Bourdakos and A. P. Monkman, *Chem. Phys. Lett.*, 2010, **490**, 76–79.

26 M. Chapran, E. Angioni, N. J. Findlay, B. Breig, V. Cherpak, P. Stakhira, T. Tuttle, D. Volyniuk, J. V Grazulevicius, Y. A. Nastishin, O. D. Lavrentovich and P. J. Skabara, *ACS Appl. Mater. Interfaces*, 2017, **9**, 4750–4757.

27 J. Luo, Z. Xie, J. W. Y. Lam, L. Cheng, B. Z. Tang, H. Chen, C. Qiu, H. S. Kwok, X. Zhan, Y. Liu and D. Zhu, *Chem. Commun.*, 2001, **381**, 1740–1741.

28 J. Teetsov and M. A. Fox, *J. Mater. Chem.*, 1999, **9**, 2117–2122.

29 S. Hofle, T. Lutz, A. Egel, F. Nickel, S. W. Kettlitz, G. Gomard, U. Lemmer and A. Colsmann, *ACS Photonics*, 2014, **1**, 968–973.

30 H. A. Méndez-pinzón, D. R. Pardo-pardo, J. P. Cuéllar-alvarado, J. Carlos, R. Vera and B. A. Páez-sierra, *Univ. Sci.*, 2010, **15**, 68–76.

31 K. Norrman, A. Ghanbari-Siahkali and N. B. Larsen, *Annu. Reports Sect. 'C'*, 2005, **101**, 174-201.

32 A. Islam, M. Rabbani, M. H. Bappy, M. A. R. Miah and N. Sakib, *2013 Int. Conf. Informatics, Electron. Vis.*, 2013, 1–5.

33 S. Burns, J. MacLeod, T. Trang Do, P. Sonar and S. D. Yambem, *Sci. Rep.*, 2017, **7**, 1–8.

34 D. Meyerhofer, *J. Appl. Phys.*, 1978, **49**, 3993–3997.

35 D. M. DeLongchamp, B. M. Vogel, Y. Jung, M. C. Gurau, C. A. Richter, O. A. Kirillov, J. Obrzut, D. A. Fischer, S. Sambasivan, L. J. Richter and E. K. Lin, *Chem. Mater.*, 2005, **17**, 5610–5612.

36 W. W. Flack, D. S. Soong, A. T. Bell and D. W. Hess, *J. Appl. Phys.*, 1984, **56**, 1199–1206.

37 M. D. Tyona, 2013, **2**, 195–208.

38 D. B. Hall, P. Underhill and J. M. Torkelson, *Polym. Eng. Sci.*, 1998, **38**, 2039–2045.

39 A. H. Reshak, M. M. Shahimin, N. Juhari and S. Suppiah, *Prog. Biophys. Mol. Biol.*, 2013, **113**, 289–294.

40 T. Chiba, Y. J. Pu and J. Kido, *Adv. Mater.*, 2015, **27**, 4681–4687.

41 S. Woo, W. Hyun Kim, H. Kim, Y. Yi, H. K. Lyu and Y. Kim, *Adv. Energy Mater.*, 2014, **4**, 1–7.

42 B. A. E. Courtright and S. A. Jenekhe, *ACS Appl. Mater. Interfaces*, 2015, **7**, 26167–26175.

43 H. C. Chen, S. W. Lin, J. M. Jiang, Y. W. Su and K. H. Wei, *ACS Appl. Mater. Interfaces*, 2015, **7**, 6273–6281.

44 S. Stolz, M. Scherer, E. Mankel, R. Lovrinčić, J. Schinke, W. Kowalsky, W. Jaegermann, U. Lemmer, N. Mechau and G. Hernandez-Sosa, *ACS Appl. Mater. Interfaces*, 2014, **6** (9), 6616-6622.

45 H. Fukagawa, K. Morii, M. Hasegawa, S. Gouda, T. Tsuzuki, T. Shimizu and T. Yamamoto, *SID Symp. Dig. Tech. Pap.*, 2015, **46**, 696–699.

46 P. de Bruyn, D. J. D. Moet and P. W. M. Blom, *Org. Electron.*, 2010, **11**, 1419–1422.

47 Y. Zhou, C. Fuentes-Hernandez, J. Shim, J. Meyer, A. J. Giordano, H. Li, P. Winget, T. Papadopoulos, H. Cheun, J. Kim, M. Fenoll, A. Dindar, W. Haske, E. Najafabadi, T. M. Khan, H. Sojoudi, S. Barlow, S. Graham, J.-L. Bredas, S. R. Marder, A. Kahn and B. Kippelen, *Science*, 2012, **336**, 327–332.

48 H. Kang, S. Hong, J. Lee and K. Lee, *Adv. Mater.*, 2012, **24**, 3005–3009.

49 S. van Reenen, S. Kouijzer, R. A. J. Janssen, M. M. Wienk and M. Kemerink, *Adv. Mater. Interfaces*, 2014, **1**, 1-34.

50 F. Wang, X. Qiao, T. Xiong and D. Ma, *Org. Electron.*, 2008, **9**, 985–993.

51 Q. Fu, J. Chen, C. Shi and D. Ma, *ACS Appl. Mater. Interfaces*, 2013, **5**, 6024–6029.

52 S. Tokito, K. Noda and Y. Taga, *J. Phys. D. Appl. Phys.*, 1996, **29**, 2750–2753.

53 C. Tao, S. Ruan, X. Zhang, G. Xie, L. Shen, X. Kong, W. Dong, C. Liu and W. Chen, *Appl. Phys. Lett.*, 2008, **93**, 1-3.

54 H. Zhang, Q. Fu, W. Zeng and D. Ma, *J. Mater. Chem. C*, 2014, **2**, 9620–9624.

55 J. Liu, X. Wu, S. Chen, X. Shi, J. Wang, S. Huang, X. Guo and G. He, *J. Mater. Chem. C*, 2014, **2**, 158–163.

56 S. Lattante, *Electronics*, 2014, **3**, 132–164.

57 X. Zhang, F. You, Q. Zheng, Z. Zhang, P. Cai, X. Xue, J. Xiong and J. Zhang, *Org. Electron. physics, Mater. Appl.*, 2016, **39**, 43–49.

58 X. Li, F. Xie, S. Zhang, J. Hou and W. C. Choy, *Light Sci. Appl.*, 2015, **4**, 1-7.

59 X. Li, W. C. H. Choy, F. Xie, S. Zhang and J. Hou, *J. Mater. Chem. A*, 2013, **1**, 6614-6621.

60 A. Soultati, A. M. Douvas, D. G. Georgiadou, L. C. Palilis, T. Bein, J. M. Feckl, S. Gardelis, M. Fakis, S. Kennou, P. Falaras, T. Stergiopoulos, N. A. Stathopoulos, D. Davazoglou, P. Argitis and M. Vasilopoulou, *Adv. Energy Mater.*, 2014, **4**, 1–10.

61 Hydrogen Peroxide Boiling Points and Freezing Poin | USP Technologies, http://www.h2o2.com/technical-library/physical-chemical-properties/physical-properties/default.aspx?pid=22, (accessed 10 March 2018).

Chapter III: Green and Red series materials for OLEDs application

I. RGB materials and OLEDs

It has been calculated that in the last years, between televisions, phones and computers, the average time spent in front of a screen can reach up to 8 or 10 hours a day.[1] Displays started to be introduced in everyday life with the development of affordable televisions in the 1950's. In the 80's and 90's, it was the turn of computers to become an essential part of every home and with time of every workplace. Finally, since 2007 with the release of the first iPhone and the development of tactile screens, smartphones are the latest participant of the display revolution.

This never-ending need for screens created a booming economical market around the development of new technologies for displays. For many years, the display market was led by the development of the liquid crystal display (LCD), due mainly to their lightweight and low power consumption. However, in the last decade, OLED technologies are slowly taking over the market. OLEDs present several advantages over LCD,[2] such as not being a photo acceptor and therefore not requiring backlighting, which simplifies the display fabrication and lowers its power consumption. Additionally, OLEDs offer the possibility to be deposited on thinner substrates, leading to the possibility of extremely thin and flexible screens.[3] An example of an OLED television screen is presented in Figure III.1.

Figure III.1: Picture of the 55" KE55S9C Series 9 Smart 3D Full HD OLED TV from Samsung.
http://www.samsung.com/uk/tvs/curved-oled-s9c/ (04/05/2018)

Every display is composed of multiple pixels, which are themselves commonly composed of three small and very close, but separate light sources: one red, one green and one blue.[4] At a certain distance, the three light sources are indistinguishable and our eyes only see one solid colour. This is due to the way we perceive colours. Indeed, the human eye is composed of three types of colour sensitive cells, called cones. Each cone is defined according to its sensibility to short (S), medium (M) or long (L) wavelength.[5] Figure III.2 represents the normalized spectral sensitivity of the human eye. When they are activated, the cones send a signal to the brain, which processes the signal in such way that each colour is perceived as a mix of three distinct primary colours. These three primary colours are additive, which means that when the three of them are added together white light can be obtained. This is in total opposition with physical colours, like paints, inks or dyes, which work on a subtractive colour model.

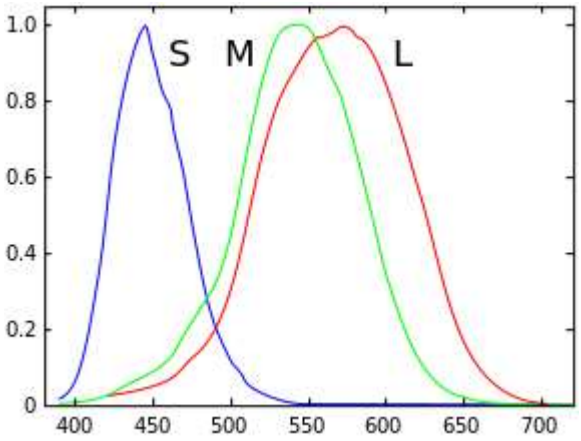

Figure III.2: The normalised spectral sensitivity of short-, middle- and long-wavelength sensitive human cones.[6]

Using this knowledge, it was found that by using a combination of three primary colours, red blue and green, and varying their intensity it was possible to trick the brain into seeing colours from the entire visible spectrum. For example, if a red light sources is turned on at high brightness with a green light source turned on at a lower brightness, the medium and long wavelength sensitive cones will be activated

and the brain will process these signals as yellow light. Nowadays, most displays are made using this technology, called the RGB system (for Red Green and Blue).

The omnipresence of displays based on the RGB system in everyday life make it important to continually develop new materials capable of emitting in the range of these three primary colours. Hence, in this chapter, we will study two series of emitting materials: one series of green emitters and one series of red emitters. Each material has been tested in a simple conventional OLED architecture and optimised to obtain the best performance.

II. Green OLED

A. Background

Organic green emitters have been intensively studied over the last few years and they often give the best results. One explanation for this is that green light is always perceived as the brightest colour by the human eye.[7] Indeed, when subjected to green light both M and L cones are activated near their maximum sensitivity. Thereby, if presented with two light sources, one green and one blue for example, delivered with the same power then the green light will always seem brighter. This selectivity of our eyes perception means that it is possible to use less powerful light source for green light and explains why many laser pointers are green.

The first efficient OLED, made by Tang and Van Slyke[8], was green and was based on the green emitting properties of Alq_3. However, Alq_3 has a highly unbalanced charge mobility, and with the evolution and the complexification of device architectures, Alq_3 is now mostly used as an electron transport layer. Nowadays, one of the most common OLED green emitters is tris[2-phenylpyridinato-C2,N]iridium(III), best known as $Ir(ppy)_3$. As a phosphorescent material, it can achieve an internal quantum efficiency close to 100%, in theory. However, used alone it was proven to suffer severely from concentration quenching,[9] indicating that a host material is required to maximise efficiency. Thus, the host materials or the percentage of $Ir(ppy)_3$ doped within the host can have a major impact on device performance. In 2000, Adachi *et al.*[10] obtained a luminance of around 4 000 cd/m^2 by

adding 7% of $Ir(ppy)_3$ into 3-(biphenyl-4-yl)-5-(4-tert-butylphenyl)-4-phenyl-4H-1,2,4-triazol (TAZ). Ten years later, Erickson *et al.*[11] through meticulously doping both the ETL (bathophenanthroline; BPhen) and the HTL (tris(4-carbazol-9-ylphenyl)amine; TCTA) of their devices obtained a luminance of around 300 000 cd/m^2. Besides being heavily impacted by the type of doping and the host material, $Ir(ppy)_3$ usually needs to be thermally evaporated. In an era where research is focussing more and more on solution processing this is an important factor to be considered.

Although solution processed materials can usually be made using straightforward synthesis, they are less present on the market. The principal reason for this is their lower overall performance compared to thermally evaporated materials. For example, in 2009, Li *et al.*[12] synthesised two green solution processable green emitters based on asymmetrical 4,7-disubstituted benzothiadiazole derivatives. Both materials were used as the emissive layer in OLEDs which exhibited a luminance of only around 1300 cd/m^2, about a hundred times lower than $Ir(ppy)_3$. More recently, Moonsin *et al.*[13] demonstrated a solution processed green OLED, with an emissive layer was based on a bis(fluorenyl)benzothiadiazole-cored carbazole dendrimer, with a luminance of up to 8 000 cd/m^2. However, a complexification of the device architecture, *via* the addition of an ETL, was necessary to obtain this result.

B. Materials

The two materials presented in this study have been synthesised by Dr Neil Findlay[14]. Both are green emitters and are based on a 2,1,3-benzothiadiazole (BT) units with two bifluorene arms on each side. The end groups are the differential point between the two materials. Green 1 possess trimethylsilane (TMS) end groups whereas Green 2 is finished with triphenylamine (TPA) groups. Figure III.3 shows the molecular structure of the two green emitter materials.

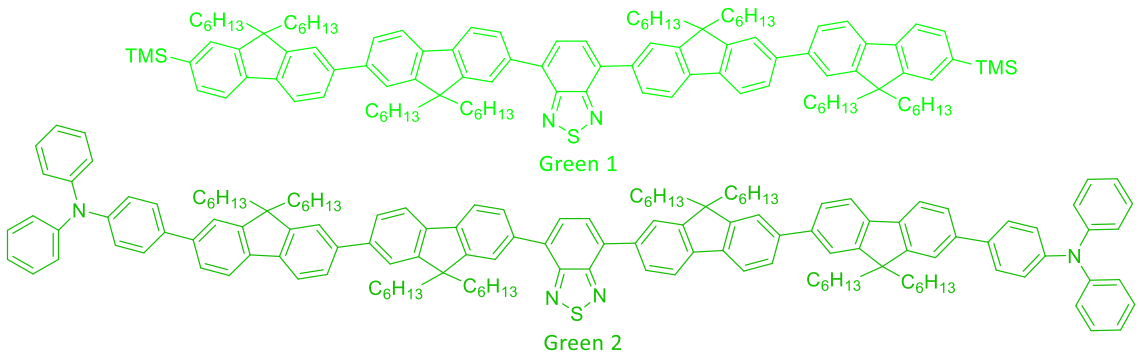

Figure III.3: Molecular structure of Green 1 and Green 2

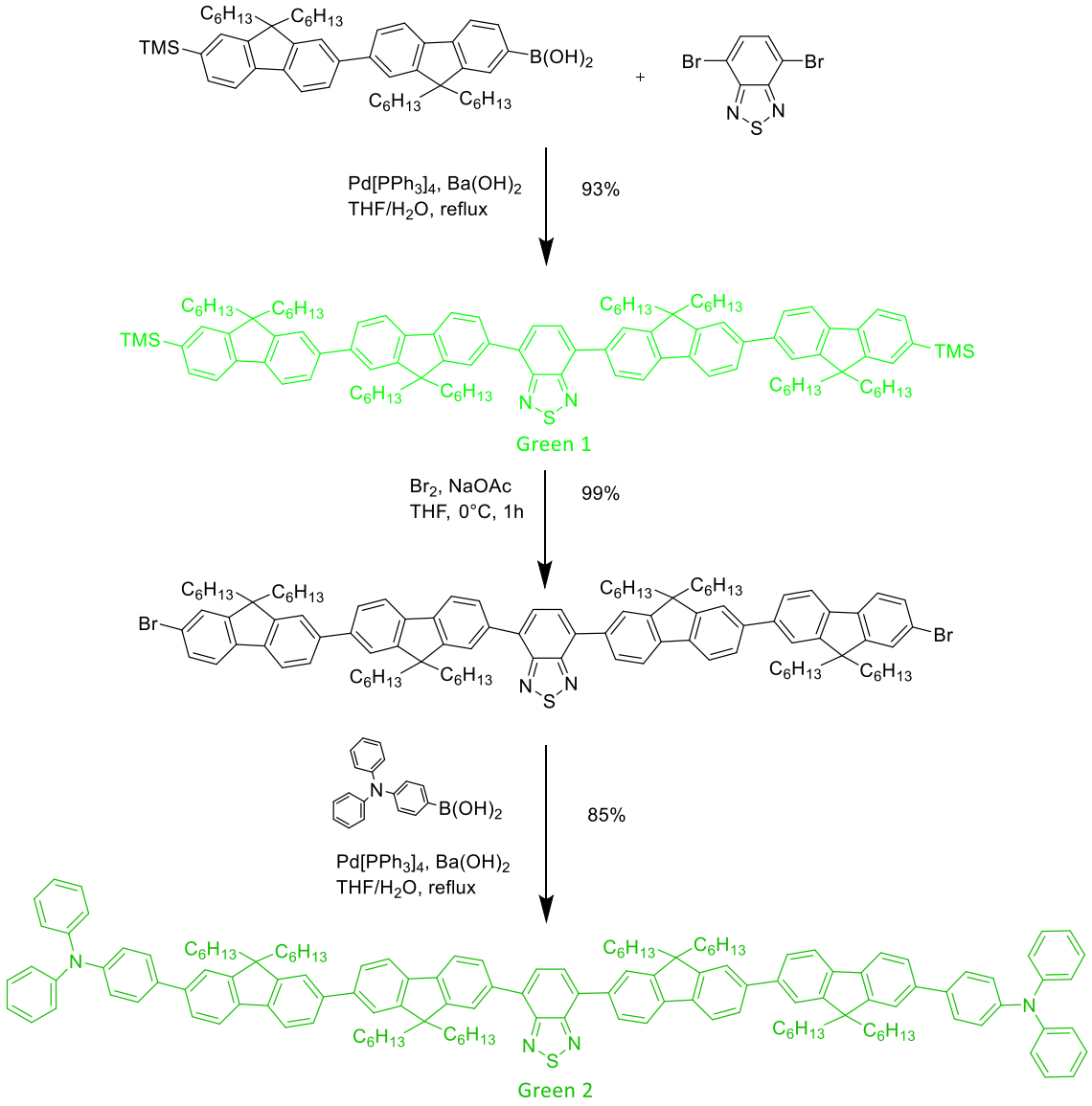

Figure III.4: Synthetic road for the fabrication of Green 1 and Green 2

Benzothiadiazole has been largely used in the design of new light emitting materials. The electron deficient character of BT units stabilise and spatially localise the lowest unoccupied molecular orbital or LUMO, in simple conjugated structures.[15] This LUMO energy reduction can allow an improved electron injection by inducing a closer match to the electrode work function or to the LUMO of the electron transport material.

The synthesis of the common core units, as well as the importance of the BT unit position in the molecule is described by Belton *et al.*[16]. The 4-7-dibromobenzothiadiazole and the corresponding oligofluorene boronic acid were connected via a simple Suzuki-Miyaura coupling, using barium hydroxide as base. This reaction resulted in the isolation of a bright yellow powder, Green 1, in over 90% yield. In order to form Green 2, the TMS groups were converted into bromides, forming an intermediate molecule. A second Suzuki-Miyaura coupling on this intermediate with 4-(diphenylamino)phenyl boronic acid lead to the formation of Green 2 with a yield of over 80%. The schemes of the reactions are presented in Figure III.4.

As previously mentioned in chapter II, thermal stability is a very important factor for any OLED emissive material. Both green materials showed a good thermal stability for temperatures up to 400°C. However, Green 1 exhibited a glass transition temperature (Tg) of 65°C and Green 2 had a Tg of 91°C. A low Tg could be a problem for the stability of the devices and an annealing test will be necessary to evaluate any possible change in the emissive layer morphology. Solution state UV-vis absorption and photoluminescence (PL) spectra were recorded as dilute solutions in dichloromethane. Green 1 presents an intense absorption band (346 nm), corresponding to a π-->π* transition of the excitons, and a less intense band at longer wavelength (425 nm), symbol of a charge transfer. In the same way, Green 2 exhibits an intense absorption band (365 nm) with a less intense shoulder (420 nm). For the PL spectra, both samples were excited at the wavelength of maximum absorption. The maximum emission wavelengths of Green 1 and 2 are at 546 and 549 nm

respectively. Both exhibited sharp emission profiles as shown in Figure III.5. This similarity in the emission spectra combined with the relative similarity of the molecular structure suggest that the emission comes from the BT core unit and it is only slightly impacted by the change of end groups.

Despite the optical HOMO-LUMO gaps of Green 1 and 2 being almost identical, the electrochemical HOMO-LUMO gap, measured by cyclic voltammetry (CV, not shown here), was narrower for Green 2 than for Green 1. Indeed, although the LUMO levels of both materials are relatively similar (3.00 eV and 2.98 eV for Green 1 and 2 respectively) with almost identical reversible reduction waves, their HOMO energies differ by 0.30 eV (5.37 eV and 5.07 eV for Green 1 and 2 respectively). This shift in the HOMO level is due to the triphenylamine groups present in Green 2.

Finally, absolute photoluminescence quantum yield (PLQY) values in the solid state for Green 1 and Green 2 were recorded as 88.5% and 65.7% respectively. These values would suggest better performances for Green 1 than for Green 2 however we will see that PLQY alone is not enough to predict the device performance of materials.

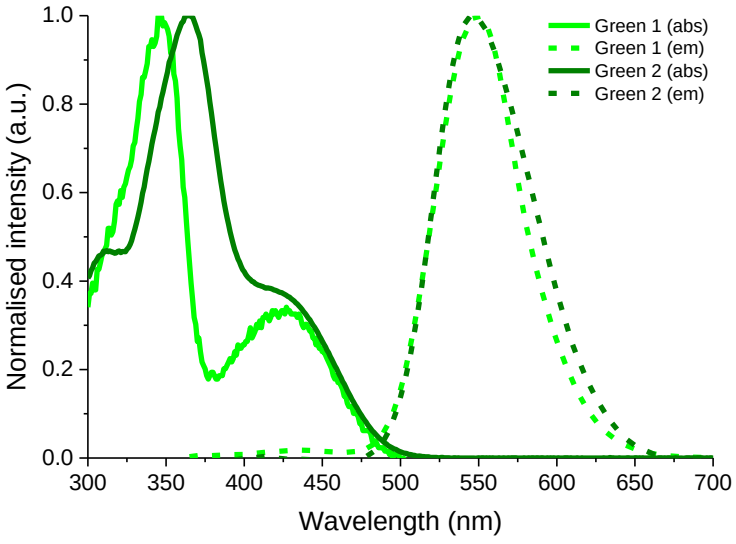

Figure III.5: Absorption and photoluminescence of Green 1 and 2

C. Devices

1. Concentration

In chapter II, it was demonstrated that the active layer thickness can have a significant impact on device performance, while determining the optimum thickness in the early stage of the optimisation is highly important. As previously explained, a thin layer is beneficial as it allows a higher current flow in to the device (lower ohmic resistance), however it will also make the device more sensitive to degradation.[17] On the other hand, a thicker layer would improves the material resistance to degradation, while also having reduced current flow and therefore limiting the luminance.[18] An equilibrium between the two is therefore necessary and can be found by doing a thickness study. In other words, by designing a series of devices where the thickness of the emissive layer is varied.

As the emissive layer is deposited by spin-coating, the easiest way to alter its thickness is to vary the concentration of the solution while keeping the same spin-coating parameters. With Super-Yellow, the concentration was varied from 4 to 6 mg/ml, any higher concentration was too thick to be properly deposited. However, for small molecules, higher concentrations are necessary to obtain a similar thickness. The solution concentration was varied from 10 mg/ml to 30 mg/ml and all solutions were spin-coated at 800 rpm for 60 s.

A simple conventional architecture was chosen: ITO/PEDOT:PSS/Green/Ca/Al (Figure III.6). The thickness of the emissive layer was measured via AFM. The results are presented in Table III.1.

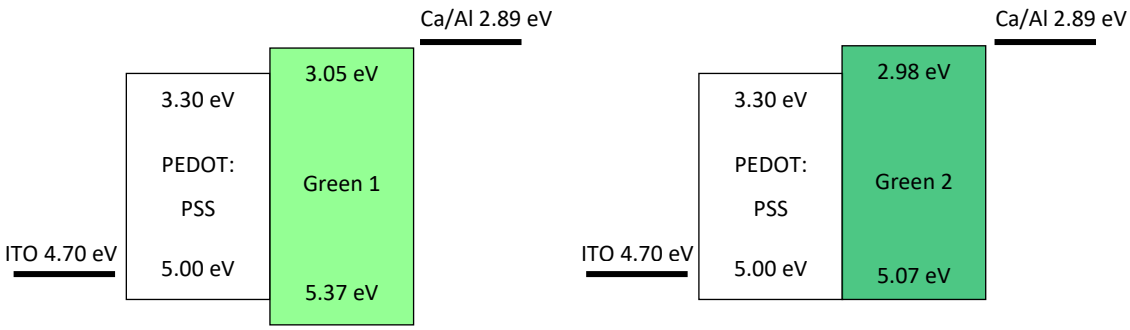

Figure III.6: Device architecture for the two materials

Table III.1: Concentration test for Green 1 and Green 2

Green	Concentration (mg/ml)	Thickness (nm)	Current efficiency (cd/A)[a]	Maximum Luminance (cd/m^2)[a]	Turn on voltage (V)[b]
1	10	30	0.59	3 033 (8.2)	3.7
	20	80	1.22	3 720 (10.2)	4.1
	30	120	0.9	2 130 (11.2)	5.0
2	10	30	1.80	14 590 (8.8)	4.0
	20	80	2.06	15 958 (9.5)	4.1
	30	120	2.15	12 085 (11.7)	4.7

[a] In brackets the operating voltage at which values were recorded (in Volts); [b] recorded for a luminance of 1 cd/m^2

Both materials exhibit their best performance at a concentration of 20 mg/ml (80 nm), as well as a turn on voltage increase following the increase in thickness. This similarity in the behaviour is expected, as the two materials share many common structural features. However, Green 2 shows a better performance than Green 1 in almost every domain. Indeed, Green 2 demonstrated a maximum luminance of 15 958 cd/m^2 against only 3 720 cd/m^2 for Green 1. At its maximum, the luminance of Green 2 is almost five times higher than the maximum reached by Green 1. Green 2 current efficiency is also improved and reaches a maximum of 2.06 cd/A at 20 mg/ml.

The large improvement of the luminance is explained by the increased current flow in the device, as shown in Figure III.7. Indeed, Green 2 can accept a higher current and therefore an increased number of charges that can reach the recombination zone. This higher current flow can be partially explained by the better HOMO match between Green 2 and PEDOT:PSS. Further explanation and discussion is provided in chapter III.

The substitution of TMS group by TPA groups is therefore extremely beneficial to the properties of the emissive materials. Indeed, as this is the only change between

the two materials, we can conclude that the TPA groups are responsible for the enhanced performance observed with Green 2.

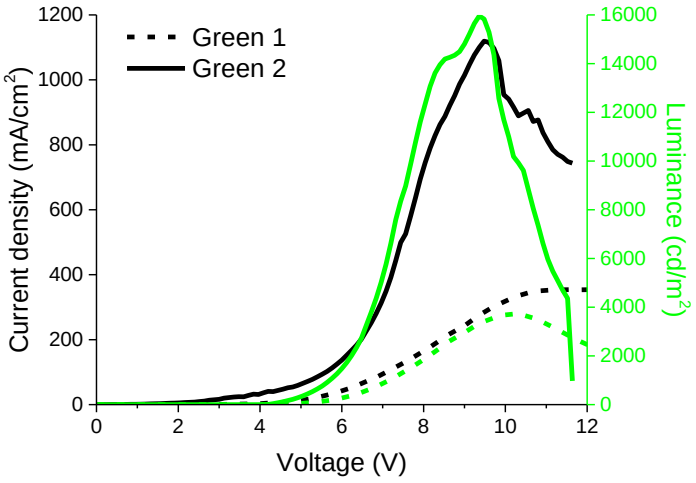

Figure III.7: Current density and Luminance versus voltage for Green 1 and Green 2

2. Annealing

Thermal analysis (by DSC) of Green 1 and Green 2 revealed that both had a relatively low glass transition temperature of 65°C and 91°C for Green 1 and 2, respectively. This low Tg is worth considering as heat induced morphological changes can have beneficial or detrimental effects on the device performance. It is why an annealing test, where a thin film of both materials is submitted to different temperatures before deposition of the next layer, is necessary. The results for this test are presented in Table III.2.

In the case of devices using Green 1, the luminance first doubles to 6 700 cd/m^2 and the current efficiency is increased to 1.74 cd/A when annealed at 40°C. However, device performance rapidly deteriorates with further heating and the luminance is reduced to only 500 cd/m^2 once heated at 80°C.

Devices fabricated with Green 2 also exhibit an increase in performance when heated at 40°C. Their luminance increases to reach a maximum of 20 388 cd/m^2 whereas both the current efficiency and the turn on voltage are stable. However, at higher temperature a similar phenomenon as the one observed with Green 1, is experienced. At 60°C, a slight decrease is observed on the devices luminance and the

current efficiency. At 80°C the devices do not emitted light anymore. In this last case, the devices initially sustained a higher current flow, compared to the devices heated at other temperatures, however, this higher current flow only leads to a short-circuit.

Table III.2: Annealing test for Green 1 and Green 2

Green (at 20 mg/ml)	Annealing temperature (°C)	Current efficiency (cd/A)[a]	Maximum Luminance (cd/m^2)[a]	Turn on voltage (V)[b]
1	no	1.22	3 720 (10.2)	4.1
	40	1.74	6 724 (9.9)	6.0
	60	1.49	4 087 (10.9)	6.8
	80	1.22	504 (10.0)	6.8
2	no	2.06	15 958 (9.4)	4.1
	40	2.00	20 388 @ (9.4)	4.2
	60	1.63	17 809 @ (9.1)	4.1
	80	-	-	-

[a] In brackets the operating voltage at which values were recorded (in Volts); [b] recorded for a luminance of 1 cd/m^2

Overall, both materials reveal a similar behaviour to annealing. First, an increase in performances with a 40°C annealing, followed by a slight decrease of luminance and current efficiency at 60°C and finally a drastic fall, or complete extinction in case of Green 2, of the performances at 80°C. The latter phenomenon is most likely due to thermal degradation as we are over or close to the glass transition temperature of both materials. Nonetheless, the turn on voltage has a different behaviour for each material. In case of Green 1, it increase from 4.1 to 6.8 V whereas with Green 2 it stay at 4.1 V. The turn on voltage is usually linked with charge injection.[19,20] Therefore, if the charge injection is stable for Green 2, it is degrading with the increase of temperature in the case of Green 1. On top of the previous improvement brought by TPA ending groups, they also help with stabilisation of charge injection.

Overall both materials exhibit their best performances when heated at 40°C, with Green 1 doubling its luminance to reach 6 724 cd/m^2 and Green 2 reaching a luminance of over 20 000 cd/m^2. A low heat treatment is therefore necessary with these green emitters in order to obtain the best performance. However, it is important to control this treatment precisely, as any overheating will be extremely damaging for the device performance.

3. CIE coordinates emission spectrum

Once optimised the electroluminescence properties of the fabricated devices were measured. The best devices were placed into an integrated sphere equipped with an optical fibre. The voltage applied corresponded to the value they showed their maximum luminance (9.9 V and 9.4 V, respectively for Green 1 and Green 2). Their electroluminescence spectra are presented in Figure III.9 and pictures of the two devices are shown in Figure III.8.

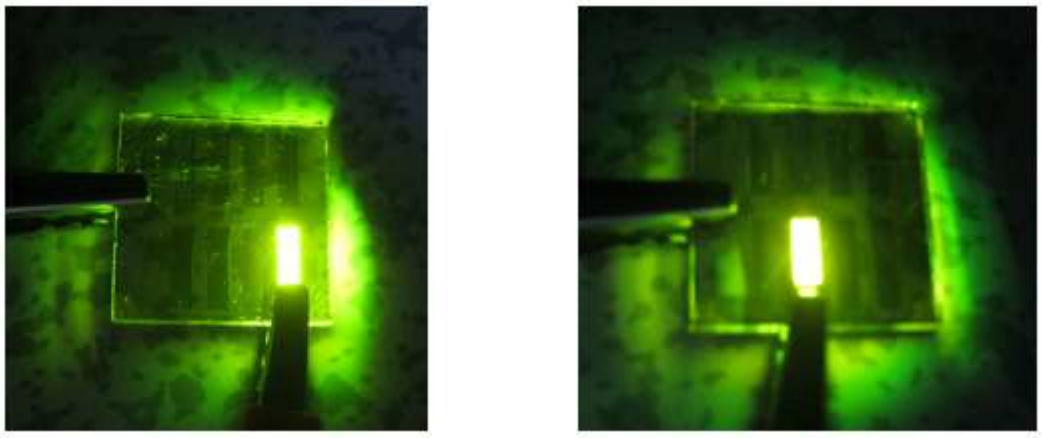

Figure III.8: Picture of Green 1 (left) and Green 2 (right) devices

Both materials presented extremely similar spectra with maximum emission peaks at 556 and 561 nm respectively for Green 1 and Green 2. This result is consistent with the photoluminescence spectra presented earlier. It was established that the emission comes from the fluorene-BT-fluorene core units that is only slightly impacted by the change of terminal groups. However, a small shift in the maximum emission is visible compared to the solution spectra (maximum 546 and 549 for Green

1 and Green 2 respectively). This bathochromic shift is most likely caused by some small aggregation sites in the thin film compared to the solution.

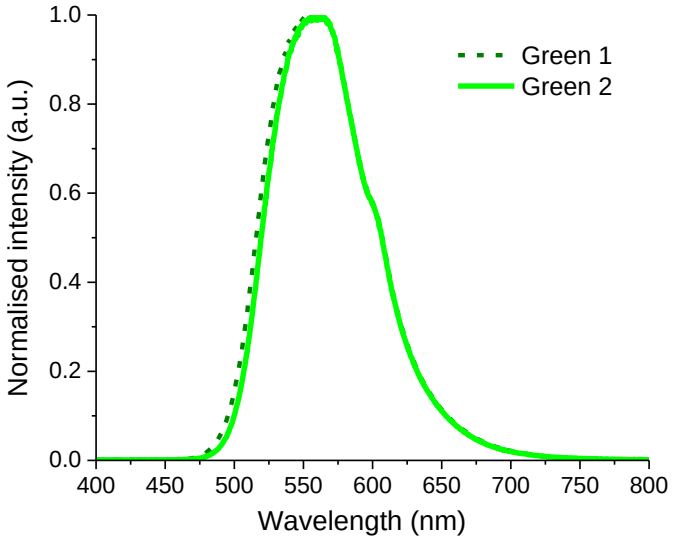

Figure III.9: Electroluminescence spectra of Green 1 and Green 2

From these emission spectra, it is possible to measure the CIE coordinates from each of these materials. Both materials exhibit identical CIE coordinates. The coordinates are presented on the chromaticity diagram in Figure III.10 and in Table III.3.

Green 1 and Green 2 have CIE coordinates close to those defined for the green primary colour of the sRGB system.[21] The latter is a colour space standard for computer screens developed in 1996 by Hewlett-Packard and Microsoft. Today this system is still the most common system used for computers screens. Therefore, these materials could potentially suit screen and display manufacturers.

Table III.3: CIE coordinate of Green 1 and Green 2

Green	x	y
1	0.39	0.60
2	0.39	0.60
sRGB	0.30	0.60

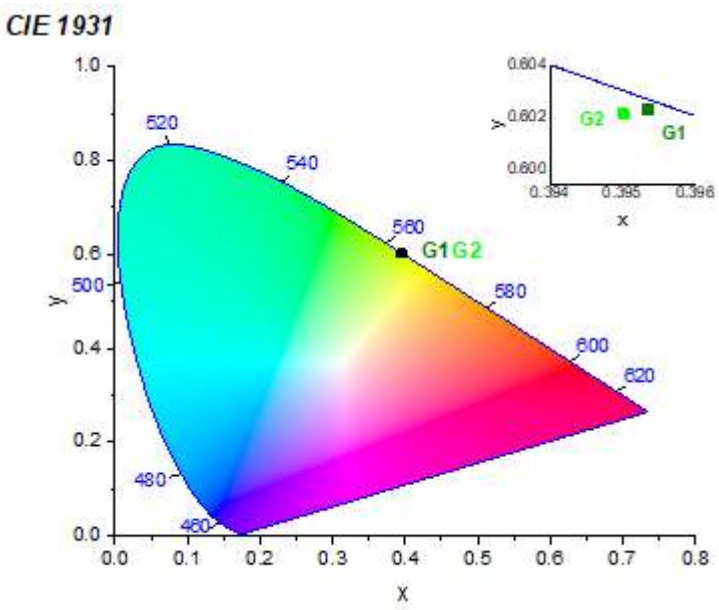

Figure III.10: CIE coordinates of Green 1 and Green 2 represented on the chromaticity diagram CIE 1931

D. Conclusion and further improvement

The substitution of trimethylsilane groups by triphenylamine groups was revealed extremely beneficial for device performance. Indeed, Green 2 demonstrated a maximum luminance of over 20 000 cd/m^2, three times higher than for the best Green 1 device. Additionally, Green 2 also offered superior performance for all other parameters such as current efficiency (2.00 cd/A instead of 1.74 cd/A) and turn on voltage (4.0 V instead of 6.0 V). This superior performance was shown to be the results of a better alignment of the HOMO energy level and a higher current flow. Both factors are consequences of the substitution of TMS group by TPA groups in Green 2 compare to Green 1.

When compared to other fluorescent green emitting small molecules, Green 2 present two advantages. Firstly, its synthesis is relatively straightforward, with only three steps and the use of commercially available materials. Secondly, the device with Green 2 exhibited very high brightness (over 20 000 cd/m^2). Indeed, fluorescent small molecules luminance is usually around a few thousands candela per square metre.[12,13]

Nevertheless, Green 2 is far from perfect. Despite its good performance, it is still quite far from the standard of high-performing green emitting devices, made from phosphorescent green emitters. As discussed, such materials can reach values of over hundreds of thousands of candela per metre squared.[11] However, as discussed, due to the fluorescent nature of Green 2, internal conversion of 100% is not possible. Another problem with Green 2 is the low current efficiency relative to the high brightness. This would suggest that good charge balance in these devices is not yet achieved and a more complex device architecture is likely necessary. The addition of a good ETL layer could prove to be beneficial to the device performances. A relatively large choice of ETL is available and a number of them would be suitable for our devices.

Dimethyl-4,7-diphenyl-1,10-phenanthroline (BCP) is commonly used with hole dominant materials, as a hole blocking materials. In their study, Moonsin *et al.*[13] made devices architectures combining PEDOT:PSS and BCP sandwiching their benzothiadiazole dendrimers and, despite exhibiting a lower luminance (4 000 to 8 000 cd/m^2) than the devices discussed here, their devices demonstrated current efficiencies of up to 10 cd/A.

Tris(8-hydroxyquinoléine)aluminium(III) (Alq_3) could also be a good match. Indeed, its LUMO is relatively close to the LUMO of Green 2 and to the work function of our electrode. At the HOMO interface of Green 2 - Alq3, an energetic barrier of 0.9 eV would help the confinement of the positive charges in the emissive material. However, Alq_3 is known to emit green light when used in a double layer type of device.[8,22,23] As such, a dual emission could be observed. However, this emission could be used to our advantage. The maximum emission of an Alq3 film is measured around 525 nm[24], therefore a hypsochromic shift could be observed, which would reduce the x axis in the CIE coordinates bringing the devices reported here closer to the sRGB standards.

III. Red OLED

A. Background

The majority of red emissive materials are either fluorescent materials used as a dopant in a matrix[25–29] or phosphorescent materials based on metal complexes,[30–32] such as iridium, ruthenium or europium. In the first category, the matrix is not always soluble and therefore only thermal evaporation is possible. Furthermore, it is important to control the exact doping level of the matrix, as there is the risk to deteriorate the colour or the luminance intensity. As for the second category of red emitters, although they generally present the highest performance, their price is also highly dependent on global supply of rare earth metals. The growing demand for such metals, whether in aerospace, surgical prostheses, supermarket case scanners or even missile guidance systems, added to their limited abundance on earth, means that they are not only scarce but expensive options for red emissive materials.

A third way to make red emitters is to develop non-doped fluorescent red materials. Such materials are often synthetically straightforward and consist of commonly available building blocks. Compared to the previous families, fewer examples of such materials are present in the literature, with even fewer cases of solution-processed materials. Wang *et al.* reported a solution-processable series of dendrimers, in which the 5,5',10,10',15,15'-hexahexyltruxene unit is employed as the node, oligo(thienylethynylene)s (OTEs) are employed as light-harvesting branching units, and 4,7-diaryl-2,1,3-benzothiadiazole is employed as the core.[33] The resulting devices showed a luminance of 2260 cd/m^2 for an efficiency of 0.11 cd/A. More recently, Khanasa *et al.*[34] reported a new molecule, CAPTB (4,7-bis{5-(*N*,*N*-bis[4-(3,6-di-tert-butylcarbazol-9-yl)phenyl]aminophenyl)-thien-2-yl}-2,1,3-benzothiadiazole). The resulting OLEDs showed a maximum luminance of 4522 cd/m^2 for devices with a single emissive layer, which increased to 12 325 cd/m^2 when an electron injection/hole blocking layer was introduced into the device.

B. Materials

The four materials presented in this study have been synthesised by Dr Neil Findlay and Valentin Fell, and will be referred to as Red 1, 2, 3 and 4. Each of these molecules have in common a 4,7-di(thiophen-2-yl)benzo[c][1,2,5]thiadiazole (BTB) core, a well-known red emitter with an emission wavelength of between 620 and 660 nm.[33–37] Red 1, 3 and 4 possess fluorene arms but differ by their end groups (TMS, TPA and benzofuran, respectively). On the contrary, Red 2 possesses the same end groups as Red 1 but the fluorene arms are extended to bifluorene. As such, Red 2 can be considered as an extended analogue of Red 1.

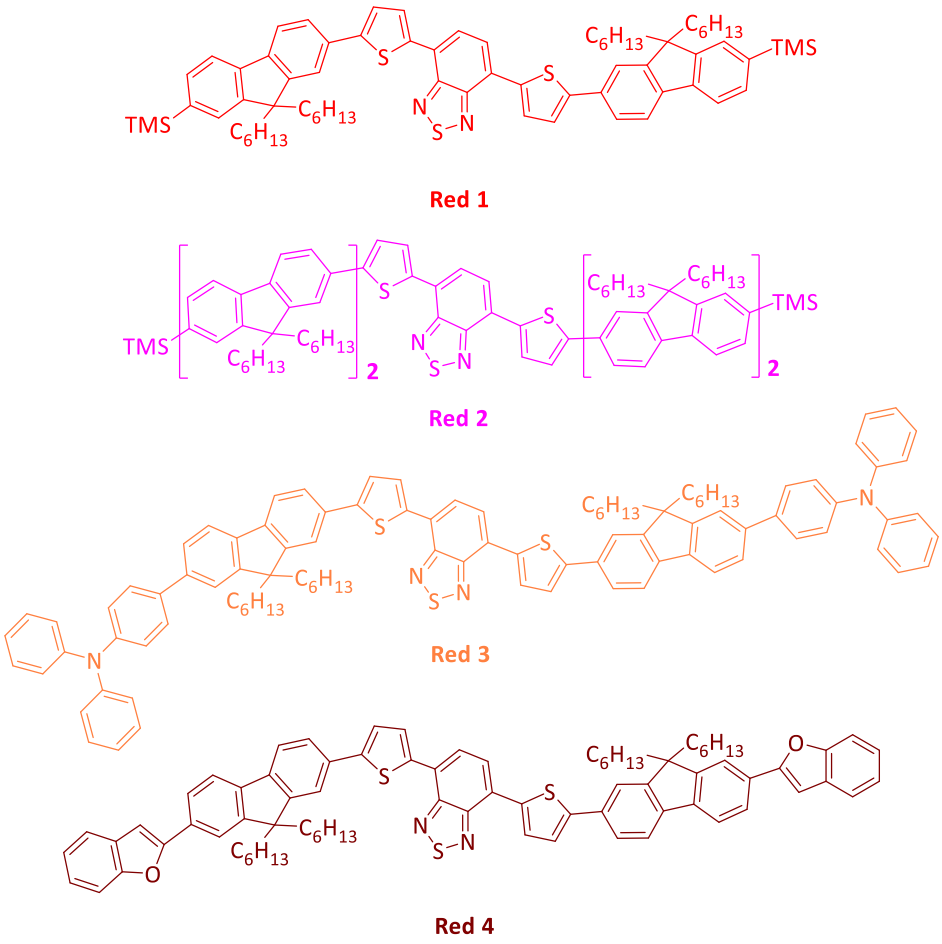

Figure III.11: Molecular structures of Red 1, 2, 3 and 4

The BTB core was constructed *via* microwave assisted Stille coupling of commercially available 4,7-dibromo-2,1,3-benzothiadiazole with 2-

(tributylstannyl)thiophene. Once formed this intermediate was brominated in the terminal α-positions using *N*-bromosuccinimide (NBS) to form the key intermediate. From there Red 1 and Red 2 were formed *via* simple Suzuki-Miyaura couplings with the appropriate mono- or bi-fluorene respectively. The synthesis of the other two compounds was more complex than expected. The first step was to brominate the terminal group of Red 1. However, this reaction showed evidence of over bromination and an alternative reaction involving the iodination of the TMS group lead to the formation of a by-product. Finally, the only working route was to use 4.4 equivalents of bromine added to a solution of Red 1 at 0 °C, followed by warming the reaction solution to room temperature overnight. This gave a conversion of 97% with an over bromination of approximately 6%. However, only a 55% yield was achieved for the formation of the brominated intermediate. The stark contrast between the efficiency of the Green 1 bromination compare to this one, suggest that the additional thiophene is the cause of these complications. The final steps in the synthesis of the two compounds were simple Suzuki-Miyaura couplings that were performed with the appropriate electron-rich terminal groups. Both reactions gave relatively low yields compared to the synthesis of other materials presented in this project, 63% and 34% for Red 3 and 4, respectively.

All the compounds showed no thermal degradation below 360°C. The increased conjugation length of Red 2 compared to Red 1 contributed to an increase of the glass transition temperature by 16°C (67°C and 83°C for Red 1 and Red 2 respectively). However, the real difference is made with the change of terminal groups. Indeed, both Red 3 and Red 4 exhibit an increased thermal stability (TGA 447°C and 408°C, respectively) and both materials show no phase transitions before their melting point at around 200°C. This higher resistance, induced by the TPA and benzofuran groups, is a positive point for the emissive layer stability.

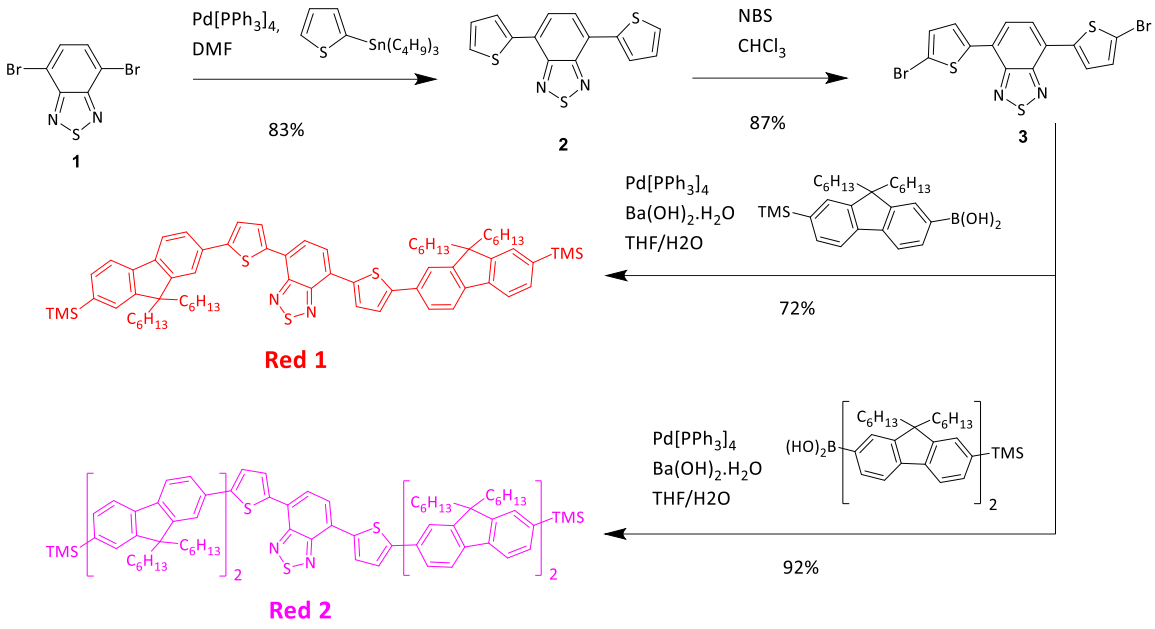

Figure III.12: Synthetic route for Red 1 and Red 2

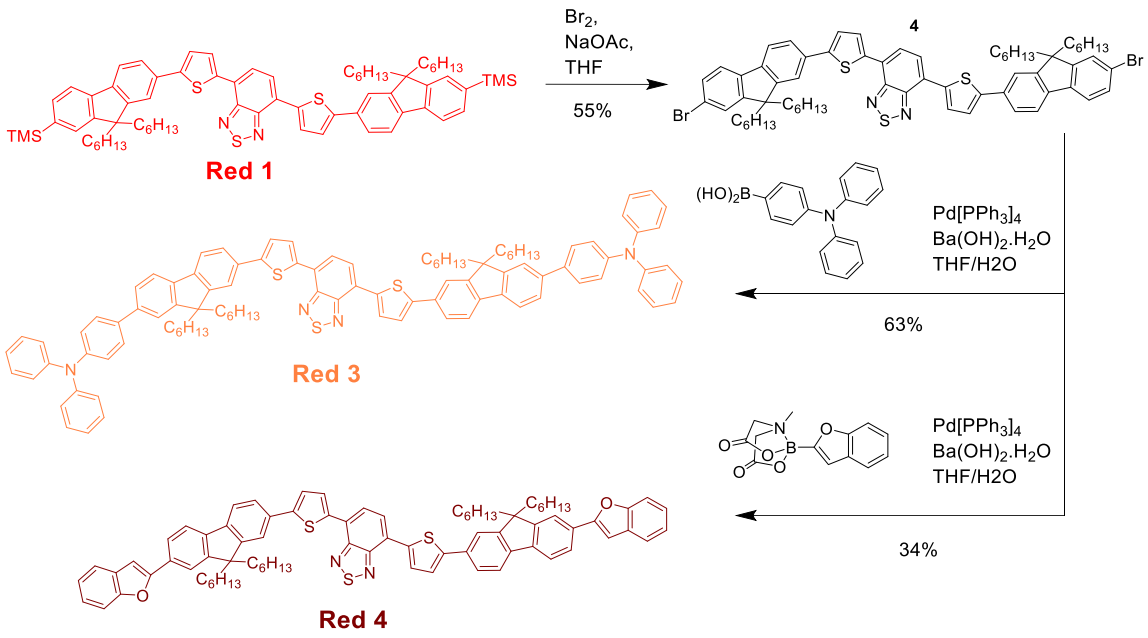

Figure III.1318: Synthetic route for the Red 3 and Red 4

The UV-Vis absorption studies were performed in dichloromethane and show similarities in the profiles but disparities in the maximum absorption wavelengths. As with the previous series, two major absorption bands were observed, with a higher intensity band at lower wavelength, which is characteristic of charge transfer. The changes made to Red 1 molecules seem to only affect the intensity of the lower

energy bands. However, a small bathochromic shift is observed for the higher energy bands. This shift follows the increased conjugation in the molecules. For the PL spectra, all solutions were excited at the wavelength of maximum absorption. The emission spectra observed for all four compounds is almost identical. This suggests that the BTB core is responsible for the emission.

The HOMO-LUMO values were determined by cyclic voltammetry (not shown). All four compounds show a very similar HOMO-LUMO gap, of around 2.0 ± 0.1 eV. Their HOMO and LUMO values are also similar with a maximum difference of 0.1 eV. These results are in contrast to the previous values obtained with the green emitters. According to the high similarity of the two series molecular structures, these limited changes in the HOMO and LUMO energy levels are attributed to the addition of thiophene to the BT core.

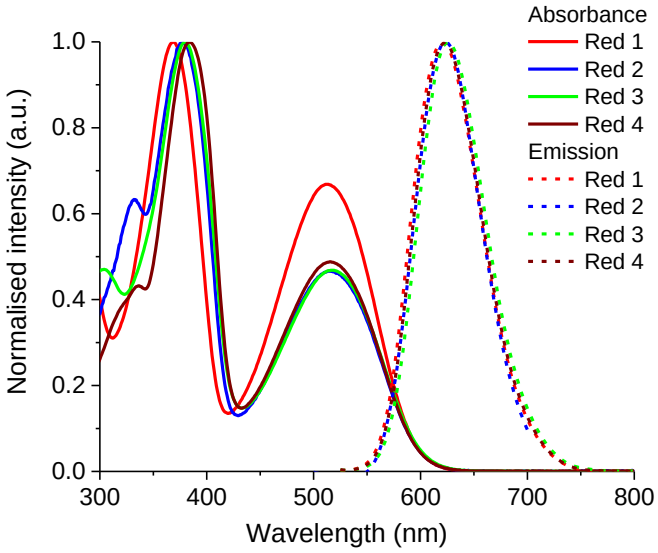

Figure III.14: Absorption and photoluminescence of Red 1, 2, 3 and 4

PLQY measurements were carried out on 90 ±10 nm thin films deposited by spin-coating on glass substrates. Red 2 and 3 showed the best results with PLQY values of over 30%. Red 4 exhibited only a small improvement with respect to Red 1 with 23.6%. Following these results Red 2 and 3 should demonstrate the best performance, followed by Red 4. Devices containing Red 1 should show the lowest

performance of the four. However, as shown for the green materials PLQY is not the only factor that influences the performance of OLEDs.

Table III.4: Optical and thermal properties of Red 1, 2, 3 and 4

Red	TGA (°C)[a]	DSC (°C)[b]	λ_{max}(abs) (nm)[c]	λ_{max}(Em) (nm)[c]	E_g(opt) (eV)[d]	PLQY[e]
1	361	67 (T_g)	369, 513	620	2.08	19.3%
2	391	83 (T_g)	377, 515	623	2.06	32.8%
3	447	241 (T_m)	380, 518	626	2.04	31.1%
4	408	210 (T_m) 224 (T_m)	384, 515	623	2.05	23.6%

[a] Temperature at which 5% mass loss occurs; [b] thermal event recorded by DSC (Tg: glass transition temperature; Tm: melting temperature); [c] recorded in dichloromethane solution (concentration of 10^{-5} M for absorption and 10^{-8} M for PL spectra); [d] calculated from the onset of the longest wavelength absorbance edge; [e] recorded from an optimised single layer device (20 mg/ml).

Table III.5: Electrochemical properties of Red 1, 2, 3 and 4

Red	HOMO (eV)[a]	LUMO (eV)[a]	E_g (eV)[b]
1	-5.24	-3.11	2.12
2	-5.14	-3.15	1.99
3	-5.24	-3.18	2.06
4	-5.30	-3.16	2.14

[a] recorded *via* cyclic voltammetry using glassy carbon, platinum wire and Ag wire as the working, counter and pseudo-reference electrodes respectively, with $(n\text{Bu})_4PF_6$ as the electrolyte in dichloromethane solution (0.1 M) at a scan rate of 100 mV/s. The data were referenced to the Fc/Fc^+ redox couple, which has a HOMO of -4.8 eV; [b] calculated by subtraction of the LUMO from the HOMO.

C. Devices

1. Concentration

As before, the first parameter that was investigated in fabrication of OLEDs containing these materials was the optimum thickness. The solution concentrations were varied from 10 mg/ml to 30 mg/ml and all solutions were spin-coated at 800

rpm for 60 s. The following conventional architecture was chosen ITO/PEDOT:PSS/Red/Ca/Al (Figure III.15).

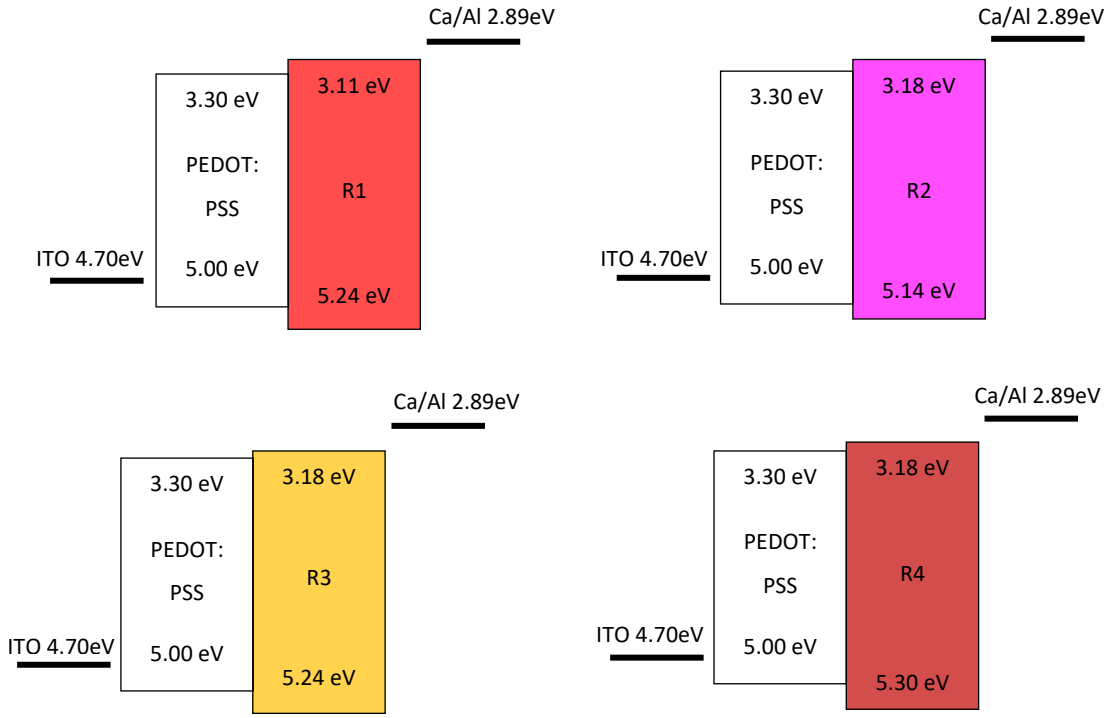

Figure III.15: Device architecture for Red 1 to 4

The results of the concentration study for Red 1 are given in Table III.6 as an example of how the emissive layer thickness influences the device performance of OLEDs made with these Red emitters (the thickness of the emissive layer was measured by AFM). The results obtained follow the trend observed with the other emissive materials from this thesis. Considering only Red 1, the turn on voltage increased by 2 volts when the thickness of the emissive layer increased from 35 to 120 nm. This increase is likely due to the increase of resistance in the emissive layer as the thickness increases. A similar effect is observed on the voltage at which the maximum luminance is recorded. The latter shows an increase of almost 6 V as a result of an increase in the thickness of the emissive layer. The luminance is also affected by this change of thickness. However, contrary to the other two factors it

does not show a continuous increase but more of a sinusoidal trend. In this example, the maximum luminance was reached with a film of 90 nm and a value of 854 cd/m^2.

A similar test was made on the other materials of the series (Annex 4). They all reveal similar behaviour and the same optimum concentration (20 mg/ml) with thickness around 90 ± 10 nm. The luminance, turn on voltage and current efficiency for each material at its optimum thickness are shown in Table III.7.

Table III.6: Concentration and thickness study on Red 1

Red	Concentration (mg/ml)	Thickness (nm)	Current efficiency (cd/A)[a]	Maximum Luminance (cd/m^2)[a]	Turn on voltage (V)[b]
1	10	35	0.03	390 (5.8)	2.7
1	20	90	0.10	854 (7.0)	2.7
1	30	120	0.06	343 (11.4)	4.6

[a]In brackets the operating voltage at which values were recorded (in Volts); [b] recorded for a luminance of 1 cd/m^2

Table III.7: Results for Red 1, 2, 3 and 4 at their optimum concentration (20 mg/ml)

Red	Thickness (nm)	Current efficiency (cd/A)[a]	Maximum Luminance (cd/m^2)[a]	Turn on voltage (V)[b]
1	90	0.10	854 (7.2)	2.7
2	100	0.15	1 561 (8.1)	2.9
3 unfiltered	80	0.051*	1 425 (14.4)	2.1
4	90	0.060	586 (7.1)	2.7

*[a]In brackets the operating voltage at which values were recorded (in Volts); [b] recorded for a luminance of 1 cd/m^2, *limited due to short circuits*

The addition of a second fluorene unit in Red 2, compare to Red 1, is shown to be beneficial to the device performance, as it allows an increase in the luminance up to 1 561 cd/m^2, which is about two times higher than Red 1. Following this increase in luminance the current efficiency is also improved and reaches 0.15 cd/A. The turn

on voltage and the operating voltage are the two factors negatively impacted. The first one increased by 0.2 V, while the second increased by 1 V. This delay in the charge injection is even more visible on the current density graphics presented in Figure III.16. Therefore, contrary to what was observed with Green 1 and Green 2, the increase of luminance is not due to improved current flow, and even happens when current flow is reduced. Instead, the PLQY of Red 2 was considerably higher than Red 1 and this better recombination rate underpins why Red 2 exhibits an improved luminance.

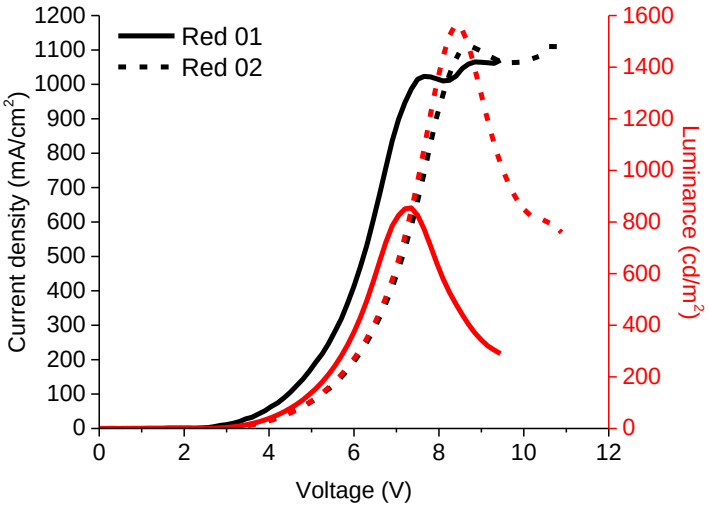

Figure III.16: Current density and Luminance versus voltage for Red 1 and Red 2

Initially Red 3 exhibited a similar luminance to Red 2, with a value of 1 425 cd/m^2 recorded. However, the current efficiency is reduced by half compared to Red 1. This is explained by the poor film quality. As seen in the optical images in Figure III.17, Red 3 presents numerous aggregates and certain areas of the substrate are not even covered by the material. Such a poor-quality film cannot properly conduct charges toward the recombination zone. To correct this problem and improve the film morphology, the solution of Red 3 was filtered through a 0.45 µm PTFE filter before deposition. As shown in Figure III.17, the filtration largely improved the film quality by removing most areas of aggregation. The results of the device made with this new film are presented in Table III.8. The new devices shown a luminance

increase of 150%, with a maximum luminance of 2 135 cd/m^2. In addition to a higher luminance, the efficiency is also increased to 0.086 cd/A compared to 0.051 cd/A for the unfiltered solution. Compared to Red 1, Red 3 (filtered) exhibits a 2.5 fold

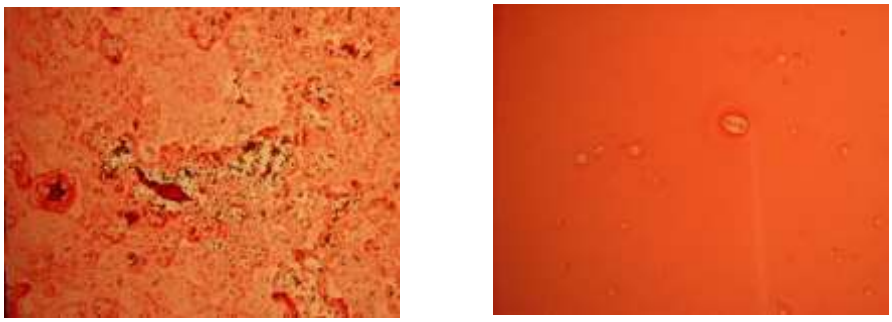

Figure III.17: Picture of the Red 3 films before (right) and after filtration (left)

increase in luminance and a lower turn on voltage at only 2.3 V. However, the current efficiency is reduced.

The overall improvement with Red 3 is due to two factors. First, as for Red 2, Red 3 showed a higher PLQY and therefore a higher recombination rate. It is most likely this factor that made Red 3 (unfiltered) luminance performed almost as well as Red 2. However, that is not a sufficient explanation alone as Red 3 (filtered) exhibits an improved performance over Red 2. The second factor is a higher current flow (Figure III.18). Indeed, Red 3 (filtered) presented a higher current flow than any other Red materials. This led to a better turn on voltage, indicative of improved charge injection, and later it will be proven to come also from a higher hole mobility (see chapter IV).

Table III.8: Devices performance before and after Red 3 filtration

Red	Current efficiency (cd/A)[a]	Maximum Luminance (cd/m^2)[a]	Turn on voltage (V)[b]
3 (unfiltered)	0.051*	1 425 (14)	2.1
3 (filtered)	0.086	2 135 (8.8)	2.3

*[a] In brackets the operating voltage at which values were recorded (in Volts); [b] recorded for a luminance of 1 cd/m^2; *limited due to short circuits.*

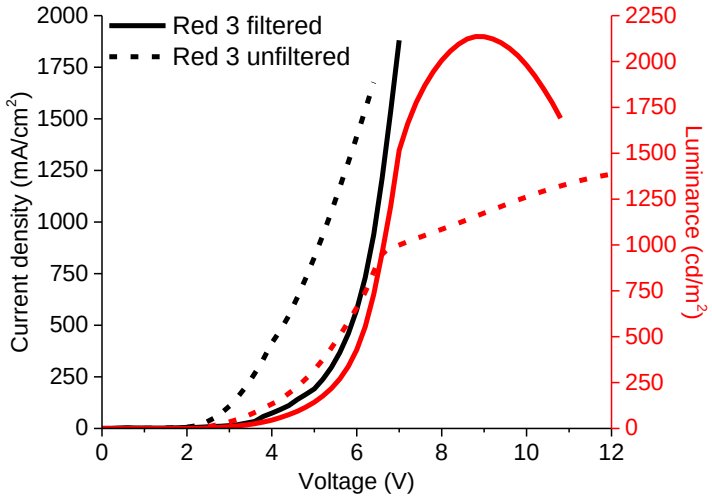

Figure III.18: Current density and Luminance versus voltage for Red 3 unfiltered and filtered

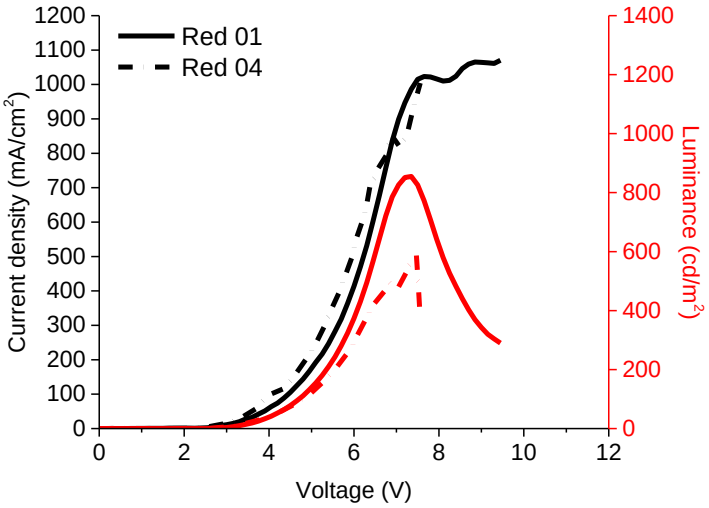

Figure III.19: Current density and Luminance versus voltage for Red1 and Red 4

With a luminance at 586 cd/m^2, a turn on voltage at 2.7 V and current efficiency of 0.6 cd/A, Red 4 exhibited the lowest performance overall. Unfortunately, the low number of results obtain with Red 4 does not allow us to properly understand why. This low number of results is primarily due to its challenging synthesis, resulting in a low amount of available product. Additionally, there was an unusually high amount of short-circuit during the tests. Of the eight OLEDs present on each

fabricated device, only two emitted light. When comparing Red 1 and Red 4, the close similarity between the current density and luminance graphs (Figure III.19) indicates that the benzofuran unit does not appear to bring any improvement in terms of charge injection or transport.

In summary, Red 3 gave the highest luminance and lowest turn on voltage over the four materials, with values of 2 135 cd/m^2 and 2.3 V recorded, respectively. The substitution of TMS groups by TPA groups was proposed to improve the recombination rate, the current flow in the device and the charge injection. However, a filtration step is necessary to obtain these results. If Red 2 is out performed in most parameters by Red 3, it does present a better current efficiency, with a maximum recorded value of 0.15 cd/A. Adding a fluorene unit on each arm seems to have increased the recombination rate (better luminance and current efficiency) compare to Red 1, however it also limited the charge injection (higher turn on voltage). The latter problem can be fixed by substituting the TMS groups by TPA groups or by adjusting the device architecture to improve charge injection.

2. Annealing

Red 1 has the lowest glass transition temperature (67°C) and an annealing test revealed that this makes it extremely sensitive to heat. Its luminance is reduced by half at 40°C, with a fourfold drop after annealing at 80°C. The average turn on voltage increased by 1.4 V when the temperature is increased to 80°C, showing an increased resistance in the material. This reduction in performance is similar to what happened with Green 1.

At first, Red 2 has a similar behaviour than Green 2. The devices performance increase at 40°C before slowly reducing after 40°C. However, contrary to Green 2, Red 2 devices do not know any drastic reduction of their performances when the annealing temperature is close to or over its *T*g (83°C). More surprisingly, the turn on voltage is stable up to 80°C and only increase by 0.3V after.

Table III.9: Values for Red 1, 2 and 3 at different annealing temperature

Red (at 20 mg/ml)	Annealing temperature (°C)	Current efficiency (cd/A)[a]	Maximum Luminance (cd/m^2)[a]	Turn on voltage (V)[b]
1	none	0.10	854 (7)	2.7
	40	0.079	440 (11)	3.6
	60	0.072	429 (10)	3.8
	80	0.060	245 (8)	3.8
2	none	0.15	1 561 (8)	2.9
	40	0.19	1 609 (9)	3,0
	60	0.17	1 409 (9)	3.1
	80	0.16	1 362 (9)	3.1
	100	0.15	1 295 (9)	3.4
3 (filtered)	none	0.086	2 135 (9)	2.3
	40	0.091	1 802 (8)	2.6
	60	0.080	1 665 (8)	2.7
	80	0.086	1 790 (8)	2.5

[a] In brackets the operating voltage at which values were recorded (in Volts); [b] recorded for a luminance of 1 cd/m^2

Red 3 only knows an improvement of its current efficiency when heated at 40°C. In counterpart, the luminance is reduced by 333 cd/m^2 and the turn on voltage is increase by 0.3 V. With further increase in temperature, the luminance oscillate between 1 660 and 1 790 cd/m^2. An oscillation that reflects on the current efficiency. As for the turn on voltage, it does not vary more than 0.1 V. Overall, after a slight reduction at first the devices performances of Red 3 seems to stabilise.

Therefore, both the increase conjugation in Red 2, via the addition of a fluorene unit, and the substitution of TMS groups by TPA groups in Red 3 are

favourable to the heat resistance of the materials. In both cases, the turn on voltage is relatively stable compare to Red 1, with a bonus for Red 2 that knows an increase only after 80°C. However, signs of thermal degradation seems to appear with Red 2, as its luminance is decreasing with the temperature after 40°C.

Therefore, both the increase conjugation in Red 2, via the addition of a fluorene unit, and the substitution of TMS groups by TPA groups in Red 3 are favourable to the heat resistance of the materials. In both cases, the turn on voltage is relatively stable compare to Red 1, with a bonus for Red 2 that knows an increase only after 80°C. However, signs of thermal degradation seems to appear with Red 2, as its luminance is decreasing with the temperature after 40°C.

D. Electroluminescence

The electroluminescence properties of the four materials were measured using the best performing devices. The four materials of the series present extremely similar EL spectra, with maximum emission peak between 650 and 656 nm. As for the Green series, a slight bathochromic shift is observed compare to the photoluminescent spectra measured in dichloromethane (maximum around 620 nm). This type of shift is expected as we pass from a solution to a thin film and it can be accorded to a phenomenon of aggregation in the film. Similarly, the widening of the emission spectra compare to the PL ones and the apparition of a small shoulder around 750 nm are common features of thiophene-benzothiadiazole based red emitting materials, when pass from solution to a thin film.[33,34,37]

The similarity between the different EL spectra confirm that the change made to the original molecules (Red 1) only have a negligible impact on the emission spectra.

Figure III.20: Pictures of devices made with Red 1 (left) Red 2 (middle) and Red 3 (right)

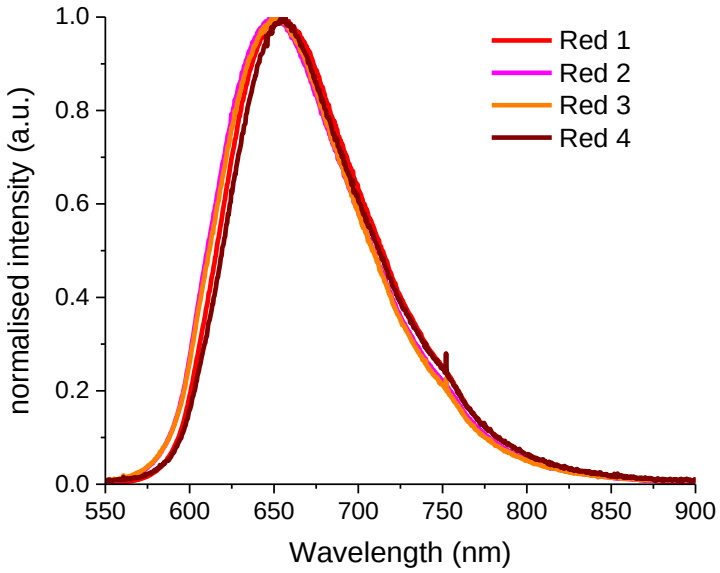

Figure III.21: Electroluminescence spectra of Red 1, 2, 3 and 4

From these emission spectra, the CIE coordinates of each material were calculated. The results are presented in the Table III.10. The CIE coordinates of the Red series do not overlap with the sRGB coordinates for primary red. This is in part due to 20% of the emission occurring in the IR (at wavelengths greater than 750 nm). This series of materials is better categorised as deep red emitters (x>0.7). However, deep red or near IR OLED emitters attracted a lot of interest lately, as the can be used in fields such as phototherapy, telecommunications or defence.[38]

Table III.10: CIE coordinate of Red 1, Red 2, Red 3 and Red 4

Red	x	y
1	0.72	0.28
2	0.71	0.29
3	0.72	0.29
4	0.73	0.28
sRGB	0.64	0.33

E. Conclusion and further work

In this series of materials, the impact of the conjugation length of the molecules on device performance was studied, *via* the insertion, in Red 1, of a second fluorene unit to form Red 2. In parallel, the trimethylsilane ending groups of Red 1 were substituted by triphenylamine (Red 3) and benzofuran (Red 4) groups in order to study their impact on the device performance.

The increased conjugation in Red 2 induced a higher recombination rate, leading to a higher luminance (1 609 cd/m^2) and the best current efficiency of the four materials (0.16 cd/A). The increase conjugation also improved the heat resistance of the devices.

The substitution of trimethylsilane by triphenylamine groups in Red 3, induce a reduction of the turn on voltage, a phenomenon which was not observed with Red 2, as well as an improvement of the luminance, by an increase of the recombination rate and a higher current flow (induced by improved mobility, see chapter IV) . Red 3 exhibits a maximum luminance of 2 135 cd/m^2 at a voltage less than 10 V and with a turn on voltage of only 2.3 V. However, the downside of this material is its current efficiency, which laboriously reached 0.09 cd/A. The similar recombination rate with Red 2 combined with a higher number of charges flowing through the device should have led to a higher efficiency than Red 2.

The overall low current efficiency observed with each molecule of the series, suggests poor confinement of the charges in the recombination zone. The potential higher charge mobility in Red 3 would hence this phenomenon, which would explain

the even lower current efficiency observed with this material. The device architecture, as well as the nature of the molecules, favour the hole mobility, therefore it is most likely that the problem is at the interface of the EM and the ETL. For example, in 2013, Prachumrak *et al.*[37], presented a solution-processed benzothiadiazole-based red emitter with a maximum luminance around 1 100 cd/m2 and a current efficiency between 0.4 and 1.15 cd/A with a simple device architecture. However, by adding a 40 nm layer of 2,9-dimethyl-4,7-diphenyl-1,10-phenanthroline (BCP), they were able to improve their device performance to 4 600 cd/m^2 and 4.80 cd/A for the luminance and the current efficiency, respectively. Due to the close structural nature of both this material and the Red series (the same BT core), if the addition of this ETL/HBL material to their device architecture was so beneficial, it is reasonable to assume that it can also boost the performance of devices containing the Red series.

The luminance performance of Red 3 is in agreement with other red emitting fluorescent material. Indeed, with a simple architecture they outperform some of the existing devices and are close to the best OLEDs presented by Wang *et al.*[33] and Li *et al.*[39] (maximum luminance of 2 260 cd/m^2 and 2 600 cd/m^2, respectively). However, Red 3 devices are largely out-performed by the devices of Khanasa *et al.*[34] with their luminance over 4 000 cd/m^2, with a simple architecture, and over 12 000 cd/m^2, when a BCP layer was added. However, in the defence of Red 3 most of these other materials discussed have CIE coordinates with an $x < 0.7$, and therefore have a lower percentage of their illumination in the IR. As the luminance sensor is calibrated to act like a human eye, with more IR emission there is a drop in luminance. The addition of an ETL layer will also induce a shift of the recombination zone away from the cathode. Rhee *et al.*[40] demonstrated that such a shift could induce a blue shift of the emission spectra, which in our case could help further improve the luminance.

IV. Bibliography

1 L. Hale and S. Guan, *Sleep Med. Rev.*, 2015, **21**, 50–58.

2 W.-J. Kim, Y.-H. Lee, T.-Y. Kim, J.-W. Hong and T.-W. Kim, *J. Korean Phys. Soc.*, 2007, **51**, 1007-1010.

3 B. Geffroy, P. le Roy and C. Prat, *Polym. Int.*, 2006, **55**, 572–582.

4 J. Marian, The illusion of RGB screens, https://jakubmarian.com/the-illusion-of-rgb-screens/, (accessed 3 May 2018).

5 A. Roorda and D. R. Williams, *Nature*, 1999, **397**, 520–522.

6 A. Stockman, D. I. A. MacLeod and N. E. Johnson, *J. Opt. Soc. Am. A*, 1993, **10**, 2491–2521.

7 K. R. Spring, T. J. Fellers and M. W. Davidson, https://www.olympus-lifescience.com/en/microscope-resource/primer/lightandcolor/humanvisionintro/, (accessed 11 October 2018).

8 C. W. Tang and S. A. Vanslyke, *Appl. Phys. Lett.*, 1987, **51**, 913–915.

9 Y. Q. Zhang, G. Y. Zhong and X. A. Cao, *J. Appl. Phys.*, 2010, **108**, 1-5.

10 C. Adachi, M. A. Baldo, S. R. Forrest and M. E. Thompson, *Appl. Phys. Lett.*, 2000, **77**, 904–906.

11 N. C. Erickson and R. J. Holmes, *Appl. Phys. Lett.*, 2010, **97**, 1-3.

12 Y. Li, A.-Y. Li, B.-X. Li, J. Huang, L. Zhao, B. Wang, J. Li, X. Zhu, J. Peng, Y. Cao, D. Ma and J. Roncali, *Org. Lett.*, 2009, **11**, 5318–5321.

13 P. Moonsin, N. Prachumrak, S. Namuangruk, S. Jungsuttiwong, T. Keawin, T. Sudyoadsuk and V. Promarak, *Chem. Commun.*, 2013, **49**, 6388–6390.

14 N. J. Findlay, B. Breig, C. Forbes, A. R. Inigo, A. L. Kanibolotsky and P. J. Skabara, *J. Mater. Chem. C*, 2016, **4**, 3774–3780.

15 J. Cornil, I. Gueli, A. Dkhissi, J. C. Sancho-Garcia, E. Hennebicq, J. P. Calbert, V. Lemaur, D. Beljonne and J. L. Brédas, *J. Chem. Phys.*, 2003, **118**, 6615–6623.

16 C. R. Belton, A. L. Kanibolotsky, J. Kirkpatrick, C. Orofi, S. E. T. Elmasly, P. N. Stavrinou, P. J. Skabara and D. D. C. Bradley, *Adv. Funct. Mater.*, 2013, **23**,

2792–2804.

17 S. Hofle, T. Lutz, A. Egel, F. Nickel, S. W. Kettlitz, G. Gomard, U. Lemmer and A. Colsmann, *ACS Photonics*, 2014, **1**, 968–973.

18 H. A. Méndez-pinzón, D. R. Pardo-pardo, J. P. Cuéllar-alvarado, J. Carlos, R. Vera and B. A. Páez-sierra, *Univ. Sci.*, 2010, **15**, 68–76.

19 I.-M. Chan, T.-Y. Hsu and F. C. Hong, *Appl. Phys. Lett.*, 2002, **81**, 1899–1901.

20 X. Zhou, M. Pfeiffer, J. Blochwitz, A. Werner, A. Nollau, T. Fritz and K. Leo, *Appl. Phys. Lett.*, 2001, **78**, 410–412.

21 R. Rehák, P. Bodrogi and J. Schanda, *Displays*, 1999, **20**, 165–170.

22 Y. Shirota, Y. Kuwabara, H. Inada, T. Wakimoto, H. Nakada, Y. Yonemoto, S. Kawami and K. Imai, [4,4',4]-tris(3-methylphenylphenylamino)triphenylamine, as a hole transport material, *Appl. Phys. Lett.*, 1994, **65**, 807–809.

23 J. U. Wallace, PhD thesis, University of Rochester, 2009.

24 G. Baldacchini, T. Baldacchini, A. Pace and R. B. Pode, *Electrochem. Solid-State Lett.*, 2005, **8**, J24–J26.

25 T. H. Liu, C. Y. Iou and C. H. Chen, *Appl. Phys. Lett.*, 2003, **83**, 5241–5243.

26 Y. S. Yao, Q. X. Zhou, X. S. Wang, Y. Wang and B. W. Zhang, *Adv. Funct. Mater.*, 2007, **17**, 93–100.

27 K. H. Lee, S. M. Kim, J. Y. Kim, Y. K. Kim and S. S. Yoon, *Bull. Korean Chem. Soc.*, 2010, **31**, 2884–2888.

28 C. H. Chen, C. W. Tang, J. Shi and K. P. Klubek, *Thin Solid Films*, 2000, **363**, 327–331.

29 H. Fu, Y. Zhan, J. Xu, X. Hou and F. Xiao, *Opt. Mater. (Amst).*, 2006, **29**, 348–354.

30 J. Kido, H. Hayase, K. Hongawa, K. Nagai and K. Okuyama, *Appl. Phys. Lett.*, 1994, **65**, 2124–2126.

31 F. Ali, P. K. Nayak, N. Periasamy and N. Agarwal, *J. Chem. Sci.*, 2017, **129**, 1391–1398.

32 W. Cho, G. Sarada, A. Maheshwaran, Y.-S. Gal, Y. Nam, J. Yong Lee and S.-H. Jin, *J. Mater. Chem. C*, 2017, **5**, 10029–10038.

33 J. L. Wang, Y. Zhou, Y. Li and J. Pei, *J. Org. Chem.*, 2009, **74**, 7449–7456.

34 T. Khanasa, N. Prachumrak, R. Rattanawan, S. Jungsuttiwong, T. Keawin, T. Sudyoadsuk, T. Tuntulani and V. Promarak, *Chem. Commun.*, 2013, **49**, 3401–3403.

35 S. Kato, T. Matsumoto, T. Ishi-i, T. Thiemann, M. Shigeiwa, H. Gorohmaru, S. Maeda, Y. Yamashita and S. Mataka, *Chem. Commun.*, 2004, **1**, 2342–2343.

36 Y. Wang, J. Huang, H. Zhou, G. Ma, S. Qian and X. H. Zhu, *Dye. Pigment.*, 2012, **92**, 573–579.

37 N. Prachumrak, S. Pojanasopa, S. Namuangruk, T. Kaewin, S. Jungsuttiwong, T. Sudyoadsuk and V. Promarak, *ACS Appl. Mater. Interfaces*, 2013, **5**, 8694–8703.

38 Y. Li, X. Gao, L. Wang and G. Tu, *RSC Adv.*, 2017, **7**, 40533–40538.

39 D. Li, K. Wang, S. Huang, S. Qu, X. Liu, Q. Zhu, H. Zhang and Y. Wang, *J. Mater. Chem.*, 2011, **21**, 15298–15304.

40 S. H. Rhee, C. S. Kim, M. Song and S. Y. Ryu, *Org. Electron.*, 2017, **42**, 343–347.

Chapter IV: Charge carrier mobility measurements and their influence on the performance of OLED devices

I. Introduction

The mechanism for organic light emitting diodes is based on the transport of charges (positive and negative) into the emissive material, where they can form an exciton.[1,2] Two parameters are therefore crucial for emissive materials: their capacity to form excitons (the recombination rate) and their capacity to transport holes and electrons (their charge carrier mobilities). The charge carrier mobility is defined as the speed (in cm/s) at which the charges move through the material, in one direction, in the presence of an electric field (V/cm). In this aspect, the charge mobility will directly influence the luminance, as it will affect the current flowing in the device.[3] The current efficiency can also be influenced by the charge carrier mobilities, either indirectly via a change in the luminance or directly via the charge balance.[4,5] As a majority of emissive materials are hole dominant[6] (their hole mobility is higher than their electron mobility) the charge balance is usually rectified by the addition of an electron transport layer or a hole blocking layer. Meerheim *et al.*[7] and Lee *et al.*[8] demonstrated that to obtain highly efficient devices the recombination zone should be broad and centred, and for that a perfect charge balance is necessary. The measurement of such charge carrier mobilities is, therefore, extremely important in order to fully understand the properties of an active material and to adapt the device architecture to improve its performances.

Mobilities in organic semiconductors are typically between 10^{-7} to 10^{-3} $cm^2/(V.s)$, while inorganic semiconductors can present mobilities of around 10^2 $cm^2/(V.s)$.[9,10] Tiwari *et al.*[11] classify the main techniques to measure an organic material mobility into four categories. The doping generated, such as charge

extraction by linearly increasing voltage (CELIV) and conductivity measurements; the photo generated, with time of flight (TOF) and Auston-Switch photoconductivity; the injection generated techniques, such as transient electroluminescence and space charge limited current (SCLC); and the electric field generated technique, based on organic field-effect transistors (OFET).[11]

Photo-generated TOF is probably the most popular method.[12] In this case, the material is sandwiched between two electrodes and charges are generated under the top electrode, usually via a short-pulsed laser. With the help of an electric field, the charges are swept across the material to reach the bottom electrode. The time these charges take to reach the second electrode is measured and related to the mobility. However, a number of constraints must be met for this technique to work. One of the main constraint with organic material is the necessity to have a strong absorption of the emitted light. With their absorption coefficient, this means a sample thickness of up to few microns.[13] Such thick layers are not always a good representation of the reality, as most devices will have layers between ten to one hundred nanometres. Another popular method is CELIV, however it requires a sufficiently conductive film, which can be challenging as most organic materials present relatively low conductivities. Additionally, the polarity of the charges measured are difficult to identify.

The two methods used in this chapter are SCLC and OFET. SCLC is becoming more and more popular as it only requires modest equipment and it most closely reproduces the layer thickness observed in devices.[14] As for OFET, it benefits largely in the continuous development of proper organic field effect transistors to offer more and more accurate measurements.

II. Organic field-effect transistors

A. Theory

The idea of a field-effect transistor (FET) was first presented and patented by Lilienfeld,[15] in 1930. He proposed that a field-effect could help the transport of carriers from a source to a drain electrode. In other words, transistors are electrical

switches that can be turned on and off according to the electrical potential applied to them. Thirty years later, Kahng and Atalla presented the first silicon-based metal-oxide-semiconductor (MOSFET), at the IRE Solid-State Devices Research Conference in Pittsburgh.[16] Nowadays, MOSFETs are probably the most used type of transistor in the world. They are used as amplifiers, current limiters or analogue switches in most electronic systems.

A majority of these field-effect transistors are based on amorphous silicon (α-Si), however more and more organic based FET are commercialised. The first organic based FET was reported in 1986 by Tsumura *et al.*[17] and it used polythiophene as a conductive material. Organic field-effect transistors (OFET) present several advantages over their inorganic counterparts, such as a lower cost of fabrication, their lightweight nature and the possibility to produce even smaller transistors. Additionally, as with OLEDs, the use of organic materials offers the possibility for solution processing and more importantly, the deposition on flexible substrates.

There are three commonly accepted OFET architectures: bottom gate – bottom contact (BGBC), bottom gate - top contact (BGTC) and top gate - bottom contact (TGBC) (Figure IV.1).

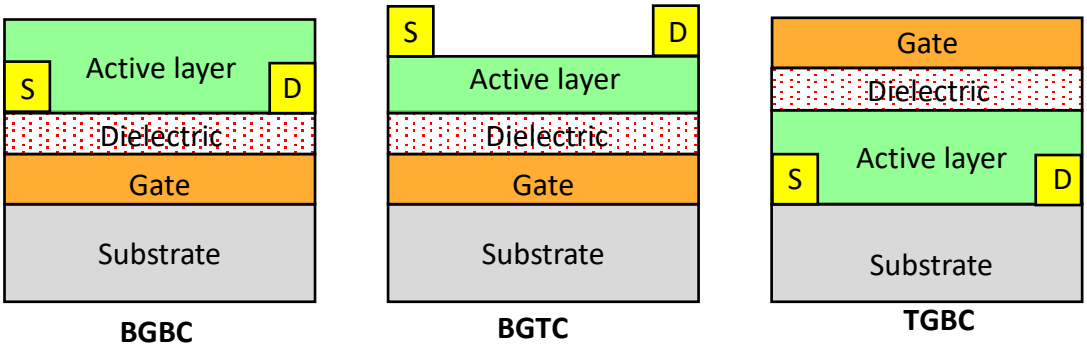

Figure IV.1: OFET architectures. S-Source and D-Drain.

The three essential components of any OFET are the three electrodes: the source, the drain and the gate. The latter is typically made of doped silicon. The other two are made of diverse metals according to the active layer material used and the type of charge carriers measured. For p-type materials high work function metals like gold, silver or platinum are used whereas for n-type materials low work function

metals such as calcium are used. In order to obtain a closer match with the HOMO or LUMO of the organic material, some layers, usually self-assembled monolayers (SAM), can be added on top of the electrodes.[18] The dielectric or insulating layer is typically composed of few hundred nanometres of thermally grown silicon oxide (SiO_2). However, insulating polymers, like poly(4-vinyl phenol) or polyvinyl alcohol, will be favoured in the case of flexible devices.[19]

In the operation of OFETs, a potential is applied at the gate (Vg), thus resulting in the generation of a large electric field at the dielectric-active layer interface. If a negative (positive) current is applied between the source and the gate then positive (negative) charges are attracted toward the dielectric-active layer interface. By applying, a second potential between the source and the drain, carriers can be injected in the semiconductor and flow from the source to the drain due to this newly generated electric field. The higher the voltage applied to the gate, the stronger the electric field will be, and more charge will be able to flow from one electrode to the other.

The performance of organic field-effect transistors is characterised by three main parameters: charge carrier mobilities (μ_h for holes, μ_e for electrons), on/off current ratio (I_{on}/I_{off}) and threshold voltage (V_{th}). The latter marks the voltage required to turn the transistor on. In other words, the minimum voltage that needs to be applied to the gate to obtain a sufficient electric field for a current to be measured at the drain. When the drain-source current (I_{ds}) is measured as a function of the drain-source voltage (V_{ds}), while keeping the gate-source voltage constant, the I-V characteristics are classified as output parameters. Transfer parameters are considered when the I_{ds} is measured as a function of the V_{gs}, while keeping the V_{ds} constant (Figure IV.2).

Two regimes are usually observed in OFET I-V curves. The linear regime, when V_{ds} is smaller than V_{gs}, the current is then linearly proportional to V_{gs} (eq. 1), and a saturation regime, when V_{ds} is bigger than (V_{gs} - V_{th}) (eq. 2).[20]

$$I_{ds} = \frac{w}{L}\mu_{lin}C_i\left(V_{gs} - V_{th}\right)V_{ds} \quad (eq.1)$$

$$I_{ds} = \frac{w}{2L}\mu_{sat}C_i(V_{gs} - V_{th})^2 \qquad (eq.2)$$

Charge carrier mobility is usually calculated from the saturation regime by plotting $\sqrt{I_{ds}}$ versus V_{gs} to extract the slope of the curve and use it in equation 3.

$$\mu_{sat} = \frac{2L}{wC_i} \times \left(\frac{\partial\sqrt{I_d}}{\partial V_g}\right)^2 \qquad (eq.3)$$

Where L is the channel length and w its width and C_i is the capacitance per unit area of the insulator material.

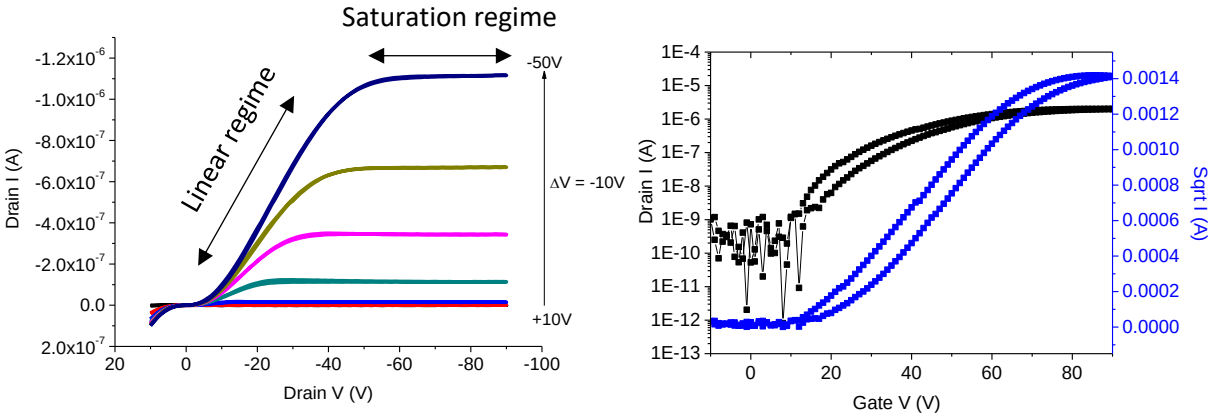

Figure IV.2: Example of output (left) and transfer (right) characteristic measure for Green 2 at a channel length of 20 µm

B. Measurement of the hole mobility for Green and Red materials

The transistors used in this study are commercially available substrates from Fraunhofer IPMS. The gate is n-doped silicon with thermally activated silicon oxide on top for the dielectric layer. The source and the drain are made of gold. The use of gold makes these transistors generally more suitable for hole mobility measurements, which is the charge carrier mobility of interest in the case of our emissive materials. As mentioned earlier most emitting materials are in fact hole dominant, which means that the current flow will be driven by hole transport.[5] Prior to the deposition of the organic materials, the transistors were washed in diverse solvents (water, acetone, isopropanol) before having their surface modified by a

combination of SAMs (necessary for a better contact) and deposition of the organic material (see chapter VI).

As Green 1 and 2 have previously been studied for potential applications in OFETs, the results presented here are the highest values obtained after optimisation.[21] On the contrary, the Red devices did not undergo any optimisation. Table IV.1 presents the OFET results obtained with the Red and the Green series, while Table IV.2 compares the hole mobility and the devices performance observed in the previous chapter. The output and transfer graphs for each materials are presented in the annex (annex 5 to 9).

Table IV.1: Green and Red series holes mobilities

Green	Hole mobility ($cm^2/(V.s)$)	V_{th} (V)	I_{on}/I_{off}
1[a]	$3.93x10^{-5} \pm 8.21x10^{-6}$	-42 ± 9	$6.38x10^{3} \pm 1.17x10^{3}$
2[b]	$2.03x10^{-4} \pm 6.60x10^{-5}$	-16 ± 7	$5.09x10^{3} \pm 3.20x10^{3}$
Red	**Hole mobility ($cm^2/(V.s)$)**	**V_{th} (V)**	**I_{on}/I_{off}**
1[a]	$7.28x10^{-6} \pm 1.52x10^{-6}$	-44 ± 2	$4.28x10^{2} \pm 2.62\ x10^{2}$
2[b]	$3.92x10^{-6} \pm 1.38x10^{-6}$	-35 ± 5	$2.17x10^{3} \pm 2.82\ x10^{3}$
3[c]	$1.81x10^{-5} \pm 3.15x10^{-6}$	-29 ± 1	$9.06x10^{3} \pm 8.61x10^{3}$

[a] Average over 3 values ; [b] Average over 4 values ; [c] Average over 7 values

Table IV.2: Device performances and mobility for the Green and Red series

Material	Highest luminance recorded (cd/m^2)	Best current efficiency (cd/A)	Hole mobility ($cm^2/(V.s)$)
Green 1	6 724	1.74	$3.93x10^{-5}$
Green 2	20 388	2.06	$2.03x10^{-4}$
Red 1	854	0.10	$7.28x10^{-6}$
Red 2	1 609	0.19	$3.92x10^{-6}$
Red 3	2 135	0.091	$1.81x10^{-5}$

A large increase of current flow, which lead to a higher luminance, was observed with Green 2 compared to the devices made with Green 1. The first factor explaining this phenomenon was the difference in HOMO levels between the two materials. Indeed, the HOMO level in Green 2 (5.07 eV) compared to Green 1 (5.37 eV) was a better match with the PEDOT:PSS HOMO (5.00 eV), thus inducing a better charge injection from the HTL to the active layer. However, a second factor explaining this luminance increase is presented here. Indeed, Green 2 exhibits a hole mobility around 10^{-4} $cm^2/(V.s)$ whereas Green 1 only exhibits a mobility of around of 10^{-5} $cm^2/(V.s)$. A hole mobility increase inevitably means that more charges are carried to the emissive layer, therefore, increasing the possibility for recombination.

As for Green 2, a higher luminance was recorded with Red 3 compare to the other materials of the same series. The first factor to explain this enhancement is a higher recombination rate. Nonetheless, it is not enough to fully explain the luminance improvement. Besides it does not explain the higher current flow observed with this material. Similarly, to Green 2, the second factor capable of explaining this enhancement is an increase of mobility, which we demonstrated here. Indeed, Red 3 exhibits a mobility of around of 10^{-5} $cm^2/(V.s)$, while the other two red materials only present a hole mobility of around of 10^{-6} $cm^2/(V.s)$.

For both Green 2 and Red 3, the trimethylsilane (TMS) ending groups, present on Green 1 and Red 1, were substituted by triphenylamine (TPA) groups. TPA moieties are known to be excellent hole transport entities and have been proven multiple time to have the capacity to enhance the hole mobility of different molecules.[22–24] TPA owes this property to the capacity of its nitrogen atom to easily oxidise, allowing for the formation of a radical cation, and to a sufficient stability of this cation to undergo numerous redox cylcles.[25] Therefore, the similarity observed in Green 2 and Red 3 mobilities enhancement can be attributed to the replacement of TMS groups by TPA groups.

Red 2 also exhibits a luminance increase over Red 1 (1 609 cd/m^2 and 854 cd/m^2 respectively), however the current flow of both series of devices follows a similar trend. After measuring the mobility of both material, we can confirm that the increase luminance is not due to a mobility improvement, as the mobility of Red 2 is even lower than Red 1. Therefore, the main factor for this enhancement is the recombination rate improvement observed with Red 2.

One aspect that was difficult to explain in the previous chapter (chapter III) was that Red 3 had the lowest current efficiency despite having the highest luminance of the three materials. Considering that the current efficiency is highly impacted by the charge balance[4,6–8] and that, in the case of the Red series, the efficiency seems to be inversely proportional to the hole mobility. The increase of hole mobility in Red 3 could be unfavourable to the charge balance. Thus, the addition of an ETL to improve the electron mobility is even more important if we want to improve the device performances. A similar theory can be assumed to explain the relatively low increase in current efficiency with Green 2 despites the large luminance increase. Of course, in order to confirm this theory the electron mobility must be measured. However, such measurements by OFET can reveal extremely tricky. First, the OFET design must be rethink, as this time electrodes near the LUMO level of our compounds are necessary. The second problem we would face is the potential low values of mobilities. Indeed, lower is the mobility harder it will be to obtain a good saturation and more important will be the noises on the graphs. Already with the hole mobility measurement of the Red series, the noises are clearly visible on the transfer graphs (see annex 5-9). Our material being hole dominant it is to assume that the electron mobilities of these materials should be even lower than the hole mobilities.

III. Space charge limited current

C. Theory

Space charge limited current (SCLC) is based on the study of I-V curves obtained from diode-like devices. The studied materials are usually sandwiched between two electrodes, chosen to carry preferentially only one type of charge

carrier. These are often termed electron or hole only devices. In theory, space charge limited current is considered as one of the simplest and most versatile forms of mobility characterisation.[26] Additionally, contrary to a number of other techniques where the measurement happens parallel to the substrate plane, in SCLC the measurement happens perpendicular to the substrate plane, which is a closer mimic to the current flow in OLEDs or OPVs.[27] The combination of these advantages, combined with the modest equipment requirement, makes SCLC a very attractive method for measurement of mobilities.

Space charge limited current is observed when the number of injected charges reaches its maximum, because their electrostatic potential prevents the injection of additional charges, and therefore a new charge can be injected in the material only when another is extracted by the counter electrode. At this moment, the current is considered transport limited and not injection limited and the contact of the electrode-organic layer is considered ohmic.[11] In these conditions and assuming a uniform charge carrier mobility in the material, the current density (J) is a function of the applied voltage (Va), the film thickness (t), the permittivity of the film (ε) and the charge carrier mobility (μ) according to the Mott Gurney law presented in equation 4.

$$J = \frac{9\,\varepsilon\,\mu\,{V_a}^2}{8\,t^3} \quad (eq.4)$$

It is important to note that for the above equation to be applicable it is necessary to make the following assumptions:

- The devices must be unipolar. Only one charge carrier (electrons or holes) is progressing through the device. This is usually achieved by choosing a suitable combination of electrodes according to their work function. For ambipolar materials, such as the majority of emissive materials, checking for light emission is a common test for bipolar charge transport. Indeed, if light is observed then electron-hole recombination is occurring and the devices are unsuitable for SCLC measurement. However, the absence of light emission does not mean

the devices are unipolar. This feature is why the measurement of ambipolar emissive materials can be extremely complicated.

- Both the carrier mobility (μ) and the dielectric permittivity (ε) are constant through the material. Although the value of ε can sometimes be difficult to measure, most organic materials are known to have a dielectric constant of between $3.0\varepsilon_0$ and $4.0\varepsilon_0$, with ε_0 the permittivity of free space. Therefore, a median value of $3.5\varepsilon_0$ is usually assumed.[14]

However, it is important to note that even when all these conditions are met certain disparity can be found in the mobility measured for the same material. In 2013, Blakesley *et al.*[14] sent identical devices to two laboratories and asked three different scientists to analyse all the data measured. They discovered that the data could vary by a few orders of magnitude according to the lab or the scientist. They linked this disparity to different experimental methods and different analysis methods. Therefore, when the aim is to measure the mobility of similar materials they recommend a "benchmark" measurement. The values are extracted from a single device, or even a single I-V and a simple analysis is applied. This type of measurement can be used for comparison only if the same experimental method is applied to the measurement of all the materials. Additionally, such values are only indicative and should not be used to compare to other mobilities using different measurement methods or different experimental procedures.

D. Space charge limited current for electron mobility measurement of ETLs/HBLs

As explained in the introduction, the addition of an electron transport layer or a hole blocking layer is relatively common to compensate for the hole dominance of most organic emissive materials. These layers can be a key part of any device architecture and their impact on the device performances is not negligible. They can serve multiple purposes from reducing the barrier of energy between the emissive layer LUMO and the cathode work function to improving the introduction of

electrons in the emissive layer or influencing the recombination zone position in the devices.[8,28,29]

An ETL is usually characterised by its electron mobility and its HOMO-LUMO levels. It was demonstrated by Rhee *et al*.,[30] *via* the study of four ETLs with different mobilities, that a change in the electron mobility can influence the zone where the recombination takes place in a device. Such a change can then improve the device performance by shifting this zone away from the electrodes and closer to the centre of the device. In the same study, they also demonstrated the importance of the hole blocking properties of an ETL on the current efficiency. Indeed, a good capacity to block the holes from leaking out of the emissive layer, a capacity usually achieved by an ETL with a higher energy HOMO than the HOMO of the emissive layer, can enhance the chances of recombination and therefore the current efficiency.[30]

The development of electron transport materials with good electron mobility, a LUMO close to the cathodic work function and with a sufficiently low HOMO level, is crucial to the development of OLEDs. In this aspect, two new TPBI derivatives were synthesised within the Skabara laboratory in order to be used as ETL/HBL in OLED devices. The molecular structure of the two derivatives is presented in Figure IV.3. TPBi or 2,2’,2"-(1,3,5-benzinetriyl)-tris(1-phenyl-1-H-benzimidazole) (Figure IV.2) was chosen as a base material, as it is already a common ETL/HBL molecule, with a LUMO of around 2.7 eV and a HOMO of around 6.2 eV.[31–33] The mismatch of HOMO levels with the materials presented here, Green and Red series (HOMO level at 5.00-5.30 eV) would perfectly enhance the hole blocking properties of TPBi. Another advantage of TPBi is that it can be deposited by solution processing, which increases its range of applications.

The aim of these two derivatives is to keep the hole blocking properties of TPBi while increasing their electron mobility. While both TPBi and OA67 are soluble in chloroform, 3-COOK is soluble in water and methanol. Emissive materials are less commonly soluble in the latter solvent. This property is extremely useful to develop all solution processed OLEDs, as it minimises the risk of damaging the active layer

while depositing the ETL/HBL. All three molecules used in this study were synthesised by Olena Avramchenko, however their synthesis will not be discussed here.

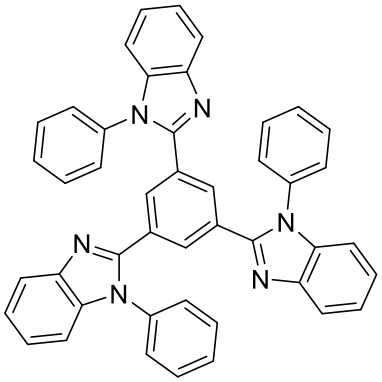

Figure IV.2: Molecular structure of TPBi

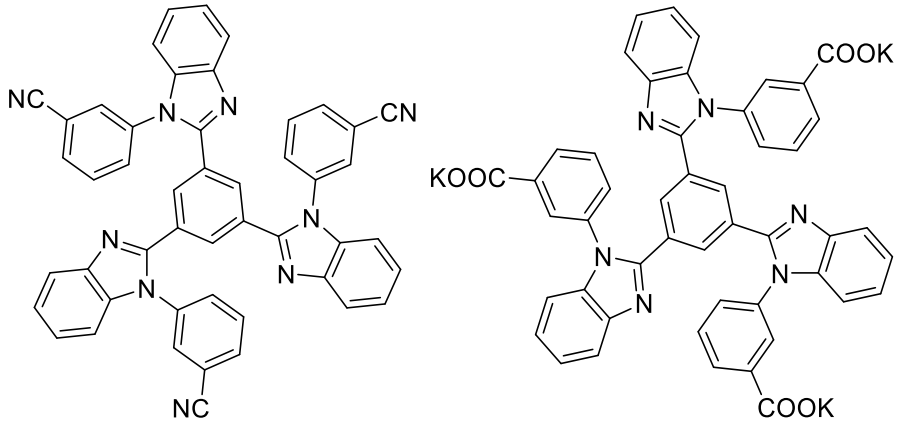

Figure IV.3: TPBI derivatives synthesised by Olena Avramchenko; OA67 (left) and 3-COOK (Right)

The SCLC technique will be used to measure the electron mobilities of all the materials. The electron mobility of TPBi will be measured as both a thermally evaporated and solution processed layer.

As mentioned previously, the device architecture in SCLC is extremely important. The HOMO and LUMO of TPBi have been reported to be around 6.2 eV and 2.7 eV, respectively. Therefore, a top electrode of calcium/aluminium ($Ø_m$: 2.9 eV) is the best option. SCLC only requires one electrode to inject the required charges (in this case, electrons) while the other blocks the injection of the opposite charge (holes). Due to the relatively high value for the HOMO of TPBi, it is possible to use

common metals such as aluminium (4.2 eV) or silver (4.7 eV), or ITO (4.7 eV) as a blocking electrode without risking hole injection into the device (Figure IV.5). A layer

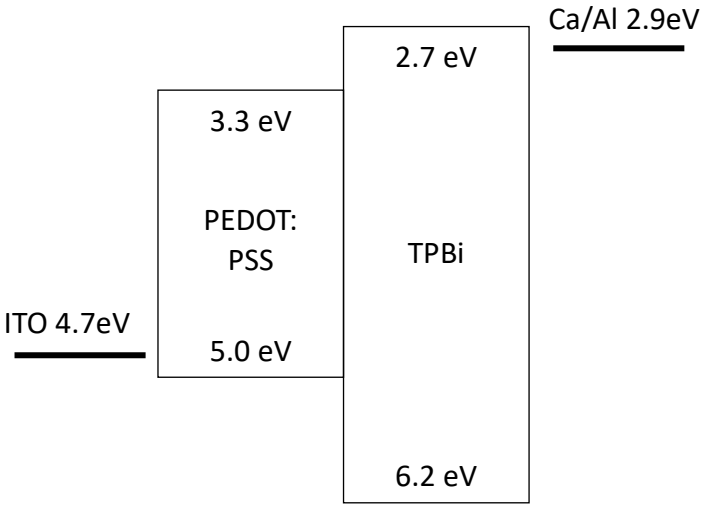

Figure IV.4: Device architecture for SCLC measurement of TPBi

of PEDOT:PSS is used on top of ITO in order to smooth its surface and favour the deposition of a thin layer of organic material.

In the first series of devices, a 120 nm layer of TPBi was thermally evaporated, whereas in second series TPBi was solution processed from a 20 mg/ml chloroform solution deposited *via* spin coating (800 rpm for 60s). The results are presented in Table IV.3. The thickness was measured via AFM (see chapter VI). The literature values[34] presented here were measured by TOF. In this case the sample was deposited *via* thermal evaporation with a thickness of 1 to 2 µm.

Table IV.3: Electron mobility for TPBi

Material	TPBi (TOF)[34]	TPBi (evap.)	TPBi (solution)
Thickness (µm)	2	0.120	0.195
Electron mobility ($cm^2/(V.s)$)	3-8 x 10^{-5}	1 x 10^{-4}	2 x 10^{-5}

The thermally evaporated series of devices exhibited the highest mobility at 10^{-4} $cm^2/(V.s)$ whereas the solution processed series was determined to be at the lower limit of the electron mobility reported in the literature. The difference in results

is not so surprising as it has been shown that solution processed TPBi can demonstrate lower performances than with devices involving thermal evaporation.[32]

The HOMO-LUMO of the two derivatives were measured by cyclic voltammetry (not shown here). OA67 exhibits a HOMO of 6.01 eV and a LUMO of 2.47 eV while 3-COOK presents a HOMO at 6.08 eV and a LUMO at 2.7 eV. These values are coherent with the TPBi ones. Therefore, the same device architecture used with TPBi can be used for the SCLC measurements of the derivatives. The results are shown in Table IV.4. As both demonstrated similar properties to TPBi and most importantly similar HOMO and LUMO energy levels, the same architecture was kept for these tests. Both materials were developed to be solution-processed materials and therefore both were deposited *via* spin-coating (800 rpm for 60 s). OA67 was also deposited from a chloroform solution (like TPBi), while 3-COOK was deposited from a methanol solution, due to its increased solubility in this solvent. The thickness was measured *via* AFM.

Table IV.4: electron mobilities for TPBi derivatives

Material	TPBi (solution)	OA67	3-COOK
Thickness (µm)	0.195	0.121	0.094
Electron mobility ($cm^2/(V.s)$)	$2x10^{-5}$	$1x10^{-4}$	$4x10^{-4}$

[a] The values presented in this table are an average over 6 values taken from 2 different devices (apart from the TOF measurement).

Both materials exhibited a mobility around or over 10^{-4} $cm^2/(V.s)$, with 3-COOK presenting the highest mobility value of $4x10^{-4}$ $cm^2/(V.s)$. However, it is important to specify that 3-COOK is a potassium salt and therefore its permittivity may be slightly higher than OA67. Thus, its real electron mobility might be slightly lower. Most importantly, both materials presented a significant improvement in their mobility compared to solution processed TPBi. As such, the addition of potassium carboxyl groups or cyano groups was proven beneficial in the development of solution processed ETL/HBL materials with high electron mobility. The possibility to deposit 3COOK from methanol gives it a high potential as a solution processable ETL.

IV. Conclusion

Charge carrier mobility is a crucial parameter to understand the inner mechanism of OLEDs. In this chapter, OFET measurements were used to calculate the hole mobilities of the different materials from the Green and Red series, presented in chapter III. From the values obtained, it can be concluded that the presence of triphenylamine (TPA) groups in Red 3 and Green 2 enhanced the hole mobility compared to their reference materials (Red 1 and Green 1, respectively). This enhancement leads to a higher current flow in the devices, one of the factors that explains the increased luminance observed in devices with these materials.

Red 2 also showed an increased luminance compared to Red 1, however no hole mobility enhancement was observed. This confirms that in this case the improvement in luminance is not due to an increased mobility of the dominant charge carrier but to the higher rate of recombination (see chapter III).

The low current efficiency of Red 3, despite its high luminance, and the inversely proportional relation between the current efficiency and the hole mobilities in the Red series led to the conclusion that the increase in hole mobility for Red 3 unfavourably affects the charge balance in the device. Therefore, in order to obtain an efficient device an ETL/HBL layer should be added to the device architecture with Red 3. Similarly, the same type of layer could be beneficial to Green 2 as well.

The two TPBi derivatives (OA67 and 3-COOK) presented in this chapter are excellent candidates for ETL/HBL. Their high LUMO levels afford good hole accumulation properties while their high electron mobilities make them very good electron transporting materials. In the development of all-solution-processed materials, 3-COOK presents the advantage of being processable via polar solvents like methanol. This property means that the 3-COOK layer could be deposited on top of Red 3 or Green 2, while minimising the chance of damaging adjacent layers with solvent and causing interlayer mixing.

V. Bibliography

1 Z. Deng, S. T. Lee, D. P. Webb, Y. C. Chan and W. a. Gambling, *Synth. Met. J. Electron. Polym. Electron. Mol. Mater.*, 1999, **107**, 107–109.

2 T. Okachi, T. Nagase, T. Kobayashi and H. Naito, *Jpn. J. Appl. Phys.*, 2008, **47**, 8965–8972.

3 H. Mu, D. Klotzkin, A. de Silva, H. P. Wagner, D. White and B. Sharpton, *J. Phys. D. Appl. Phys.*, 2008, **41**, 235109.

4 B. Krummacher, M. K. Mathai, V. E. Choong, S. A. Choulis, F. So and A. Winnacker, *Org. Electron. physics, Mater. Appl.*, 2006, **7**, 313–318.

5 G. Nenna, PhD thesis, Universita degli studi di napoli federico II, 2009.

6 N. Chopra, J. Lee, Y. Zheng, S. H. Eom, J. Xue and F. So, *ACS Appl. Mater. Interfaces*, 2009, **1**, 1169–1172.

7 R. Meerheim, S. Scholz, S. Olthof, G. Schwartz, S. Reineke, K. Walzer and K. Leo, *J. Appl. Phys.*, 2008, **104**, 1–8.

8 W. H. Lee, D. H. Kim, P. Justin Jesuraj, H. Hafeez, J. C. Lee, D. K. Choi, T.-S. Bae, S. M. Yu, M. Song, C. S. Kim and S. Y. Ryu, *Mater. Res. Express*, 2018, **5**, 1–8.

9 R. Liu, PhD thesis, Iowa State University, 2012.

10 Y. Karzazi, *Environ. Sci*, 2014, **5**, 1–12.

11 S. Tiwari and N. C. Greenham, *Opt. Quantum Electron.*, 2009, **41**, 69–89.

12 Z. B. Wang, M. G. Helander, M. T. Greiner, J. Qiu and Z. H. Lu, *J. Appl. Phys.*, 2010, **107**, 2–5.

13 J. U. Wallace, PhD thesis, University of Rochester, 2009.

14 J. C. Blakesley, F. A. Castro, W. Kylberg, G. F. A. Dibb, C. Arantes, R. Valaski, M. Cremona, J. S. Kim and J. S. Kim, *Org. Electron. physics, Mater. Appl.*, 2014, **15**, 1263–1272.

15 US Pat. 1 745 175A 1930.

16 G. Horowitz, *Adv. Mater.*, 1998, **10**, 365–377.

17 A. Tsumura, H. Koezuka and T. Ando, *Appl. Phys. Lett.*, 1986, **49**, 1210–1212.

18 S. Li, D. Guérin and K. Lmimouni, *Microelectron. Eng.*, 2018, **195**, 62–67.

19 R. Parashkov, E. Becker, G. Ginev, T. Riedl, H.-H. Johannes and W. Kowalsky, *J. Appl. Phys.*, 2004, **95**, 1594–1596.

20 L. Torsi, M. Magliulo, K. Manoli and G. Palazzo, *Chem. Soc. Rev.*, 2013, **42**, 8612.

21 R. Doran, Master thesis, University of Strathclyde, 2015.

22 M. Stolka, D. M. Pai, D. S. Renfer and J. F. Yanus, *J. Polym. Sci. Polym. Chem. Ed.*, 1983, **21**, 969–983.

23 Y.-K. Wang, Z.-C. Yuan, G.-Z. Shi, Y.-X. Li, Q. Li, F. Hui, B.-Q. Sun, Z.-Q. Jiang and L.-S. Liao, *Adv. Funct. Mater.*, 2016, **26**, 1375–1381.

24 R. Rybakiewicz, M. Zagorska and A. Pron, *Chem. Pap.*, 2017, **71**, 243–268.

25 B. Souharce, PhD thesis, Bergischen Universität Wuppertal, 2008.

26 J. Dacuña and A. Salleo, *Phys. Rev. B*, 2011, **84**, 195209.

27 T. Yasuda, Y. Yamaguchi, D. C. Zou and T. Tsutsui, *Japanese J. Appl. Physics, Part 1 Regul. Pap. Short Notes Rev. Pap.*, 2002, **41**, 5626–5629.

28 C. Rothe, B. Wallikewitz, M. Zöllner, O. Fadhel and A. Werner, *SID Symp. Dig. Tech. Pap.*, 2014, **45**, 498–500.

29 W. Ma, P. K. Iyer, X. Gong, B. Liu, D. Moses, G. C. Bazan and A. J. Heeger, *Adv. Mater.*, 2005, **17**, 274–277.

30 S. H. Rhee, K. B. Nam, C. S. Kim, M. Song, W. Cho, S.-H. Jin and S. Y. Ryu, *ECS Solid State Lett.*, 2014, **3**, 19–22.

31 Z.-Y. Liu, S.-R. Tseng, Y.-C. Chao, C.-Y. Chen, H.-F. Meng, S.-F. Horng, Y.-H. Wu and S.-H. Chen, *Synth. Met.*, 2011, **161**, 426–430.

32 J.-D. You, S.-R. Tseng, H.-F. Meng, F.-W. Yen, I.-F. Lin and S.-F. Horng, *Org. Electron.*, 2009, **10**, 1610–1614.

33 N. Aizawa, Y. J. Pu, M. Watanabe, T. Chiba, K. Ideta, N. Toyota, M. Igarashi, Y. Suzuri, H. Sasabe and J. Kido, *Nat. Commun.*, 2014, **5**, 1–7.

34 W. Y. Hung, T. H. Ke, Y. T. Lin, C. C. Wu, T. H. Hung, T. C. Chao, K. T. Wong and C. I. Wu, *Appl. Phys. Lett.*, 2006, **88**, 2004–2007.

Chapter V: Conclusion and further work

I. Conclusion

The potential of organic materials for light emitting applications has been known since 1959, yet it was only in 1987 that Tang and Van Slyke demonstrated the first efficient organic light emitting diode. In the last two decades, the interest for OLEDs has continually grown, and nowadays their potential to replace inorganic LEDs is recognised in a variety of domains. As of today, OLEDs are mainly used in displays, with applications in smartphones, televisions and cameras. Displays are a massive economic market and OLED technologies have clearly found a place in it. However, as for any technology, it is necessary to continuously push for the development of new materials, new architectural design, etc. for OLEDs to continue to be the technology of tomorrow and not become a technology of the past. If the performance of some OLEDs are already comparable to LCD devices (the main concurrent in display), it is also important to develop materials with properties unique to organic materials. Indeed, their strength also lies in their easier synthesis and functionalisation but also in their potential to lower the cost of production of any display, by example *via* the use of relatively cheap commercially available organic materials or by the development of deposition methods by “wet-processing” (Roll to roll, 3D printing,…).

In this thesis, we first studied a commercially available emissive material, Super-Yellow, in order to understand the different parameters that can affect the performances of the devices made with it. A variety of optimisation techniques were applied in the research of better performances but also in the research of a better understanding of the mechanic behind these improvements.

Initially, we focused our attention on the optimisation on the emissive layer. For that we used a conventional bottom-emitting architecture (ITO/PEDOT:PSS/SY/Ca/Al). The thickness of the emissive layer was initially adjusted

by changing the concentration of the SY solution. It was demonstrated that a simple variation of 1 mg/ml of the SY solution concentration led to a thickness increase of 15 to 20 nm and more importantly an improvement of the luminance by 10 000 cd/m^2 and a variation of the current efficiency by almost 3 cd/A, thereby proving that the thickness of the EM is a crucial parameter in the characterisation of an OLED. Another option to adjust the thickness of a layer deposited by spin-coating, as it is the case here for the emissive layer, is to change the spin-speed. Using the same solution, a variation of the speed from 800 rpm to 1 400 rpm induced a thickness reduction of 20 nm. However, it was shown that such variation does not only affect the thickness but can also affect the way the molecules are spread on the substrate.

The combination of a 5 mg/ml SY concentration and a spin-speed of 1 400 rpm for 60 s exhibits the highest performance. Such devices present a current efficiency of 9.40 cd/A at 2 234 cd/m^2 (8.4 cd/A at 10 000 cd/m^2), a maximum luminance of 66 456 cd/m^2 at 9.7 V and a turn on voltage at 2.3 V.

In a second part, we changed the device architecture to study the impact of the layers alongside the emissive layer. The following bottom-emitting inverted architecture was chosen: ITO/ZnO/PEI/SY/MoO_3/Al. By analogy to the emissive layer, a variation in the thickness of either of the layers alongside the EM can have a huge impact on the device performance. Similarly, both layers presented their best performance with a thickness equal to or under 10 nm. However, in the case of PEI, the molecular weight of this polymer also has a role on the device performance. Indeed, the reduction of the Mw from 1 800 to 800 g/mol induced a reduction of the turn on voltage by 0.6 V and an increase of the current efficiency of 0.2 cd/A. However, the amount of current supported by the devices before degradation was also reduced, which induced a small reduction of the luminance.

After optimisation, the best devices with an inverted architecture exhibit a current efficiency of 10.02 cd/A at 1466 cd/m^2 (8.7 cd/A at 10 000 cd/m^2), a maximum luminance of 35 853 cd/m^2 at 10.1 V and a turn on voltage at 2.6 V.

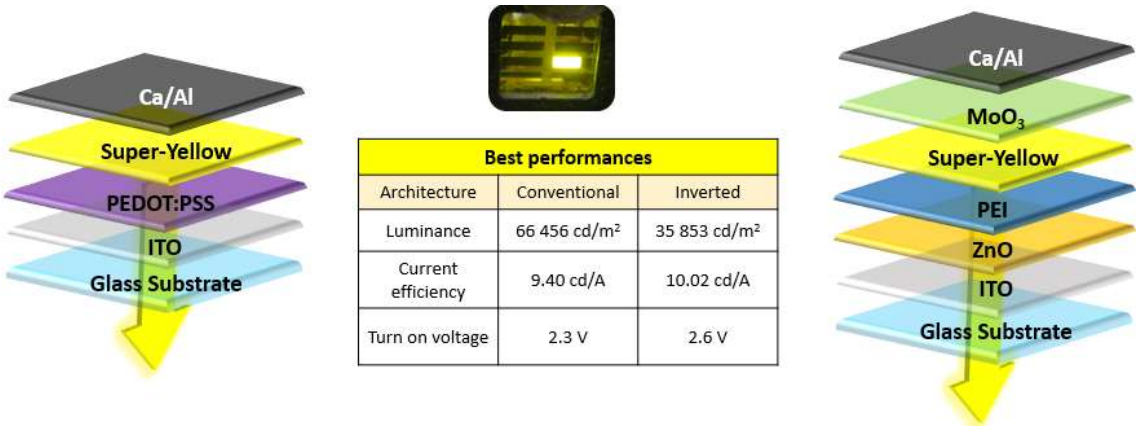

Best performances		
Architecture	Conventional	Inverted
Luminance	66 456 cd/m²	35 853 cd/m²
Current efficiency	9.40 cd/A	10.02 cd/A
Turn on voltage	2.3 V	2.6 V

Figure V.1: Best performances according to the devices architecture

Overall, this study demonstrated the importance of the thickness of each layers constituting an OLED. The optimisation of the emissive layer was the most important as it led to the bigger improvement, but when the device architecture becomes more complex it is important to also optimise the other layers. This study also showed that reporting a thickness alone is not enough. Indeed, in the case of solution-processed materials, if a change in the concentration can influence the thickness the same phenomenon can be achieved by adjusting the spin-speed. However, if a similar thickness can be achieved with both methods the results can be different. Therefore, when reporting the thickness of a solution process layer it is important to specify the conditions used to obtain it.

In a second part of this thesis, two series of novel solution-processable green and red emitting materials were characterised and optimised. The series of green emitters is composed of two materials, Green 1 and Green 2, both based on a benzothiadiazole core a bifluorene arms. However, where Green 1 has trimethylsilane (TMS) ending groups, Green 2 has triphenylamine (TPA) moieties. Similarly the red series is also composed of four materials, Red 1, Red 2, Red 3 and Red 4, all based on the same dithiophenylbenzothidiazole core. Both Red 1, Red 3 and Red 4 possess the same fluorene arms however their ending groups are TMS, TPA and benzofuran respectively. In the contrary, Red 2 possess the same ending

groups as Red 1 however a second fluorene unit was inserted in the arms of the molecules.

To characterise these different materials each of them have been inserted in a simple conventional bottom emitting OLED (ITO/PEDOT:PSS/Green or Red /Ca/Al). As it was shown earlier, the thickness of the emissive layer is a crucial characteristic of any device. In this respect, the concentration of each materials was varied from 10 to 30 mg/ml and all six materials exhibit their best performances with a solution of 20 mg/ml in toluene deposited at 800 rpm for 60 s.

After optimising the thickness, all materials except Red 4, were submitted to an annealing test. First, this test revealed that for both Green 1, Green 2 and Red 2 annealing at 40°C for 20 min after deposition of the emissive layer was beneficial to the device performance. For the other materials, no significant improvement was observed. The second information revealed by this test is the low resistance to heat of Green 1, Green 2 and Red 1. If Red 2 and Red 3 also present a variation of their performance with temperature, it is far less than the one observed with Green 1, Green 2 and Red 1.

Finally the hole mobility of the different compounds was measured by using the OFET technique. Green 2 exhibits the highest mobility with 2×10^{-4} $cm^2/(V.s)$, one order of magnitude higher than Green 1. In the Red series, it is Red 3 that present the highest hole mobility with 2×10^{-5} $cm^2/(V.s)$, while Red 1 and Red 2 demonstrated mobilities of 7×10^{-6} $cm^2/(V.s)$ and 4×10^{-6} $cm^2/(V.s)$.

In a simple conventional device architecture (ITO/PEDOT:PSS/EM/Ca/Al) and after optimisation, Green 2 displayed the highest performance of all, with a maximum luminance of over 20 000 cd/m^2 and a current efficiency of 2.00 cd/A. For the red emitters, the best luminance was reached with Red 3, with values for luminance of just over 2 000 cd/m^2. However, devices with Red 2 exhibit the highest current efficiency of the red series, at 0.19 cd/A.

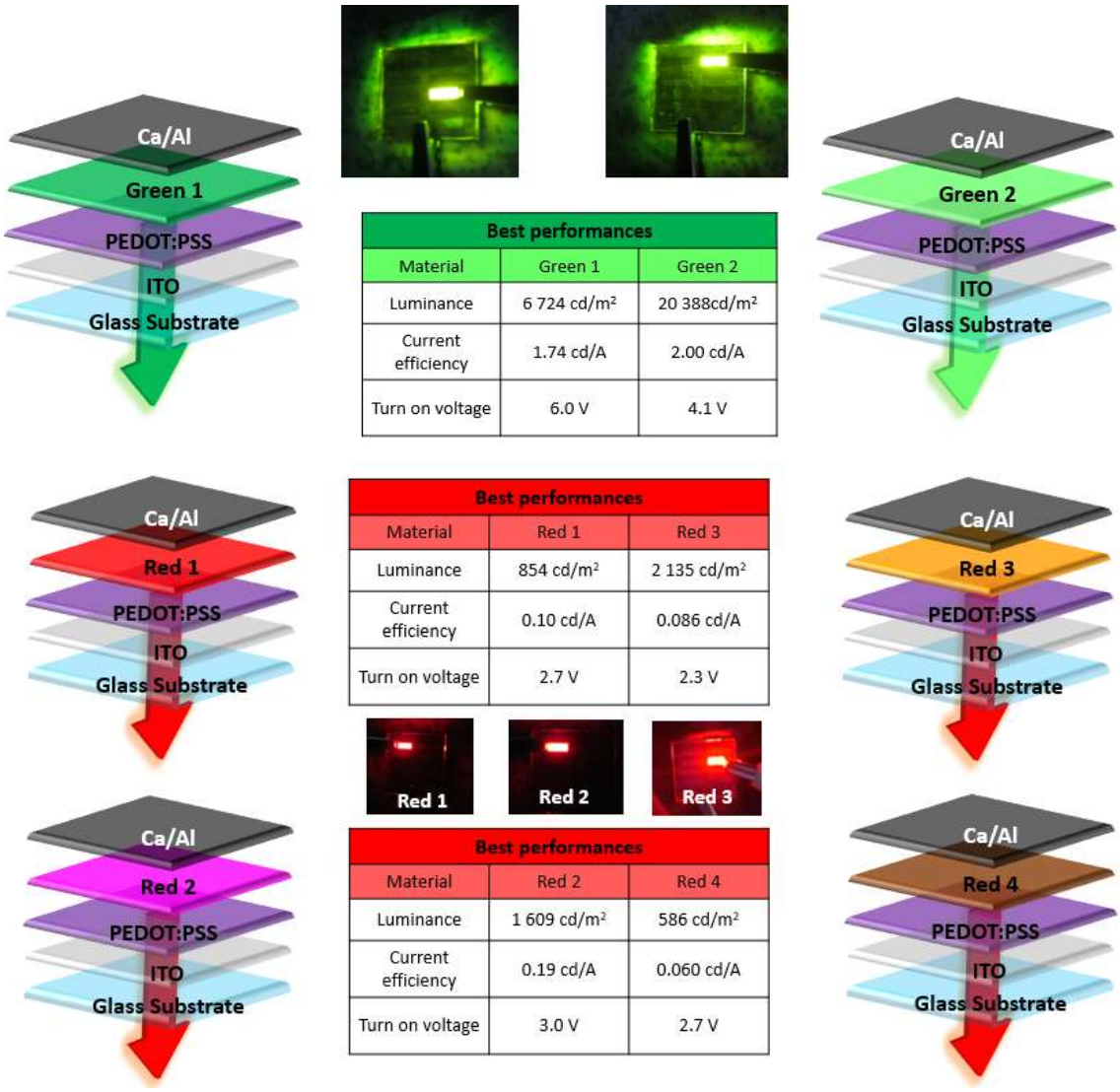

Best performances		
Material	Green 1	Green 2
Luminance	6 724 cd/m²	20 388cd/m²
Current efficiency	1.74 cd/A	2.00 cd/A
Turn on voltage	6.0 V	4.1 V

Best performances		
Material	Red 1	Red 3
Luminance	854 cd/m²	2 135 cd/m²
Current efficiency	0.10 cd/A	0.086 cd/A
Turn on voltage	2.7 V	2.3 V

Best performances		
Material	Red 2	Red 4
Luminance	1 609 cd/m²	586 cd/m²
Current efficiency	0.19 cd/A	0.060 cd/A
Turn on voltage	3.0 V	2.7 V

Figure V.2: Best performing devices for each materials of the Green and Red series

The performance enhancement observed with Green 2 are the results of the substitution of TMS groups by TPA groups. Indeed, after the substitution a variation of the HOMO level from 5.37 eV (Green 1) to 5.07 eV (Green 2) was measured. Such change reduced the initial mismatch with the HOMO level of PEDOT:PSS, thus inducing a better hole injection in the emissive material and explaining, at least partially, the lower turn on voltage observed with Green 2. The higher luminance measured with Green 2 was linked to the higher current density in the material, itself induced by a higher hole mobility. Such a phenomenon was observed in both Green 2 and Red 3, the two materials that had their ending groups change for TPA entities.

Therefore, it was concluded that this end-groups also plays a part in the enhancement of luminance observed with both Green 2 and Red 3.

Contrary to what happened with the Green series, the substitution by TPA groups did not induce any change in the HOMO level of Red 3. However, it did induce an increase of the PLQY, which in turn is linked to an increase in recombination rate in the material. Therefore, the luminance increase is not only due the higher hole mobility but also to a better recombination rate.

Similarly, Red 2 presents a higher PLQY resulting in a higher luminance. Since the end-groups of Red 2 were not changed, this enhancement of the recombination can only be linked to the increased conjugation induced by the addition of a fluorene unit. It is worthwhile noting that contrary to the previous two materials this enhancement was not due to an improvement in hole mobility.

Overall, in this thesis, we first highlighted the importance of optimising the thickness of the different layers constituting an OLED. Secondly, we characterised two series of novel and linear green and red fluorescent small molecules containing an electron deficient benzothiadiazole core and electron-rich fluorene arms. Both series of materials are relatively easy to synthesise and they also present the great advantage of being solution-processable.

II. Further work

In this thesis, we were able to fully study 5 out of the 6 materials synthesised for these two series of emitters. Indeed, due to a lack of materials further study on Red 4 were postponed. Despite the challenging synthesis, the initial chemical characterisation of Red 4 led us to believe that this material would show better performance than Red 1. Indeed, its HOMO-LUMO gap is quite similar to Red 3 and the PLQY measurements revealed a higher value than Red 1. However, the majority of the devices made with this material end up short-circuiting. It is relatively difficult with only few data to give an explanation to what happened with these devices.

Nonetheless, a problem of film morphology can be considered. If it is the case, then a variation of the spin-speed could be interesting. Indeed, we demonstrated with Super-Yellow, that such variation could lead to an improvement of the film morphology. Another option would be to try other solvents with different evaporation properties and different polarity. Obviously, in order to make any of these tests, another batch of Red 4 should be synthesised first.

Computational chemistry could also reveal useful information concerning the properties of the materials of these two series, especially the influence of the different end-groups on the twisting of the molecules and the subsequent effect on the film morphology and device performance.

From the characterisation of the Red series of materials, we established that both TPA end-groups and an extension of the conjugation length were beneficial to the device performance. However, it will be interesting to see if the combination of both aspects on the same molecule would further improve their performances, or on the contrary cancel each other.

The next step of optimisation for these materials will be to insert an electron transport layer in the device architecture. Indeed, although our devices exhibit sufficient luminance performance, their current efficiencies were extremely low, especially in the case of the Red series. Such a low efficiency is usually the sign of poor charge balance in the devices. The lower efficiency observed with Red 3, despite a higher luminance, tend to confirm this hypothesis. Therefore, the addition of an ETL would help to rebalance the charges in the devices. Another important effect of the addition of an ETL, would be to shift the recombination zone away from the cathode, which could result in further enhancement of the luminance and efficiency. Shifting the recombination zone could also induce a narrowing of the electroluminescent spectra, which in the case of the red series could be beneficial to the luminance as less emission would take place in the infrared. Overall, the addition of an ETL would be beneficial to our devices in many ways.

The well-known electron transport material TPBI, could be an excellent candidates for our devices. Indeed, its LUMO at 2.7 eV will be close enough to the work function for the Ca/Al electrode (2.9 eV) we use in our devices to induce good electron injection. At the same time, its HOMO of 6.2 eV will create a large mismatch with the HOMO of our materials and therefore induce good hole blocking capacity. However, in this study we present two derivatives of TPBI with similar electrochemical properties but with a higher electron mobility. The second of these derivatives, 3-COOK, presents a second advantage, its solubility in methanol, whereas the other two are mainly soluble in chloroform. Indeed, the main problems to make all-solution-processable OLEDs is the challenge not to damage or partially dissolve the under layer when depositing a subsequent layer. Our materials have a relatively low solubility in methanol and a high solubility in chloroform, therefore the risk of damaging the emissive layer while depositing the ETL would be minimised with 3-COOK.

The first task if we want to insert this material in our device architecture would be to find the optimum condition of deposition. For that the solution concentration, the spin-speed and the annealing temperature should be varied one at the time, as we did with the EM layer in this study. This study would be obviously time-consuming but could well result in a large enhancement of device performance.

Chapter VI: Experimental

I. OLED

A. Fabrication

1. Cleaning

Pre-patterned indium tin oxide slides, with a resistance of 7 ohm/sq, were purchased from Kintec Company. A 9x15 mm ITO rectangle is coated on a 15x15x1.1

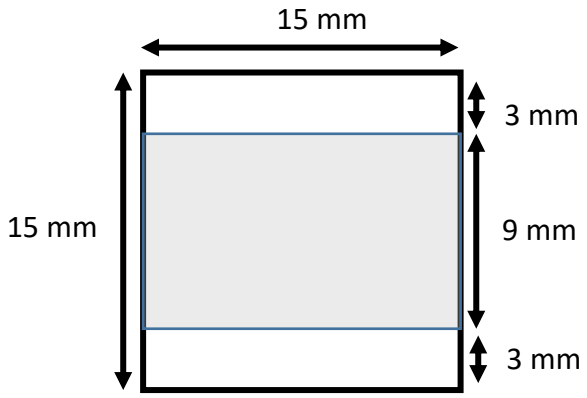

Figure VI.1: Scheme of the pre-patterned indium tin oxide slides

mm polished glass slide, according to the scheme below.

Before device fabrication, it is important to remove any possible contaminants from the glass/ITO slide. As such, they are washed with solvents according to the following procedure:

- Substrates are carefully placed on a support, which itself is placed in a beaker
- Substrates are washed for 2 min with water and soap in an ultrasonic bath
- Beaker and substrates are rinsed with acetone
- Substrates are washed for 2 min with acetone in an ultrasonic bath
- Beaker and substrates are rinsed with isopropanol
- Substrates are washed for 2 min with ethanol in an ultrasonic bath

After being dried with compressed air, the devices undergo surface treatment/cleaning via oxygen plasma for 2 min. This plasma is very effective in breaking organic bonds of the contaminants such as oils and grease. At the same time ionised oxygen atoms, created by the plasma, bond with the organic contaminants, mostly to form water or carbon dioxide. These new molecules are pumped away during the process leaving a pristine surface. Using oxygen plasma on ITO has been shown to reduce the driving voltage, enhancing the brightness, efficiency and improving the optical and electrical properties of OLEDs.[170,171] However, these improvements decay as the aging time after the surface treatment increases. That why it is important to limit the time between the treatment and the deposition of the first layer.

2. Conventional Architecture

In the conventional architecture device, the first layer deposited is a hole transport layer. Poly(3,4-ethylenedioxythiophene)poly(styrenesulfonate) or PEDOT:PSS is the commonly used HTL in these devices. Purchased from Heraeus, under the name *Clevios™ P VP AI 4083,* the HTL is deposited on top of ITO by spin-coatspin-coating at a spin-speed of 3000 rotation per minutes (rpm) for 60 seconds. The thickness of the layer was measured to be 40±10 nm. Following its deposition, PEDOT:PSS is annealed at 120°C for 20 minutes. An increase of PEDOT:PSS conductivity has been observed upon annealing.[172]

Any further steps are carried out inside the glovebox, where the oxygen and water level are kept below 0.1 ppm. The light emitting material is dissolved in toluene and then deposited on top of the PEDOT:PSS. The concentration of the solution and the spin-speed can vary according to the material.

The devices are then transported to a thermal evaporator, where the top electrode made of calcium and aluminium (ratio 40/60 nm) is evaporated at a steady rate of 1 Å/s. The devices were not encapsulated as the main part of the testing occurs in the glovebox.

3. Inverted architecture

In an inverted architecture OLED, ITO becomes the electron donating electrode. However, this causes some problems, as it is necessary to lower the ITO work function before deposition of the emissive material. Indeed, without a modification layer a large energetic barrier will separate the ITO work function (4.7 eV) and the emissive material LUMO (between 2.8 and 3.3 eV), resulting in inefficient devices. One way to overcome this problem is to use modification layers.

The combination of zinc oxide (ZnO) and polyethyleneimine (PEI) are well known modification layers in organic electronics.[64,81–84,86,173] ZnO is largely used in organic electronics thanks to its good n-type properties, air stability and because as a film it is transparent to visible light.[64] The deposition of ZnO is performed according to the method developed by Bruyn *et al.*[87]Hence, zinc acetylacetonate hydrate ($Zn(acac)_2$, Sigma-Aldrich) was dissolved in ethanol (20 mg/mL) and stirred for 24 h at 50 °C. Following this, the solution was filtered through a 0.2 µm polytetrafluoroethylene (PTFE) filter, to remove precursor aggregates. The solution was then spin-coatspin-coated on top of ITO at 2000 rpm for 45 seconds before being annealed at 120°C for 30 seconds. This thin layer of zinc oxide can reduced the work function of ITO by 0.6 to 1 eV.[82,83] However, a work function of between 4.1 and 3.7 eV is still too high for many emissive materials. Additionally, Sungho Woo *et al.* demonstrated that the roughness of zinc oxide can decrease the performance of the device. That is why a second surface modification layer is usually deposited on top of the metal oxide.

Most commonly, polyethyleneimine (PEI) is used to reduce further the electrode work function and allow a better contact with the emissive layer. With an electron affinity and ionization potential energy values of 0.3 eV and 6.5 eV (band gap of 6.2 eV), respectively, PEI should act as an insulating layer.[88] However, it has been demonstrated that the amine in the PEI backbone can protonate and absorb to the surface of the underlying layer, resulting in the formation of an interfacial dipole. This dipole induces a vacuum level shift leading to a reduction of the work function

of the electrode.[83,89,90] Zhou *et al.*[88] describe a simple way to make and deposit PEI on ZnO. The PEI is dissolved in 2-methoxyethanol solution (Sigma-Aldrich) at 0.4 wt.% before being spin-coated, on top of ZnO, at 5000 rpm for 50s. The samples are then annealed at 100°C for 10 min and then rinsed to remove any PEI surplus.

The combination of these two layers has shown an increased stability to ambient air compared to electrodes made of calcium and good thermal stability to 150-190°C.

B. Characterisation

A Keithley Semiconductor Characterisation (SCS) 4200 is used to power up OLEDs and to measure the applied voltage as well the current flowing through the device.

Luminance (Lu) measurements were recorded by using a Macom L203 photometer with a calibrated Silicon photo detector and a photoptic filter placed at a known distance D from the point source (Figure VI.2). These calibrations can be traced back to the National Physical Laboratory, London standards.

The light output is first recorded in lux (lx). Then candela (cd) and candela by square meter (cd/m^2) are calculated by using a simple conversion, with A_1 being the lighting area of the device, in our case $7.5x10^{-5}$ m^2 (1.5 cm by 0.5cm):

$$Lu\ (cd) = Lux\ (lx) \times D^2 \qquad \text{and} \qquad Lu\ (cd/m^2) = L\ (cd)/\ (A_1)$$

By dividing the luminance by the current at a specific voltage the current efficiency, in cd/A, is obtained. Other characteristics such as current density, light intensity and power efficiency can also be easily calculated from the luminance and current recorded.

The values presented in this thesis are the maximum values obtained out of 6 to 8 devices.

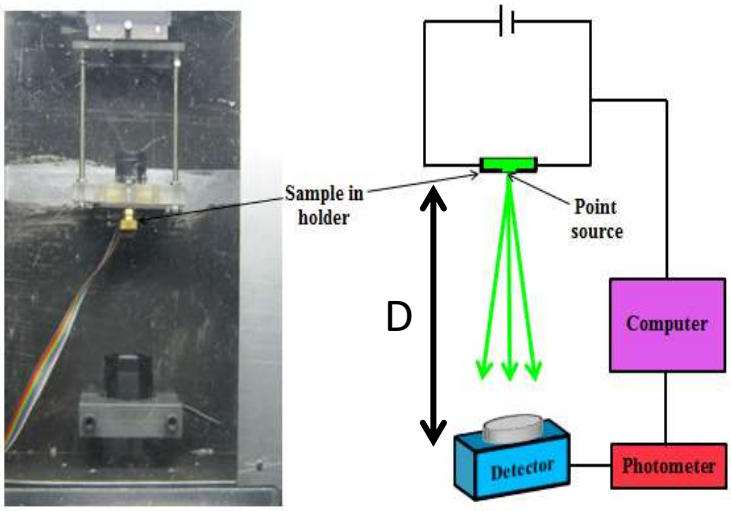

Figure VI.2: Scheme of the OLED testing box

C. Emission spectra and CIE coordinates

OLEDs were fabricated according to the procedure presented earlier. The devices were then moved to an integrated sphere equipped with an optical fibre. Once powered up by a Keithley Semiconductor Characterisation (SCS) 4200, the resulting emission spectrum was measured.

The CIE coordinates were extrapolated from this spectrum using the CIE coordinates calculator MATLAB program available online.[174]

II. Charge carrier measurement

A. SCLC

The same pre-patterned ITO slide used for OLEDs are used to make SCLC measurements. The same cleaning process is also used as well as the same method for the deposition of PEDOT:PSS.

The tested organic layer is then deposited *via* thermal evaporation, at a steady rate of 1 Å/s, or *via* spin-coating, at 800 rpm for 60 s. Further to the deposition of the organic layer, the top electrode made of calcium and aluminium (ratio 40/60 nm) is evaporated at a steady rate of 1 Å/s. The devices were not encapsulated as all testing occurred inside the glovebox.

The devices were placed in the OLED testing box and the same Keithley Semiconductor Characterisation (SCS) 4200 that powered up the OLEDs and assisted with their measurements is used to characterise the SCLC slide. On top of giving us the data necessary for SCLC measurement, the use of the box allows control so that no light emission is occurring during the measurement.

Once the data was obtained, a current density versus voltage graph is plotted and the following equation (eq. 4) is used to find the electron mobility:

$$J = \frac{9\,\varepsilon\,\mu\,{V_a}^2}{8\,t^3} \quad (eq.4)$$

B. OFET fabrication

The substrate for bottom-gate, bottom contact organic field effect transistors was purchased from the Fraunhofer Institute for Photonic Microsystems (IPMS). The substrates are n-doped silicon chips of 15x15 mm^2 with 230 nm of thermally grown SiO_2 and prefabricated interdigitated Au fingers (50 nm S/D electrodes) having a capacitance per unit area of 1.7×10^{-8} F/cm^2. Each chip has 16 transistors with a width of 10 mm. However, the length of the transistors is varied. They are divided into four groups of four devices with channel lengths of 2.5, 5, 10 and 20 µm.

To remove any possible contaminants the substrates were subsequently dipped for 2 min in distilled water, acetone and isopropanol. All the chips were then treated with Pentafluorobenzenethiol (PFBT, Sigma-Aldrich) in order to increase the work function of gold from 5.1 to 5.4 eV.[175] The solution of PFBT (13.3 µl in 10 ml of isopropanol) was dropcasted on the substrate and washed with isopropanol after two minutes to remove any excess of PFBT.

After that the chips for the measurement of the Green series of materials were treated with octadecyltrichlorosilane (OTS). The OTS solution was prepared by adding 30 µl of OTS to 6 ml of toluene. The chips were immerged in the solution for 20 min before being rinsed with toluene to remove the excess material. The substrates were then dried with compressed air before depositing the organic layer.

The latter was deposited via spin-coating (1500 rpm for 60 s) from a 20 mg/ml solution in chloroform. The chips were annealed at 40°C before characterisation.

The chips used for the Red series were treated with hexamethyldisilazane (HDMS, Sigma-Aldrich) in order to improve the wettability[176,177] of the chip surface. The HDMS was spin-coated at 5 000 rpm for 60 s and successively annealed at 150°C for 10 min. The active materials (20 mg/ml in toluene) were then deposited, on top, by spin-coating (800 rpm for 60 s). Annealing was performed is it was proven beneficial to the materials.

The electrical characteristic of the transistors was measured inside the glovebox using a Keithley Semiconductor Characterisation (SCS) 4200 and a custom-made probe station (Figure VI.3). The field effect mobilities (μ) and threshold voltages (V_{Th}) were calculated in the saturation regime by plotting the square root of the current source drain ($\sqrt{I_{DS}}$) versus the voltage source gate (V_{GS}) at a voltage drain source (V_{DS}) equal to -50V, using the following equation:

$$\mu_{sat} = \frac{2L}{wC_i} \times \left(\frac{\partial\sqrt{I_{DS}}}{\partial V_g}\right)^2, \qquad V_T = \frac{\sqrt{I_0}}{\left(\frac{\partial\sqrt{I_{DS}}}{\partial V_g}\right)}$$

Where I_{DS} is the source drain current, μ is the carrier mobility, $\partial(I_{DS})^{1/2}/\partial V_G$ is the slope and $(I_0)^{1/2}$ is the intercept of the plot. V_g is the gate voltage, L is the channel length, W is the channel width and C is the capacitance per unit area of an insulating material.

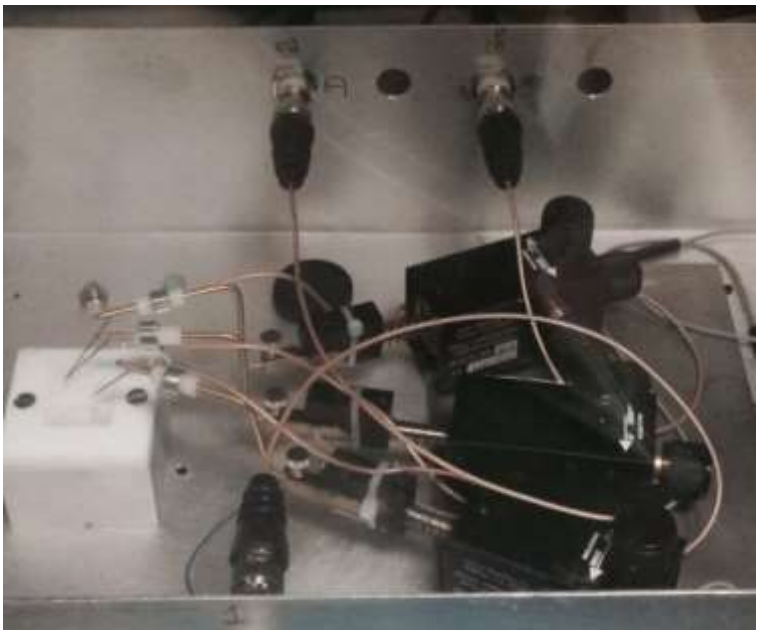

Figure VI.3: Custom made probe station for OFET measurement

III. PLQY

The photoluminescence quantum yield of the different emitting material was measured according to the method described by J.C De Mello *et al*.[67] This technique induces photoluminescence *via* a monochromatic laser beam (OL 750D Monochromator) while the material is placed in an integrated sphere (a hollow sphere with its inner surface coated with a reflecting material, typically polytetrafluoroethylene). The resulting light emission is measured with a CCD spectrometer linked to the sphere by an optical fibre (Ocean Optics 2000+). To prevent direct illumination of the optical fibre a barium sulphate coated baffle is positioned just in front of it. The laser beam is directed into the sphere through a 3 mm entrance hole and its wavelength is chosen to match the maximum absorbance wavelength of the emissive material.

Three measurements are necessary. In the first experiment (experiment a) the integrated sphere is empty, the laser beam hits the back of the sphere directly, and the laser light is the only light detected by the spectrometer. For the other two experiments, a sample is placed inside the integrated sphere. The sample consist of the emitting material deposited by spin-coating onto a clean substrate. The latter

must be transparent to the laser beam wavelength. It is usually made of quartz or glass. In the second experiment (experiment b), the sample is placed in the integrated sphere in a way that it does not enter in direct contact with the laser beam. Finally, in experiment (c) the laser beam is directed on to the sample. Typically, the sample is positioned with a certain angle (around 70° to 90°) compared to the laser beam in order to avoid reflected light from escaping the sphere through the laser entrance hole. For each experiment, an emission spectrum from 300 to 800 nm is registered.

In experiment c, the absorbed light is composed of two variables. A fraction *A*, which is the laser beam light directly absorbed by the material, and a fraction μ, which corresponds to the initially non-absorbed light that scattered on the wall of the sphere and was then absorbed by the material. The latter fraction can be measured in experiment b, as it is the only variable in this case.

$$Lb = La(1-\mu) \text{ and } Lc = La(1-A)(1-\mu)$$

$$\text{Soit } A = \left(1 - \frac{Lc}{Lb}\right)$$

With L the area under the laser profile curve of the corresponding experiment (a, b or c). This area is proportional to the amount of unabsorbed light.

The PLQY, which is equal to the number of photons emitted divided by the number of photons absorbed, was demonstrated to be equal to:

$$PLQY = \frac{Pc \; - \; (1-A) \; \times \; Pb}{La \; \times \; A}$$

With P the area under the emission curve of the corresponding experiment (b or c). It is proportional to the amount of emitted light.

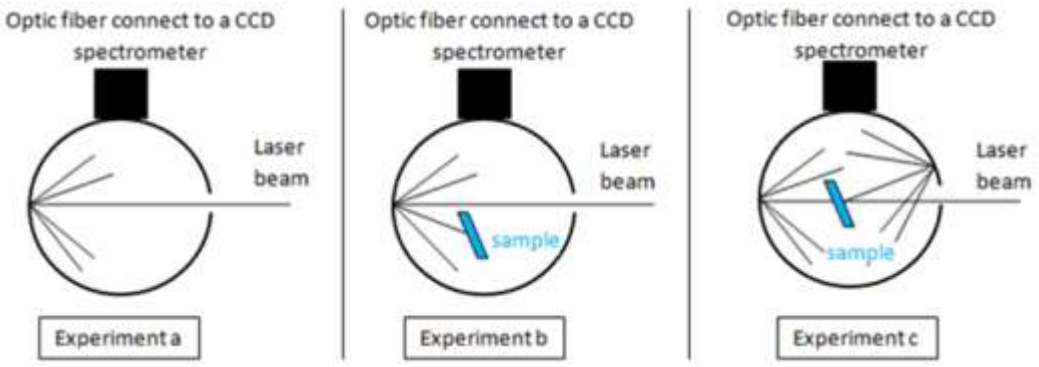

Figure VI.4: PLQY measurement

IV. Thickness measurement AFM

A glass slide of 15x15 mm was coated with the organic material by spin-coating. The parameters of the solution and of the spin-coating method depends on the tested material. Sharp cuts were then made on the deposited material. An AFM (atomic force microscope) was used to map out the surface of the material around the cuts. This results in the possibility to form a graph of the height versus length (Figure VI.5). As the materials are relatively smooth, the large change of height, observed on the graph, can only correspond to the cut made earlier. Therefore, the difference in height between the surface before the cut and where the material has been removed due to the cut gives the thickness of the layer. A minimum of 10 values were measured before calculating an average.

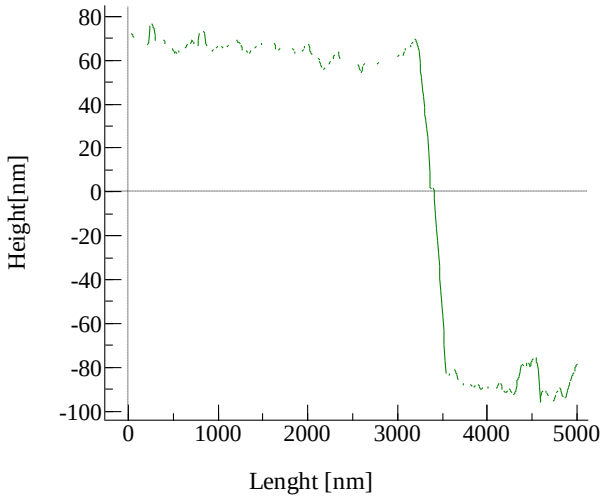

Figure VI.5: Example of a height versus length used to measure the thickness of the organic layer deposited by spin-coating.

V. Bibliography

1 Wu, C. C.; Wu, C. I.; Sturm, J. C.; Kahn, *Appl. Phys. Lett.,* **1997**, *70* (11), 1348–1350.

2 You, Z. Z.; Dong, J. Y. *Vacuum,* **2007**, *81* (7), 819–825.

3 Kim, Y.; Ballantyne, A. M.; Nelson, J.; Bradley, D. D. C., *Org. Electron. physics, Mater. Appl.,* **2009**, *10* (1), 205–209.

4 Chiba, T.; Pu, Y. J.; Kido, J., *Adv. Mater.,* **2015**, *27* (32), 4681–4687.

5 Woo, S.; Hyun Kim, W.; Kim, H.; Yi, Y.; Lyu, H. K.; Kim, Y., *Adv. Energy Mater.,* **2014**, *4* (7), 1–7.

6 Courtright, B. A. E.; Jenekhe, S. A., *ACS Appl. Mater., Interfaces* **2015**, *7* (47), 26167–26175.

7 Kim, Y. H.; Han, T. H.; Cho, H.; Min, S. Y.; Lee, C. L.; Lee, T. W., *Adv. Funct. Mater.,* **2014**, *24* (24), 3808–3814.

8 Chen, H. C.; Lin, S. W.; Jiang, J. M.; Su, Y. W.; Wei, K. H., *ACS Appl. Mater. Interfaces,* **2015**, *7* (11), 6273–6281.

9 Stolz, S.; Scherer, M.; Mankel, E.; Lovrinčić, R.; Schinke, J.; Kowalsky, W.; Jaegermann, W.; Lemmer, U.; Mechau, N.; Hernandez-Sosa, G., *ACS Appl. Mater. Interfaces,* **2014**, 6 (9), 6616-6622.

10 Fukagawa, H.; Morii, K.; Hasegawa, M.; Gouda, S.; Tsuzuki, T.; Shimizu, T.; Yamamoto, T., *SID Symp. Dig. Tech. Pap.,* **2015**, *46* (1), 696–699.

11 de Bruyn, P.; Moet, D. J. D. J. D.; Blom, P. W. M. W. M., *Org. Electron.,* **2010**, *11* (8), 1419–1422.

12 Zhou, Y.; Fuentes-Hernandez, C.; Shim, J.; Meyer, J.; Giordano, A. J.; Li, H.; Winget, P.; Papadopoulos, T.; Cheun, H.; Kim, J.; et al., *Science.,* **2012**, *336* (6079), 327–332.

13 Kang, H.; Hong, S.; Lee, J.; Lee, K., *Adv. Mater.,* **2012**, *24* (22), 3005–3009.

14 van Reenen, S.; Kouijzer, S.; Janssen, R. A. J.; Wienk, M. M.; Kemerink, M., *Adv. Mater. Interfaces,* **2014**, *1* (8), 1-34.

15 CIE Coordinate Calculator - File Exchange - MATLAB Central https://ch.mathworks.com/matlabcentral/fileexchange/29620-cie-coordinate-calculator (accessed Aug 2, 2018).

16 Kimura, T.; Kobayashi, K.; Yamada, H. Direct, *Org. Electron. physics, Mater. Appl.,* **2016**, *38*, 74–78.

17 Sonar, P.; Oldridge, L.; Grimsdale, A. C.; Müllen, K.; Surin, M.; Lazzaroni, R.; Leclère, P.; Pinto, J.; Chua, L. L.; Sirringhaus, H.; et al., *Synth. Met.,* **2010**, *160* (5–6), 468–474.

18 Hosoi, Y.; Tsunami, D.; Ishii, H.; Furukawa, Y., *Chem. Phys. Lett.,* **2007**, *436* (1–3), 139–143.

19 de Mello, J. C.; Wittmann, F. H.; Friend, R. H.,. *Adv. Mater.,* **1997**, *9* (3), 230–232.

Annex

Annex 1: Current density, Luminance and current efficiency versus voltage for the annealing test on Super-Yellow

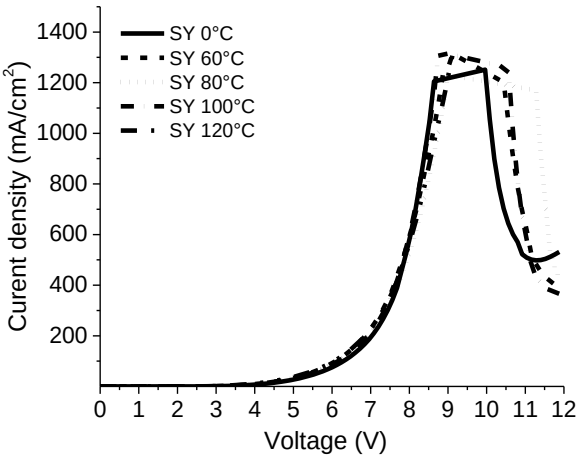

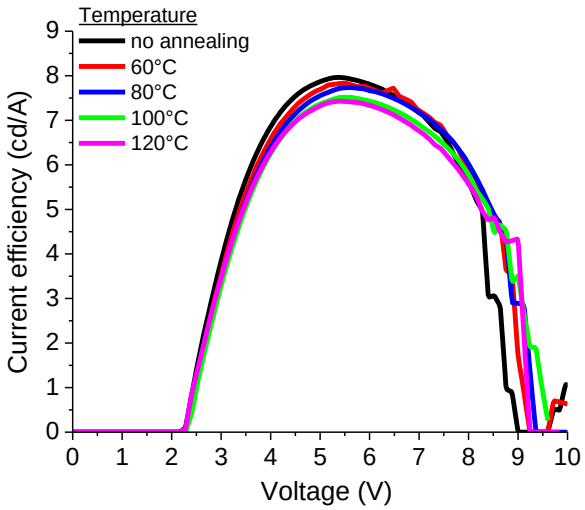

Annex 2: Luminance and current efficiency versus voltage for the spin-speed test on Super-Yellow

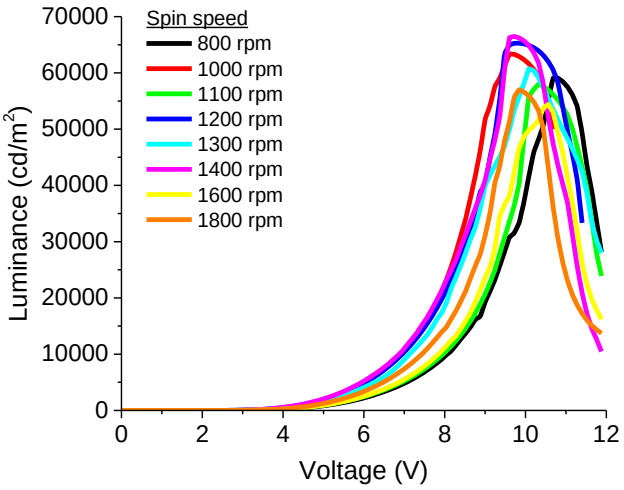

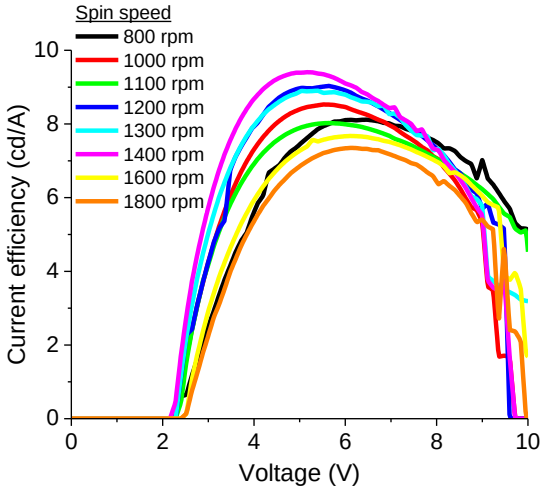

Annex 3: Current density, Luminance and current efficiency versus voltage for the thickness test on MoO_3

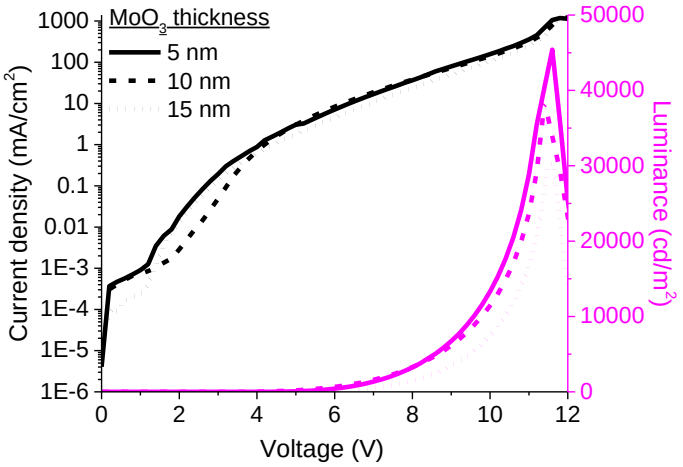

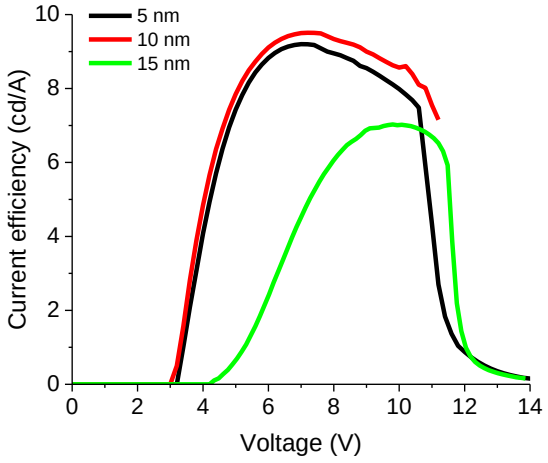

Annex 4: Results obtain from the concentration test made with Red 2 and Red 3

Material	Concentration (mg/ml)	Current efficiency (cd/A)[a]	Maximum Luminance (cd/m^2)[a]	Turn on voltage (V)[b]
R2	10	719 @ 7.2	0.06	2.7
	20	1561 @ 8 V	0.15	2.9
	30	720 @ 9.2 V	0.16	3.3
R3 (unfiltered)	10	239 @ 20 V	0,012*	1,9
	20	1425 @ 14 V	0.051*	2.1
	30	1054 @ 19 V	0,040*	2,1

*[a]In brackets the operating voltage at which values were recorded (in Volts); [b] recorded for a luminance of 1 cd/m^2, *limited due to short circuits*

Annex 5: Output (left) and transfer (right) characteristic measure for Green 1 at a channel width of 10 µm

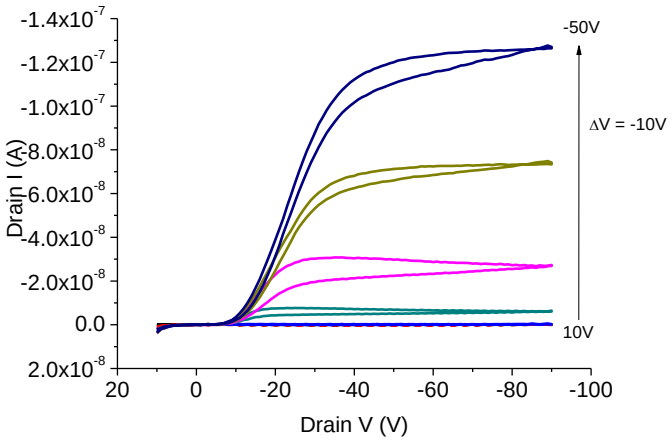

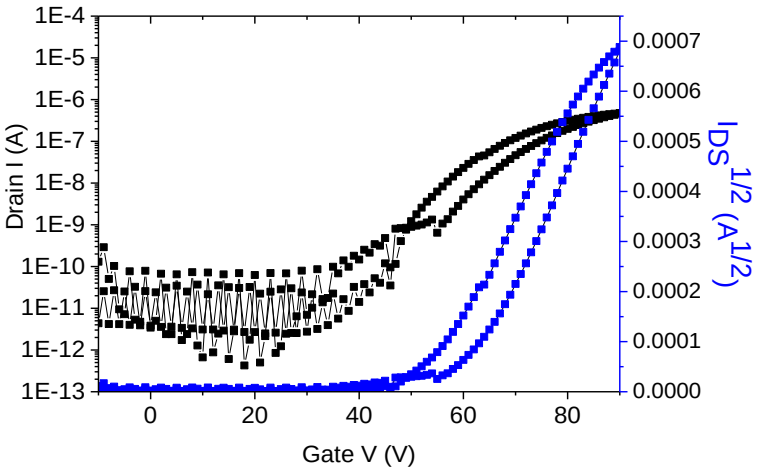

Annex 6: Output (left) and transfer (right) characteristic measure for Green 2 at a channel width of 20 µm

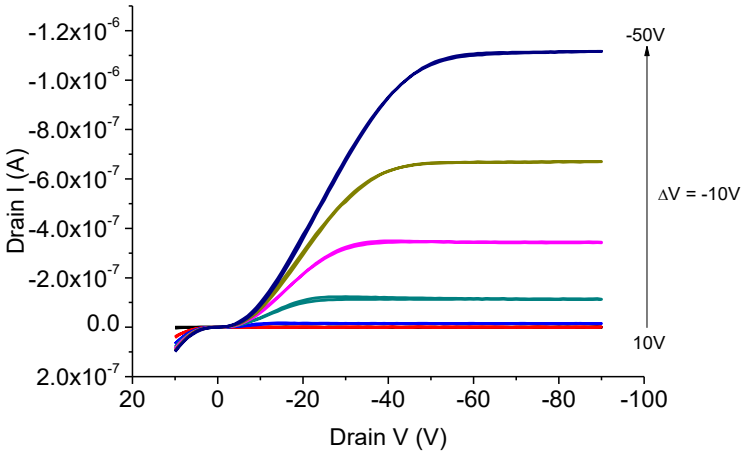

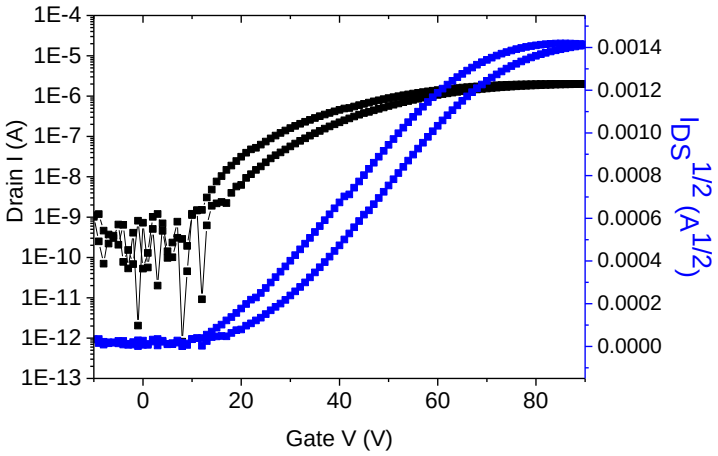

Annex 7: Output (left) and transfer (right) characteristic measure for Red 1 at a channel width of 10 µm

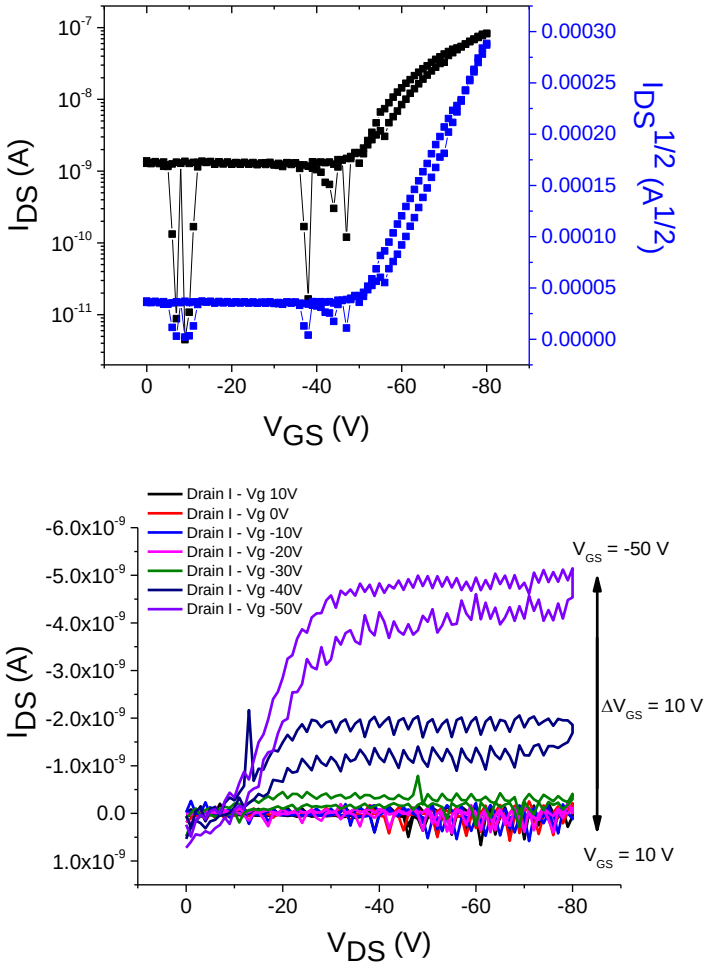

Annex 8: Output (left) and transfer (right) characteristic measure for Red 2 at a channel width of 2.5 µm

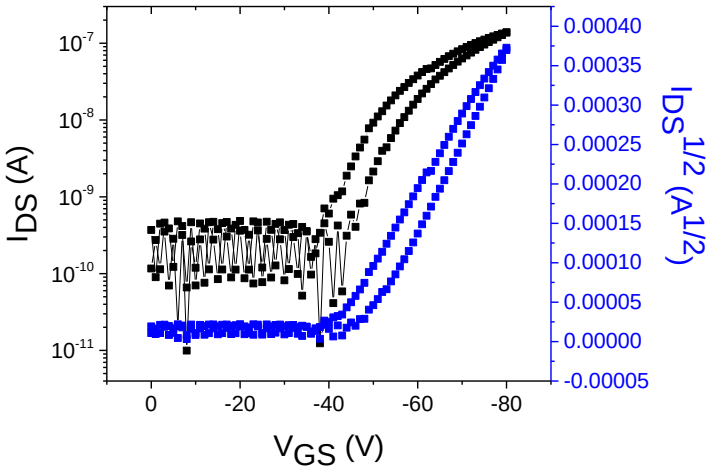

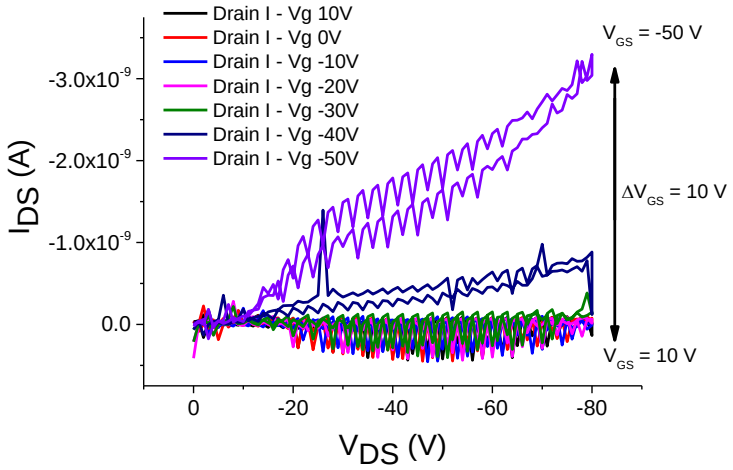

Annex 9: Output (left) and transfer (right) characteristic measure for Red 3 at a channel width of 2.5 µm

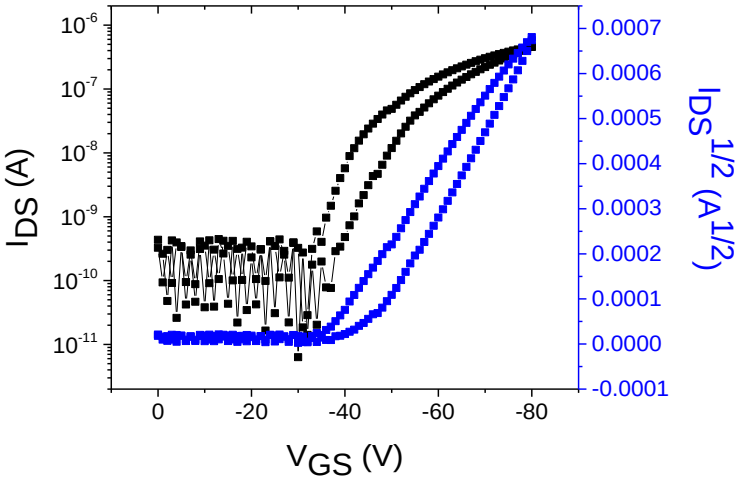

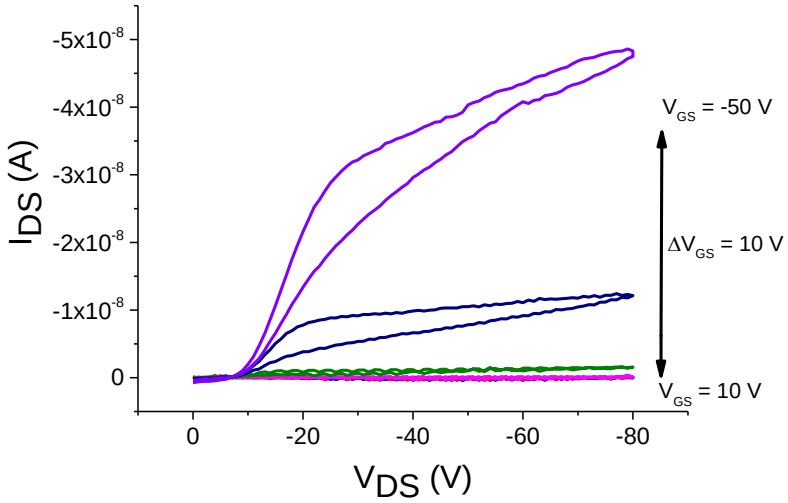

Annex 10: Electron mobility extracted from SCLC method for TPBi, OA67 and 3-COOK